CHAPTER 12

Magnetic Resonance Basics: Magnetic Fields, Nuclear Magnetic Characteristics, Tissue Contrast, Image Acquisition

Nuclear magnetic resonance (NMR) is the spectroscopic study of the magnetic properties of the *nucleus* of the atom. The protons and neutrons of the nucleus have a *magnetic* field associated with their nuclear spin and charge distribution. *Resonance* is an energy coupling that causes the individual nuclei, when placed in a strong external magnetic field, to selectively absorb, and later release, energy unique to those nuclei and their surrounding environment. The detection and analysis of the NMR signal has been extensively studied since the 1940s as an analytic tool in chemistry and biochemistry research. NMR is not an imaging technique but rather a method to provide spectroscopic data concerning a sample placed in a small volume, high field strength magnetic device. In the early 1970s, it was realized that magnetic field gradients could be used to localize the NMR signal and to generate images that display magnetic properties of the proton, reflecting clinically relevant information, coupled with technological advances and development of "body-size" magnets. As clinical imaging applications increased in the mid-1980s, the "nuclear" connotation was dropped, and magnetic resonance imaging (MRI), with a plethora of associated acronyms, became commonly accepted in the medical community.

MR applications continue to expand clinical relevance with higher field strength magnets, improved anatomic, physiologic, and spectroscopic studies. The high contrast sensitivity to soft tissue differences and the inherent safety to the patient resulting from the use of nonionizing radiation have been key reasons why MRI has supplanted many CT and projection radiography methods. With continuous improvements in image quality, acquisition methods, and equipment design, MRI is often the modality of choice to examine anatomic and physiologic properties of the patient. There are drawbacks, however, including high equipment and siting costs, scan acquisition complexity, relatively long imaging times, significant image artifacts, patient claustrophobia, and MR safety concerns.

This chapter reviews the basic properties of magnetism, concepts of resonance, tissue magnetization and relaxation events, generation of image contrast, and basic methods of acquiring image data. Advanced pulse sequences, illustration of image characteristics/artifacts, MR spectroscopy, MR safety, and biologic effects, are discussed in Chapter 13.

12.1 Magnetism, Magnetic Fields, and Magnets

Magnetism

Magnetism is a fundamental property of matter; it is generated by moving charges, usually electrons. Magnetic properties of materials result from the organization and motion of the electrons in either a random or a nonrandom alignment of magnetic "domains," which are the smallest entities of magnetism. Atoms and molecules have electron orbitals that can be paired (an even number of electrons cancels the magnetic field) or unpaired (the magnetic field is present). Most materials do not exhibit overt magnetic properties, but one notable exception is the permanent magnet, in which the individual magnetic domains are aligned in one direction.

Unlike the monopole electric charges from which they are derived, magnetic fields exist as dipoles, where the north pole is the origin of the magnetic field lines and the south pole is the return (Fig. 12-1A). One pole cannot exist without the other. As with electric charges, "like" magnetic poles repel and "opposite" poles attract. *Magnetic field strength, B* (also called the magnetic flux density), can be conceptualized as the number of magnetic lines of force per unit area, which decreases roughly as the inverse square of the distance from the source. The SI unit for *B* is the Tesla (T). As a benchmark, the earth's magnetic field is about 1/20,000 = 0.00005 T = 0.05 mT. An alternate (historical) unit is the gauss (G), where 1 T = 10,000 G.

Magnetic Fields

Magnetic fields can be induced by a moving charge in a wire (e.g., see the section on transformers in Chapter 6). The direction of the magnetic field depends on the sign and the direction of the charge in the wire, as described by the "right hand rule": The fingers point in the direction of the magnetic field when the thumb points in the direction of a moving positive charge (i.e., opposite to the direction of electron movement). Wrapping the current-carrying wire many times in a coil causes a superimposition of the magnetic fields, augmenting the overall strength of

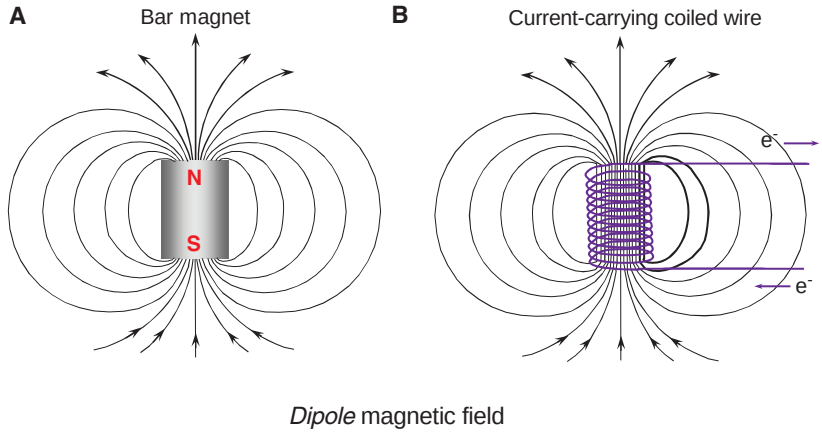

■ **FIGURE 12-1** **A.** The magnetic field has two poles with magnetic field lines emerging from the north pole (*N*), and returning to the south pole (*S*), as illustrated by a simple bar magnet. **B.** A coiled wire carrying an electric current produces a magnetic field with characteristics similar to a bar magnet. Magnetic field strength and field density are dependent on the amplitude of the current and the number of coil turns.

the magnetic field inside the coil, with a rapid falloff of field strength outside the coil (see Fig. 12-1B). Amplitude of the current in the coil determines the overall magnitude of the magnetic field strength. The magnetic field lines extending beyond the concentrated field are known as fringe fields.

Magnets

The magnet is the heart of the MR system. For any particular magnet type, performance criteria include field strength, temporal stability, and field homogeneity. These parameters are affected by the magnet design. Air core magnets are made of wire-wrapped cylinders of approximately 1-m diameter and greater, over a cylindrical length of 2 to 3 m, where the magnetic field is produced by an electric current in the wires. When the wires are energized, the magnetic field produced is parallel to the long axis of the cylinder. In most clinically designed systems, the magnetic field is horizontal and runs along the cranial–caudal axis of the patient lying supine (Fig. 12-2A). Solid core magnets are constructed from permanent magnets, a wire-wrapped iron core "electromagnet," or a hybrid combination. In these solid core designs, the magnetic field runs between the poles of the magnet, most often in a vertical direction (Fig. 12-2B). Magnetic fringe fields extend well beyond the volume of the cylinder in air core designs. Fringe fields are a potential hazard, and are discussed further in Chapter 13.

To achieve a high magnetic field strength (greater than 1 T) requires the electromagnet core wires to be superconductive. Superconductivity is a characteristic of certain metals (e.g., niobium–titanium alloys) that when maintained at extremely low temperatures (liquid helium; less than 4°K) exhibit no resistance to electric current.

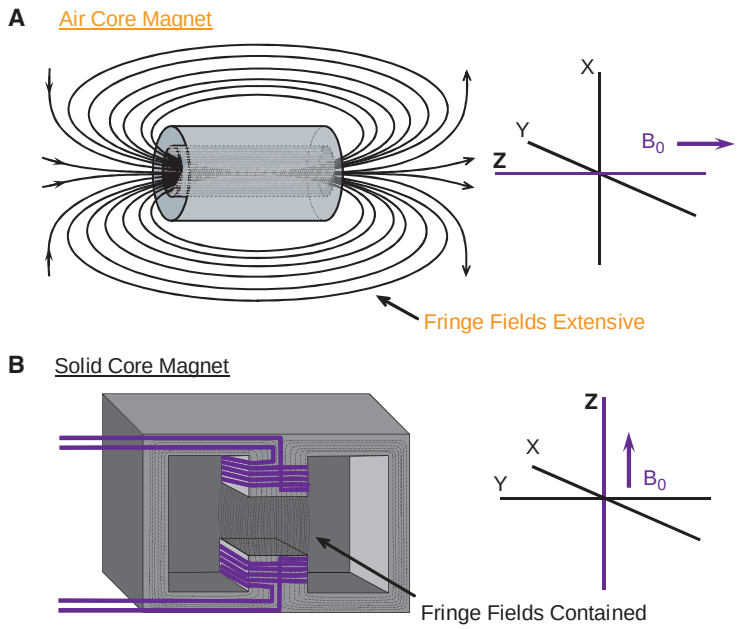

■ **FIGURE 12-2** **A.** Air core magnets typically have a horizontal main field produced in the bore of the electrical windings, with the z-axis (B_0) along the bore axis. Fringe fields for the air core systems are extensive and are increased for larger bore diameters and higher field strengths. **B.** The solid core magnet has a vertical field, produced between the metal poles of a permanent or wire-wrapped electromagnet. Fringe fields are confined with this design. In both types, the main field is parallel to the z-axis of the Cartesian coordinate system.

Superconductivity allows the closed-circuit electromagnet to be energized and ramped up to the desired current and magnetic field strength by an external electric source. Replenishment of the liquid helium must occur continuously, because if the temperature rises above a critical value, the loss of superconductivity will occur and resistance heating of the wires will boil the helium, resulting in a "quench." Superconductive magnets with field strengths of 1.5 to 3 T are common for clinical systems, and 4 to 7 T clinical large bore magnets are currently used for research applications, with possible future clinical use.

A cross section of the internal superconducting magnet components shows integral parts of the magnet system including the wire coils and cryogenic liquid containment vessel (Fig. 12-3). In addition to the main magnet system, other components are also necessary. *Shim coils* interact with the main magnetic field to improve homogeneity (minimal variation of the magnetic flux density) over the volume used for patient imaging. *Radiofrequency (RF) coils* exist within the main bore of the magnet to transmit energy to the patient as well as to receive returning signals. *Gradient coils* are contained within the main bore to produce a linear variation of magnetic field strength across the useful magnet volume.

A magnetic field gradient is obtained by superimposing the magnetic fields of two or more coils carrying a direct current of specific amplitude and direction with a precisely defined geometry (Fig. 12-4). The bipolar gradient field varies over a predefined field of view (FOV), and when superimposed upon B_0, a small, continuous variation in the field strength occurs from the center to the periphery with distance from the center point (the "null"). Interacting with the much, much stronger main magnetic field, the subtle linear variations are on the order of 0.005 T/m (5 mT/m) and are essential for localizing signals generated during the operation of the MR system.

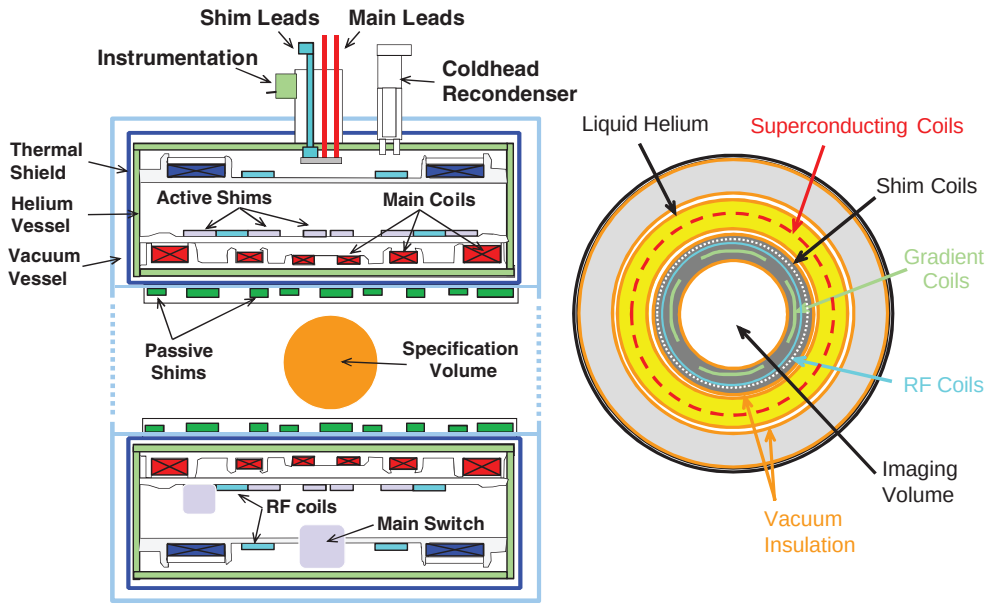

■ **FIGURE 12-3** Internal components of a superconducting air-core magnet are shown. On the left is a cross section through the long axis of the magnet illustrating relative locations of the components, and on the right is a simplified cross section across the diameter.

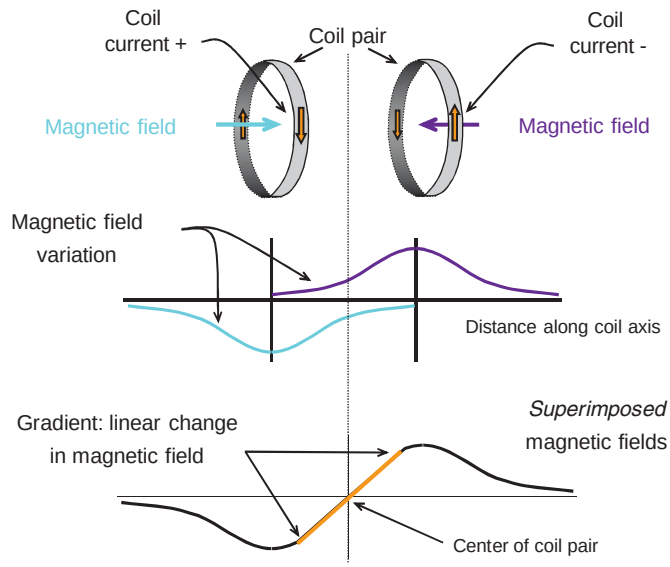

■ **FIGURE 12-4** Gradients are produced inside the main magnet with coil pairs. Individual conducting wire coils are separately energized with currents of opposite direction to produce magnetic fields of opposite polarity. Magnetic field strength decreases with distance from the center of each coil. When combined, the magnetic field variations form a linear change between the coils, producing a linear magnetic field gradient, as shown in the lower graph.

The MR System

The MR system is comprised of several components including those described above, orchestrated by many processors and control subsystems, as shown in Figure 12-5. Detail of the individual components, methods of acquiring the MR signals and reconstruction of images are described in the following sections. But first, characteristics of the magnetic properties of tissues, the resonance phenomenon, and geometric considerations are explained.

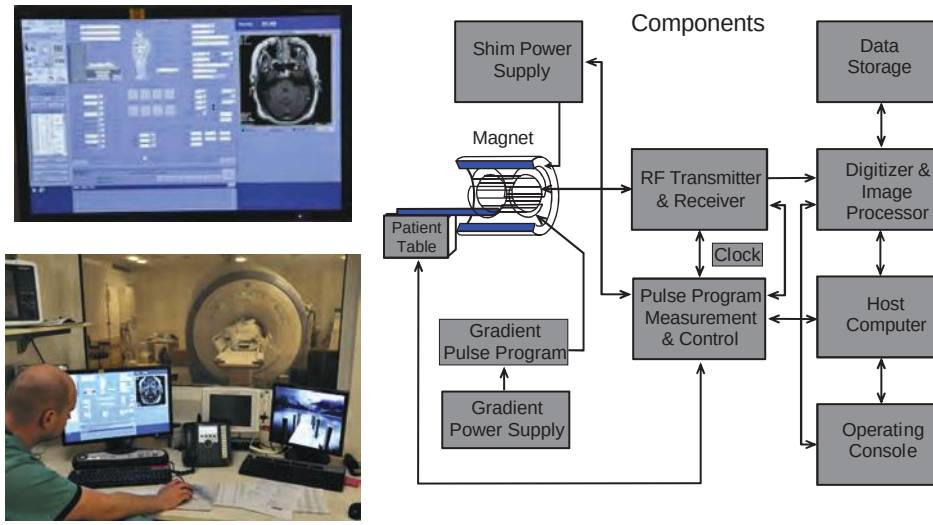

■ **FIGURE 12-5** The MR system is shown **(lower left)**, the operators display **(upper left)**, and the various subsystems that generate, detect, and capture the MR signals used for imaging and spectroscopy.

Magnetic Properties of Materials

Magnetic *susceptibility* describes the extent to which a material becomes magnetized when placed in a magnetic field. Induced internal magnetization opposes the external magnetic field and lowers the local magnetic field surrounding the material. On the other hand, the internal magnetization can form in the same direction as the applied magnetic field, and increase the local magnetic field. Three categories of susceptibility are defined: *diamagnetic, paramagnetic*, and *ferromagnetic*, based upon the arrangement of electrons in the atomic or molecular structure. Diamagnetic elements and materials have slightly negative susceptibility and oppose the applied magnetic field, because of paired electrons in the surrounding electron orbitals. Examples of diamagnetic materials are calcium, water, and most organic materials (chiefly owing to the diamagnetic characteristics of carbon and hydrogen). Paramagnetic materials, with unpaired electrons, have slightly positive susceptibility and enhance the local magnetic field, but they have no measurable self-magnetism. Examples of paramagnetic materials are molecular oxygen (O_2), deoxyhemoglobin, some blood degradation products such as methemoglobin, and *gadolinium*-based contrast agents. Locally, these diamagnetic and paramagnetic agents will deplete or augment the local magnetic field (Fig. 12-6), affecting MR images in known, unknown, and sometimes unexpected ways. Ferromagnetic materials are "superparamagnetic"—that is, they augment the external magnetic field substantially. These materials, containing iron, cobalt, and nickel, exhibit "self-magnetism" in many cases, and can significantly distort the acquired signals.

Magnetic Characteristics of the Nucleus

The nucleus, comprising protons and neutrons with characteristics listed in Table 12-1, exhibits magnetic characteristics on a much smaller scale than for atoms/molecules and their associated electron distributions. Magnetic properties are influenced by spin and charge distributions intrinsic to the proton and neutron. A magnetic dipole is created for the proton, with a positive charge equal to the electron charge but of opposite sign, due to nuclear "spin." Overall, the neutron is electrically uncharged, but subnuclear charge inhomogeneities and an associated nuclear spin result in a magnetic field of opposite direction and approximately the same strength as the proton. Magnetic characteristics of the nucleus are described by the *nuclear magnetic moment,* represented as

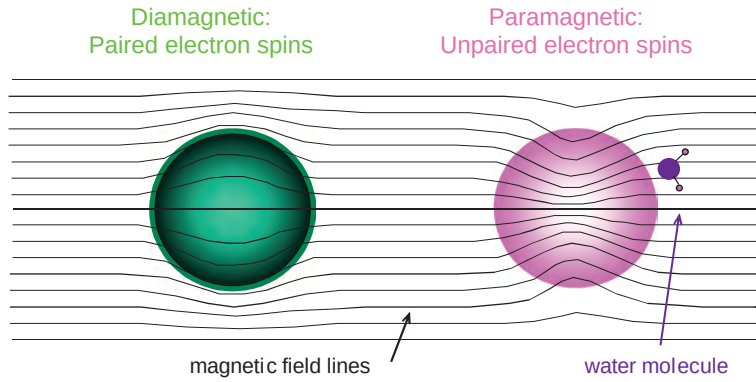

■ **FIGURE 12-6** The local magnetic field can be changed in the presence of diamagnetic (depletion) and paramagnetic (augmentation) materials, with an impact on the signals generated from nearby signal sources such as the hydrogen atoms in water molecules.

TABLE 12-1 PROPERTIES OF THE NEUTRON AND PROTON

CHARACTERISTIC	NEUTRON	PROTON
Mass(kg)	1.674×10^{-27}	1.672×10^{-27}
Charge (coulomb)	0	1.602×10^{-19}
Spin quantum number	½	½
Magnetic moment (J/T)	-9.66×10^{-27}	1.41×10^{-26}
Magnetic moment (nuclear magneton)	−1.91	2.79

a vector indicating magnitude and direction. For a given nucleus, the nuclear magnetic moment is determined through the pairing of the constituent protons and neutrons. If the sum of the number of protons (P) and number of neutrons (N) in the nucleus is even, the nuclear magnetic moment is essentially zero. However, if N is even and P is odd, or N is odd and P is even, the resultant noninteger nuclear spin generates a nuclear magnetic moment. A single nucleus does not generate a large enough nuclear magnetic moment to be observable, but the conglomeration of large numbers of nuclei ($\sim 10^{15}$) arranged in a nonrandom orientation generates an observable nuclear magnetic moment of the sample, from which the MRI signals are derived.

Nuclear Magnetic Characteristics of the Elements

Biologically relevant elements that are candidates for producing MR signals are listed in Table 12-2. Key features include the strength of the nuclear magnetic moment, the physiologic concentration, and the isotopic abundance. Hydrogen, having the largest magnetic moment and greatest abundance, chiefly in water and fat, is by far the best element for general clinical utility. Other elements are orders of magnitude less sensitive. Of these, ^{23}Na and ^{31}P have been used for imaging in limited situations, despite their relatively low sensitivity. Therefore, the nucleus of the hydrogen atom, the proton, is the principal focus for generating MR signals.

TABLE 12-2 MAGNETIC RESONANCE PROPERTIES OF MEDICALLY USEFUL NUCLEI

NUCLEUS	SPIN QUANTUM NUMBER	% ISOTOPIC ABUNDANCE	MAGNETIC MOMENT[b]	% RELATIVE ELEMENTAL ABUNDANCE[a]	RELATIVE SENSITIVITY
^{1}H	½	99.98	2.79	10	1
^{3}He	½	0.00014	−2.13	0	–
^{13}C	−½	0.011	0.70	18	–
^{17}O	5/2	0.04	−1.89	65	9×10^{-6}
^{19}F	½	100	2.63	<0.01	3×10^{-8}
^{23}Na	3/2	100	2.22	0.1	1×10^{-4}
^{31}P	½	100	1.13	1.2	6×10^{-5}

[a]moment in nuclear magneton units = 5.05×10^{-27} J T^{-1}.
[b]*Note:* by mass in the human body (all isotopes).

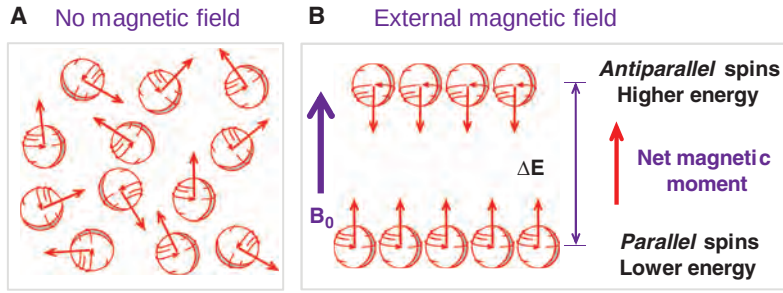

■ **FIGURE 12-7** Simplified distributions of "free" protons without and with an external magnetic field are shown. **A.** Without an external magnetic field, a group of protons assumes a random orientation of magnetic moments, producing an overall magnetic moment of zero. **B.** Under the influence of an applied external magnetic field, B_0, the protons assume a nonrandom alignment in two possible orientations: parallel and antiparallel to the applied magnetic field. A slightly greater number of protons exist in the parallel direction, resulting in a measurable *net magnetic moment* in the direction of B_0.

Magnetic Characteristics of the Proton

The spinning proton or "*spin*" (spin and proton are used synonymously herein) is classically considered to be a tiny bar magnet with north and south poles, even though the magnetic moment of a single proton is undetectable. Large numbers of unbound hydrogen atoms in water and fat, those unconstrained by molecular bonds in complex macromolecules within tissues, have a random orientation of their protons (nuclear magnetic moments) due to thermal energy. As a result, there is no observable magnetization of the sample (Fig. 12-7A). However, when placed in a strong static magnetic field, B_0, magnetic forces cause the protons to align with the applied field in parallel and antiparallel directions at two discrete energy levels (Fig. 12-7B). Thermal energy within the sample causes the protons to be distributed in this way, and at equilibrium, a slight majority exists in the low-energy, parallel direction. A stronger magnetic field increases the energy separation of the low- and high-energy levels and the number of excess protons in the low-energy state. At 1.0 T, the number of excess protons in the low-energy state is approximately 3 protons per million (3×10^{-6}) at physiologic temperatures. Although this number seems insignificant, for a typical voxel volume in MRI, there are about 10^{21} protons, so there are $3 \times 10^{-6} \times 10^{21}$, or approximately 3×10^{15} more protons in the low-energy state! This number of excess protons produces an observable "sample" nuclear magnetic moment, initially aligned with the direction of the applied magnetic field.

In addition to energy separation of the parallel and antiparallel spin states, the protons also experience a torque in a perpendicular direction from the applied magnetic field that causes *precession*, much the same way that a spinning top wobbles due to the force of gravity (Fig. 12-8). The precession occurs at an angular frequency (number of rotations/sec about an axis of rotation) that is proportional to the magnetic field strength B_0. The *Larmor equation* describes the dependence between the magnetic field, B_0, and the angular precessional frequency, ω_0:

$$\omega_0 = \gamma B_0$$

where γ is the gyromagnetic ratio unique to each element. This is expressed in terms of linear frequency as

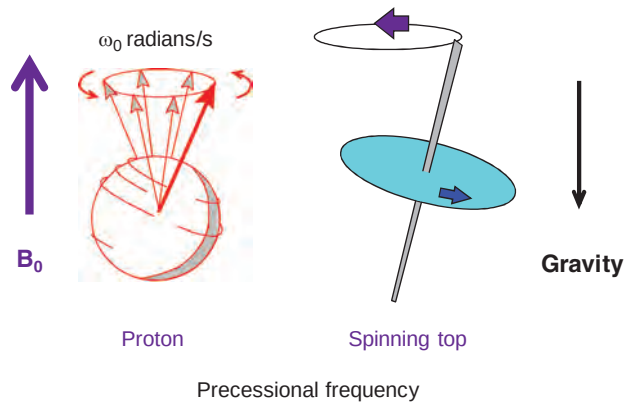

■ **FIGURE 12-8** A single proton *precesses* about its axis with an angular frequency, ω, proportional to the externally applied magnetic field strength, according to the *Larmor* equation. A well-known example of precession is the motion a spinning top makes as it interacts with the force of gravity as it slows.

$$f_0 = \frac{\gamma}{2\pi} B_0$$

where $\omega = 2\pi f$ and $\gamma/2\pi$ is the *gyromagnetic ratio*, with values expressed in millions of cycles per second (MHz) per Tesla, or MHz/T.

Each element with a nonzero nuclear magnetic moment has a unique gyromagnetic ratio, as listed in Table 12-3.

Energy Absorption and Emission

The protons precessing in the parallel and antiparallel directions result in a quantized distribution (two discrete energies) with the net magnetic moment of the sample at equilibrium equal to the vector sum of the individual magnetic moments in the direction of B_0 as shown in Figure 12-9. The magnetic field vector components of the sample in the perpendicular direction are randomly distributed and sum to zero. Briefly irradiating the sample with an electromagnetic RF energy pulse tuned to the Larmor (resonance) frequency promotes protons from the low-energy, parallel direction to the higher energy, antiparallel direction, and the magnetization along the direction of the applied magnetic field shrinks. Subsequently, the more energetic sample returns to equilibrium conditions when the protons revert to the parallel direction and release RF energy at the

TABLE 12-3 GYROMAGNETIC RATIO FOR USEFUL ELEMENTS IN MAGNETIC RESONANCE

NUCLEUS	$\gamma/2\pi$ (MHz/T)
^{1}H	42.58
^{13}C	10.7
^{17}O	5.8
^{19}F	40.0
^{23}Na	11.3
^{31}P	17.2

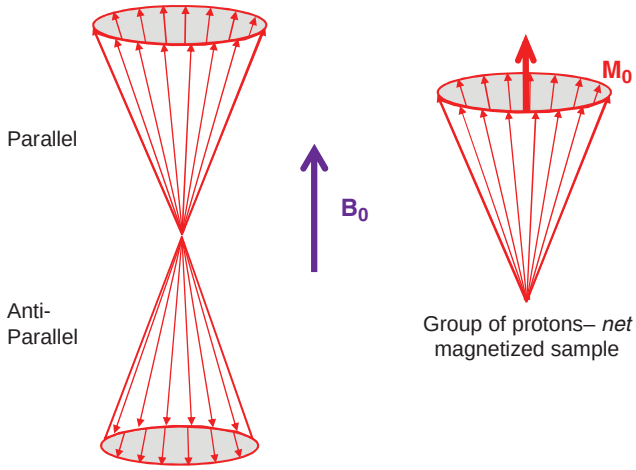

■ **FIGURE 12-9** A group of protons in the parallel and antiparallel energy states generates an equilibrium magnetization, M_0, in the direction of the applied magnetic field B_0. The protons are distributed randomly over the surface of the cone, and produce no magnetization in the perpendicular direction.

same frequency. This energy emission is detected by highly sensitive antennas to capture the basic MR signal.

Typical magnetic field strengths for MR systems range from 0.3 to 4.0 T. For protons, the precessional frequency is 42.58 MHz/T, and increases or decreases with an increase or decrease in magnetic field strength, as calculated in the example below. Accuracy of the precessional frequency is necessary to ensure that the RF energy will be absorbed by the magnetized protons. Precision of the precessional frequency must be on the order of cycles/s (Hz) out of millions of cycles/s (MHz) in order to identify the location and spatial position of the emerging signals, as is described in Section 12.6.

EXAMPLE: What is the frequency of precession of ^{1}H and ^{31}P at 0.5 T? 1.5 T? 3.0 T? The Larmor frequency is calculated as $f_0 = (\gamma/2\pi)B_0$.

	FIELD STRENGTH		
ELEMENT	0.5 T	1.5 T	3.0 T
^{1}H	42.58 × 0.5 = 21.29 MHz	42.58 × 1.5 = 63.87 MHz	42.58 × 3.0 = 127.74 MHz
^{31}P	17.2 × 0.5 = 8.6 MHz	17.2 × 1.5 = 25.8 MHz	17.2 × 3 = 51.6 MHz

The differences in the gyromagnetic ratios and corresponding precessional frequencies allow the selective excitation of one element from another in the same magnetic field strength.

Geometric Orientation, Frame of Reference, and Magnetization Vectors

By convention, the applied magnetic field B_0 is directed parallel to the z-axis of the three-dimensional Cartesian coordinate axis system and perpendicular to the x and y axes. For convenience, two frames of reference are used: the *laboratory frame* and the *rotating frame*. The laboratory frame (Fig. 12-10A) is a stationary reference frame from the observer's point of view. The sample magnetic moment vector precesses about the

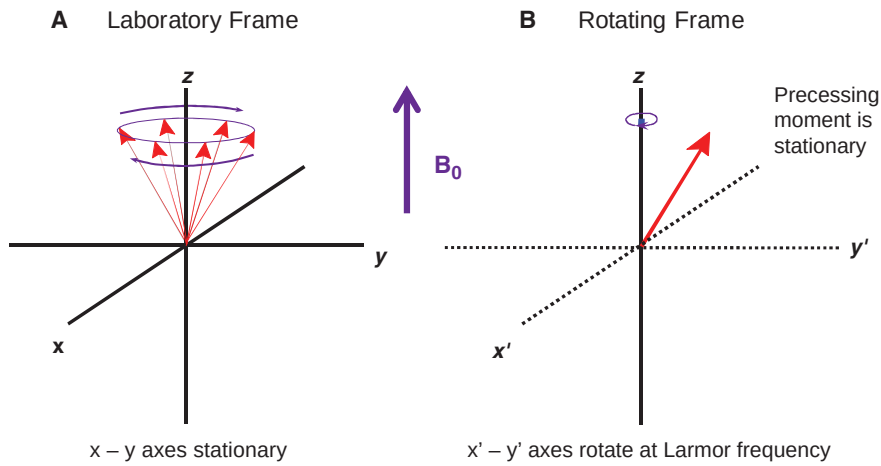

■ **FIGURE 12-10** **A.** The *laboratory frame of reference* uses stationary three-dimensional Cartesian coordinates: x, y, z. The magnetic moment precesses around the z-axis at the Larmor frequency as the illustration attempts to convey. **B.** The *rotating frame of reference* uses rotating Cartesian coordinate axes that *rotate about the z-axis* at the Larmor precessional frequency, and the other axes are denoted: *x′* and *y′*. When precessing at the Larmor frequency, the sample magnetic moment is stationary.

z-axis in a circular geometry about the x-y plane. The rotating frame (Fig. 12-10B) is a *spinning* axis system, whereby the x′-y′ axes rotate at an angular frequency equal to the Larmor frequency. In this frame, the sample magnetic moment vector appears to be stationary when rotating at the resonance frequency. A slightly higher precessional frequency is observed as a slow clockwise rotation, while a slightly lower precessional frequency is observed as a slow counterclockwise rotation. The magnetic interactions between precessional frequencies of the tissue magnetic moments with the externally applied RF (depicted as a rotating magnetic field) can be described more clearly using the rotating frame of reference, while the observed returning signal and its frequency content is explained using the laboratory (stationary) frame of reference.

The net magnetization vector of the sample, M, is described by three components. *Longitudinal magnetization*, M_z, along the z direction, is the component of the magnetic moment parallel to the applied magnetic field, B_0. At equilibrium, the longitudinal magnetization is maximal and is denoted as M_0, the *equilibrium magnetization*. The component of the magnetic moment perpendicular to B_0, M_{xy}, in the x-y plane, is *transverse magnetization*. At equilibrium, M_{xy} is zero. When the protons in the magnetized sample absorb energy, M_z is "tipped" into the transverse plane, and M_{xy} generates the all-important MR signal. Figure 12-11 illustrates this geometry.

12.2 The Magnetic Resonance Signal

Application of RF energy synchronized to the precessional frequency of the protons causes absorption of energy and displacement of the sample magnetic moment from equilibrium conditions. The return to equilibrium results in the emission of energy proportional to the number of excited protons in the volume. This occurs at a rate that depends on the structural and magnetic characteristics of the sample. Excitation, detection, and acquisition of the signals constitute the basic information necessary for MRI and and MR spectroscopy (MRS).

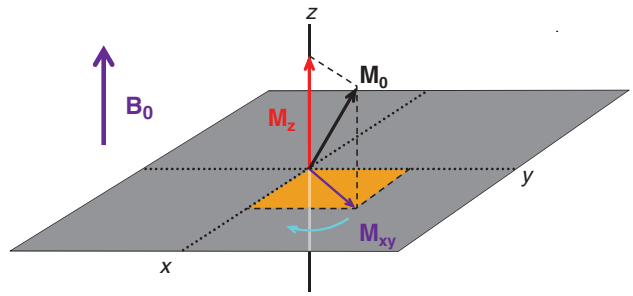

■ **FIGURE 12-11** *Longitudinal magnetization,* M_z, is the vector component of the magnetic moment in the z direction. *Transverse magnetization,* M_{xy}, is the vector component of the magnetic moment in the *x-y* plane. *Equilibrium magnetization,* M_0, is the maximal longitudinal magnetization of the sample, and is shown displaced from the z-axis in this illustration.

Resonance and Excitation

Displacement of the equilibrium magnetization occurs when the magnetic component of the RF excitation pulse, known as the B_1 field, is precisely matched to the precessional frequency of the protons. The *resonance* frequency corresponds to the energy separation between the protons in the parallel and antiparallel directions.

The **quantum mechanics model** considers the RF energy as photons (quanta) instead of waves. Protons oriented parallel and antiparallel to the external magnetic field, separated by an energy gap, ΔE, will transition from the low- to the high-energy level only when the RF pulse is equal to the precessional frequency. The number of protons that undergo an energy transition is dependent on the amplitude and duration of the RF pulse. M_z changes from the maximal positive value at equilibrium, through zero, to the maximal negative value (Fig. 12-12). Continued

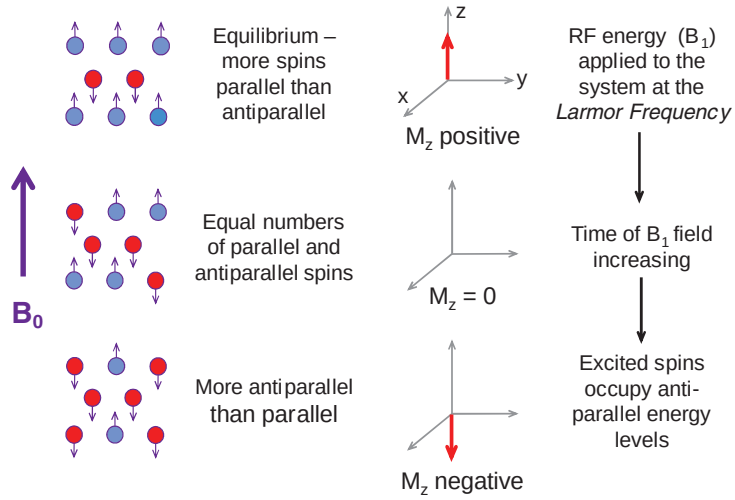

■ **FIGURE 12-12** A simple quantum mechanics process depicts the discrete energy absorption and the time change of the longitudinal magnetization vector as RF energy equal to the energy difference of the parallel and antiparallel spins is applied to the sample (at the Larmor frequency). Discrete quanta absorption changes the proton energy from parallel to antiparallel. With continued application of the RF energy at the Larmor frequency, M_z is displaced from equilibrium, through zero, to the opposite direction (high energy state).

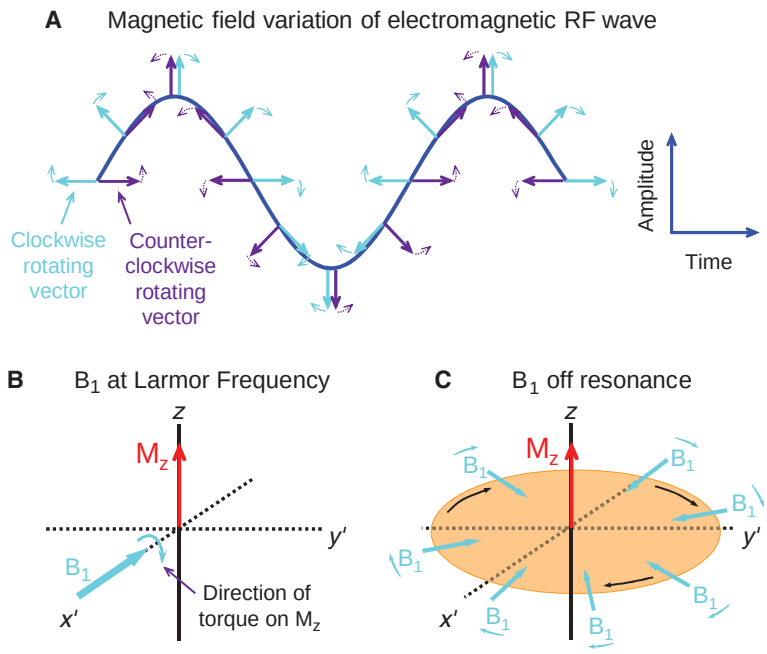

■ **FIGURE 12-13** **A.** A classical physics description of the magnetic field component of the RF pulse (the electric field is not shown). Clockwise (*solid*) and counterclockwise (*dotted*) rotating magnetic vectors produce the magnetic field variation by constructive and destructive interaction. At the Larmor frequency, one of the magnetic field vectors rotates synchronously in the rotating frame and is therefore stationary (the other vector rotates in the opposite direction and does not synchronize with the rotating frame). **B.** In the *rotating frame,* the RF pulse (B_1 field) is applied at the Larmor frequency and is stationary in the x′-y′ plane. The B_1 field interacts at 90 degrees to the sample magnetic moment and produces a torque that displaces the magnetic vector away from equilibrium. **C.** The B_1 field is not tuned to the Larmor frequency and is not stationary in the rotating frame. No interaction with the sample magnetic moment occurs.

irradiation can induce a return to equilibrium conditions, when an incoming RF quantum of energy causes the reversion of a proton in the antiparallel direction to the parallel direction with the energy-conserving spontaneous emission of two excess quanta. While this model shows how energy absorption and emission occurs, there is no clear description of how M_{xy} evolves, which is better understood using classical physics concepts.

In the **classical physics model**, the linear B_1 field is described with two magnetic field vectors of equal magnitude, rotating in opposite directions, representing the sinusoidal variation of the magnetic component of the electromagnetic RF wave as shown in Figure 12-13. One of the two rotating vectors is synchronized to the precessing protons in the magnetized sample, and in the rotating frame is stationary. If the RF energy is not applied at the precessional (Larmor) frequency, the B_1 field will not interact with M_z. Another description is that of a circularly polarized B_1 transmit field from the body coil that rotates at the precessional frequency of the magnetization.

Flip Angles

Flip angles represent the degree of M_z rotation by the B_1 field as it is applied along the x′-axis (or the y′-axis) perpendicular to M_z. A torque is applied on M_z, rotating it from the longitudinal direction into the transverse plane. The rate of rotation occurs

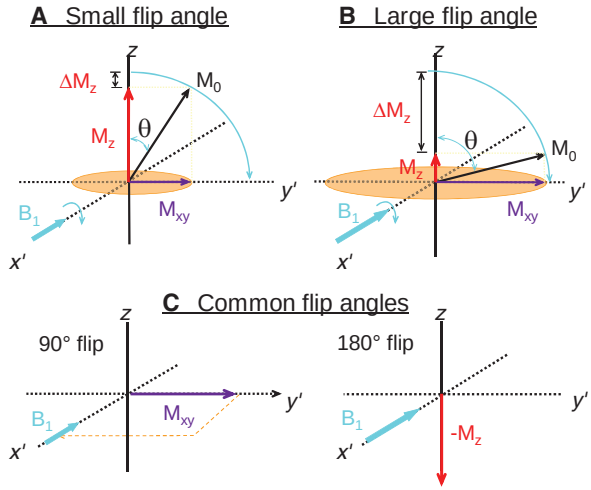

■ **FIGURE 12-14** Flip angles are the result of the angular displacement of the longitudinal magnetization vector from the equilibrium position. The rotation angle of the magnetic moment vector is dependent on the duration and amplitude of the B_1 field at the Larmor frequency. Flip angles describe the rotation of M_z away from the z-axis. **A.** Small flip angles (less than 45 degrees) and **B.** Large flip angles (75 to 90 degrees) produce small and large transverse magnetization, respectively.

at an angular frequency equal to $\omega_1 = \gamma B_1$, as per the Larmor equation. Thus, for an RF pulse (B_1 field) applied over a time t, the magnetization vector displacement angle, θ, is determined as $\theta = \omega_1 t = \gamma B_1 t$, and the product of the pulse time and B_1 amplitude determines the displacement of M_z. This is illustrated in Figure 12-14.

Common flip angles are 90 degrees ($\pi/2$) and 180 degrees (π), although a variety of smaller and larger angles are chosen to enhance tissue contrast in various ways. A 90-degree angle provides the largest possible M_{xy} and detectable MR signal, and requires a known B_1 strength and time (on the order of a few to hundreds of μs). The displacement angle of the sample magnetic moment is linearly related to the product of B_1 field strength and time: For a fixed B_1 field strength, a 90-degree displacement takes half the time of a 180-degree displacement. With flip angles smaller than 90 degrees, less time is needed to displace M_z, and a larger transverse magnetization per unit excitation time is achieved. For instance, a 45-degree flip takes half the time of a 90 degrees yet creates 70% of the signal, as the magnitude of M_{xy} is equal to the sine of 45 degrees, or 0.707. With fast MRI techniques, small displacement angles of 10 degrees and less are often used.

12.3 Magnetization Properties of Tissues

Free Induction Decay: T2 Relaxation

After a 90-degree RF pulse is applied to a magnetized sample at the Larmor frequency, an initial phase coherence of the individual protons is established and maximum M_{xy} is achieved. Rotating at the Larmor frequency, the transverse magnetic field of the excited sample induces signal in the receiver antenna coil (in the laboratory frame of reference). A damped sinusoidal electronic signal, known as the *free induction decay* (FID), is produced (Fig. 12-15).

The FID amplitude decay is caused by loss of M_{xy} phase coherence due to intrinsic micromagnetic inhomogeneities in the sample's structure, whereby individual protons

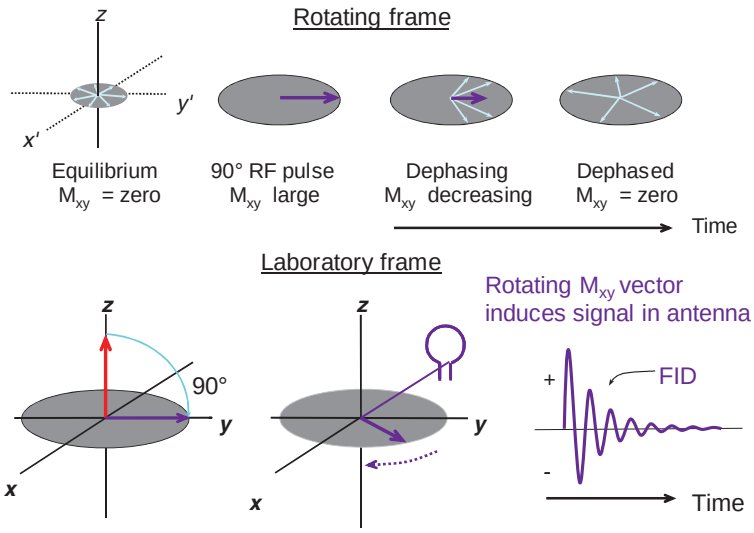

■ **FIGURE 12-15** **Top.** Conversion of longitudinal magnetization, M_z, into transverse magnetization, M_{xy}, results in an initial phase coherence of the individual spins of the sample. The magnetic moment vector precesses at the Larmor frequency (stationary in the rotating frame), and dephases with time. **Bottom.** In the laboratory frame, M_{xy} precesses and induces a signal in an antenna receiver sensitive to transverse magnetization. A FID signal is produced with positive and negative variations oscillating at the Larmor frequency, and decaying with time due to the loss of phase coherence.

in the bulk water and hydration layer coupled to macromolecules precess at incrementally different frequencies arising from the slight changes in local magnetic field strength. Phase coherence is lost over time as an exponential decay. Elapsed time between the peak transverse signal (e.g., directly after a 90-degree RF pulse) and 37% of the peak level (1/*e*) is the T2 relaxation time (Fig. 12-16A). Mathematically, this is expressed as

$$M_{xy}(t) = M_0 e^{-t/T2}$$

where $M_{xy}(t)$ is the transverse magnetic moment at time t for a sample that has M_0 transverse magnetization at $t = 0$. When $t = T2$, then $e^{-1} = 0.37$ and $M_{xy} = 0.37\, M_0$.

The molecular structure of the magnetized sample and characteristics of the bound water protons strongly affects its T2 decay value. Amorphous structures (e.g., cerebral spinal fluid [CSF] or highly edematous tissues) contain mobile molecules with fast and rapid molecular motion. Without structural constraint (e.g., lack of a hydration layer), these tissues do not support intrinsic magnetic field inhomogeneities, and thus exhibit long T2 values. As molecular size increases for specific tissues, constrained molecular motion and the presence of the hydration layer produce magnetic field domains within the structure and increase spin dephasing that causes more rapid decay with the result of shorter T2 values. For large, nonmoving structures, stationary magnetic inhomogeneities in the hydration layer result in these types of tissues (e.g., bone) having a very short T2.

Extrinsic magnetic inhomogeneities, such as the imperfect main magnetic field, B_0, or susceptibility agents in the tissues (e.g., MR contrast materials, paramagnetic or ferromagnetic objects), add to the loss of phase coherence from intrinsic inhomogeneities and further reduce the decay constant, known as T2* under these conditions (Fig. 12-16B).

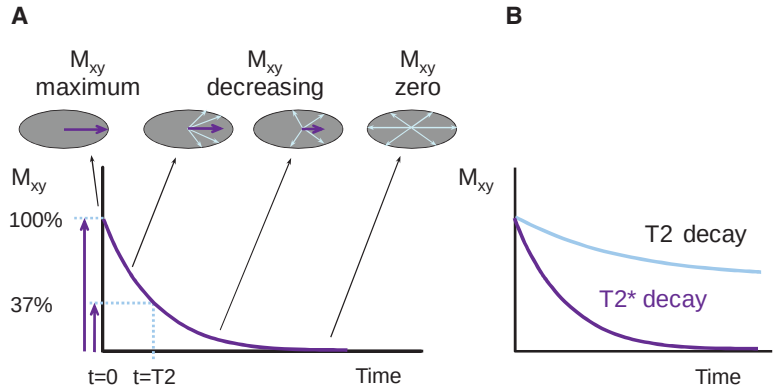

■ **FIGURE 12-16** **A.** The loss of M_{xy} phase coherence occurs exponentially caused by intrinsic spin-spin interactions in the tissues and extrinsic magnetic field inhomogeneities. The exponential decay constant, T2, is the time over which the signal decays to 37% of the initial transverse magnetization (e.g., after a 90-degree pulse). **B.** T2 is the decay time resulting from *intrinsic* magnetic properties of the sample. T2* is the decay time resulting from *both intrinsic and extrinsic magnetic field variations*. T2 is always longer than T2*.

Return to Equilibrium: T1 Relaxation

Longitudinal magnetization begins to recover immediately after the B_1 excitation pulse, simultaneous with transverse decay; however, the return to equilibrium conditions occurs over a longer time period. *Spin-lattice relaxation* is the term describing the release of energy back to the *lattice* (the molecular arrangement and structure of the hydration layer), and the regrowth of M_z. This occurs exponentially as

$$M_z(t) = M_0(1 - e^{-t/T1})$$

where $M_z(t)$ is the longitudinal magnetization at time t and $T1$ is the time needed for the recovery of 63% of M_z after a 90-degree pulse (at $t = 0$, $M_z = 0$, and at $t = T1$, $M_z = 0.63\ M_0$), as shown in Figure 12-17. When $t = 3 \times T1$, then $M_z = 0.95\ M_0$, and for $t > 5 \times T1$, then $M_z \approx M_0$, and full longitudinal magnetization equilibrium is established.

Since M_z does not generate an MR signal directly, determination of T1 for a specific tissue requires a specific "sequence," as shown in Figure 12-18. At equilibrium, a 90-degree pulse sets $M_z = 0$. After a delay time, ΔT, the recovered M_z component is converted to M_{xy} by a second 90-degree pulse, and the resulting peak amplitude

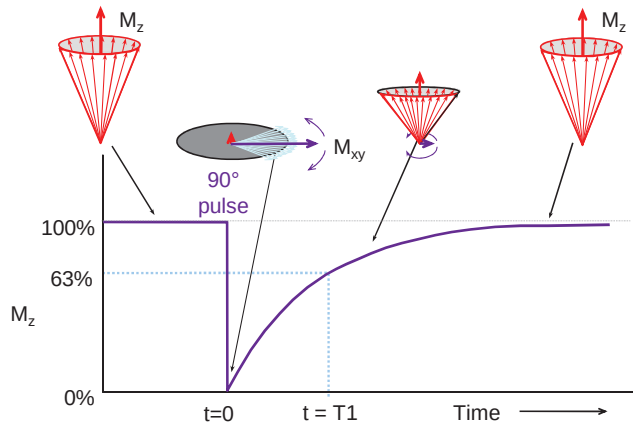

■ **FIGURE 12-17** After a 90-degree pulse, M_z is converted from a maximum value at equilibrium to $M_z = 0$. Return of M_z to equilibrium occurs exponentially and is characterized by the spin-lattice T1 relaxation constant. After an elapsed time equal to T1, 63% of the longitudinal magnetization is recovered. Spin-lattice recovery takes longer than spin-spin decay (T2).

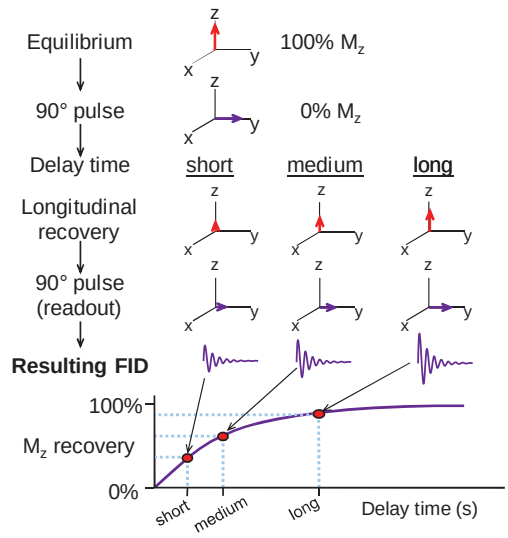

■ **FIGURE 12-18** Spin-lattice relaxation for a sample can be measured by using various delay times between two 90-degree RF pulses. After an initial 90-degree pulse, $M_z = 0$, another 90-degree pulse separated by a known delay is applied, and the longitudinal magnetization that has recovered during the delay is converted to transverse magnetization. The maximum amplitude of the resultant FID is recorded as a function of delay times between initial pulse and readout (three different delay time experiments are shown in this example), and the points are fit to an exponential recovery function to determine T1.

is recorded. By repeating the sequence from equilibrium conditions with different delay times, ΔT between 90-degree pulses, data points that lie on the recovery curve are fit to an exponential equation and T1 is estimated.

The T1 relaxation time depends on the rate of energy dissipation into the surrounding molecular lattice and hydration layer and varies substantially for different tissue structures and pathologies. This can be explained from a classical physics perspective by considering the "tumbling" frequencies of the protons in bulk water and the hydration layers present relative to the Larmor precessional frequency of the protons. Energy transfer is most efficient when a maximal overlap of these frequencies occurs. Small molecules and unbound, bulk water have tumbling frequencies across a broad spectrum, with low-, intermediate-, and high-frequency components. Large, slowly moving molecules have a very tight hydration layer and exhibit low tumbling frequencies that concentrate in the lowest part of the frequency spectrum. Moderately sized molecules (e.g., proteins) and viscous fluids have a moderately bound hydration layer that produce molecular tumbling frequencies more closely matched to the Larmor frequency. This is more fully described in the "Two Compartment Fast Exchange Model" (Fullerton, et.al, 1982; Bottomley, et. al, 1984). The water in the hydration layer and bulk water exchange rapidly (on the order of 100,000 transitions per second) so that a weighted average of the T1 is observed. Therefore, the T1 time is strongly dependent on the physical characteristics of the tissues and their associated hydration layers. Therefore for solid and slowly moving structures, the hydration layer permits only low-frequency molecular tumbling frequencies and consequently, there is almost no spectral overlap with the Larmor frequency. For unstructured tissues and fluids in bulk water, there is also only a small spectral overlap with the tumbling frequencies. In each of these situations, release of energy is constrained and T1 relaxation time is long. For structured and moderately sized proteins and fatty tissues, molecular tumbling frequencies are most conducive to spin-lattice relaxation because of a larger overlap with the Larmor frequency and result in a relatively short T1 relaxation time, as shown in Figure 12-19. Typical T1 values are in the range of 0.1 to 1 s for soft tissues, and 1 to 4 s in aqueous tissues (e.g., CSF).

As the main magnetic field strength increases, a corresponding increase in the Larmor precessional frequency causes a decrease in the overlap with the molecular tumbling frequencies and a longer T1 recovery time. Gadolinium chelated with

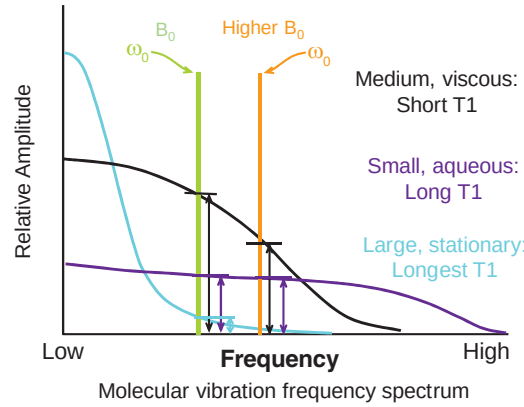

■ **FIGURE 12-19** A classical physics explanation of spin-lattice relaxation is based upon the tumbling frequency of the protons in water molecules of a sample material and its frequency spectrum. Large, stationary structures have water protons with tight hydration layers that exhibit little tumbling motion and a low-frequency spectrum (*aqua* curve). Bulk water and small-sized, aqueous materials have frequencies distributed over a broad range (*purple* curve). Medium-sized, proteinacious materials have a hydration layer that slows down the tumbling frequency of protons sufficiently to allow tumbling at the Larmor frequency (*black* curve). The overlap of the Larmor precessional frequency (vertical bar) with the molecular vibration spectrum indicates the likelihood of spin-lattice relaxation. With higher field strengths, the T1 relaxation becomes *longer* as the tumbling frequency spectrum overlap is decreased.

complex macromolecules are effective in decreasing T1 relaxation time of local tissues by creating a hydration layer that forms a spin-lattice energy sink and results in a rapid return to equilibrium.

Comparison of T1 and T2

T1 is on the order of 5 to 10 times longer than T2. Molecular motion, size, and interactions influence T1 and T2 relaxation (Fig. 12-20). Because most tissues of interest for clinical MR applications are intermediate to small-sized molecules, tissues

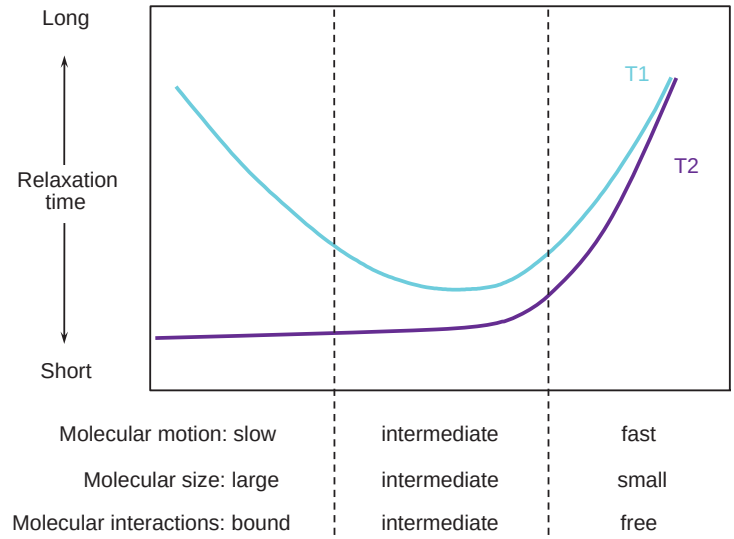

■ **FIGURE 12-20** Factors affecting T1 and T2 relaxation times of different tissues are generally based on molecular motion, size, and interactions that have an impact on the local magnetic field variations (T2 decay) and structure with intrinsic tumbling frequencies coupling to the Larmor frequency (T1 recovery). The relaxation times (vertical axis) are different for T1 and T2.

TABLE 12-4 T1 AND T2 RELAXATION CONSTANTS FOR SEVERAL TISSUES[a]

TISSUE	T1, 0.5 T (ms)	T1, 1.5 T (ms)	T2 (ms)
Fat	210	260	80
Liver	350	500	40
Muscle	550	870	45
White matter	500	780	90
Gray matter	650	900	100
Cerebrospinal fluid	1,800	2,400	160

[a]Estimates only, as reported values for T1 and T2 span a wide range.

with a longer T1 usually have a longer T2, and those with a shorter T1 usually have a shorter T2. In Table 12-4, a comparison of T1 and T2 values for various tissues is listed. Depending on the main magnetic field strength, measurement methods, and biological variation, these relaxation values vary widely. Agents that disrupt the local magnetic field environment, such as paramagnetic blood degradation products, elements with unpaired electron spins (e.g., gadolinium), or any ferromagnetic materials, cause a significant decrease in T2*. In situations where a macromolecule binds free water into a hydration layer, T1 is also significantly decreased.

To summarize, T1 > T2 > T2*, and the specific relaxation times are a characteristic of the tissues. T1 values are longer for higher field strength magnets, while T2 values are unaffected. Thus, the T1, T2, and T2* decay constants, as well as proton density are fundamental properties of tissues, and can be exploited by machine-dependent acquisition techniques in MRI and MRS to aid in the diagnosis of pathologic conditions such as cancer, multiple sclerosis, or hematoma.

12.4 Basic Acquisition Parameters

Emphasizing the differences of T1 and T2, relaxation time constants, and proton density of the tissues is the key to the exquisite contrast sensitivity of MR images, but at the same time, the need to spatially localize the tissues is also required. First, basic machine-based parameters are described.

Time of Repetition

Acquiring an MR image relies on the repetition of a sequence of events in order to sample the volume of interest and periodically build the complete dataset over time. The time of repetition (TR) is the period between B_1 excitation pulses. During the TR interval, T2 decay and T1 recovery occur in the tissues. TR values range from extremely short (millisecond) to extremely long (10,000 ms) time periods, determined by the type of sequence employed.

Time of Echo

Excitation of protons with the B_1 RF pulse creates the M_{xy} FID signal. To separate the RF energy deposition and returning signal, an "echo" is induced to appear at a later time, with the application of a 180-degree RF inversion pulse. This can also be achieved with a gradient field and subsequent polarity reversal. The time of echo (TE) is the time between the excitation pulse and the appearance of the peak amplitude of

an induced echo, which is determined by applying a 180-degree RF inversion pulse or gradient polarity reversal at a time equal to TE/2.

Time of Inversion

The TI is the time between an initial inversion/excitation (180 degrees) RF pulse that produces maximum tissue saturation, and a 90-degree readout pulse. During the TI, M_z recovery occurs. The readout pulse converts the recovered M_z into M_{xy}, which is then measured with the formation of an echo at time TE as discussed above.

Partial Saturation

Saturation is a state of tissue magnetization from equilibrium conditions. At equilibrium, the protons in a material are *unsaturated*, with full M_z amplitude. The first excitation (B_1) pulse in the sequence produces the largest transverse magnetization, and recovery of the longitudinal magnetization occurs at the T1 time constant over the TR interval. However, because the TR is less than at least five times the T1 of the sample, M_z recovery is incomplete. Consequently, less M_{xy} amplitude is generated in the second excitation pulse. After the third pulse, a "steady-state" equilibrium is reached, where the amount of M_z recovery and M_{xy} signal amplitude are constant, and the tissues achieve a state of *partial saturation* (Fig. 12-21). Tissues with short T1 have relatively less saturation than tissues with long T1. Partial saturation has an impact on tissue contrast, and explains certain findings such as unsaturated protons in blood outside of the volume moving into the volume and generating a bright vascular signal on entry slices into the volume.

12.5 Basic Pulse Sequences

Three major pulse sequences perform the bulk of data acquisition (DAQ) for imaging: spin echo (SE), inversion recovery (IR), and gradient echo (GE). When used in conjunction with spatial localization methods, "contrast-weighted" images are obtained. In the following sections, the salient points and considerations of generating tissue contrast are discussed.

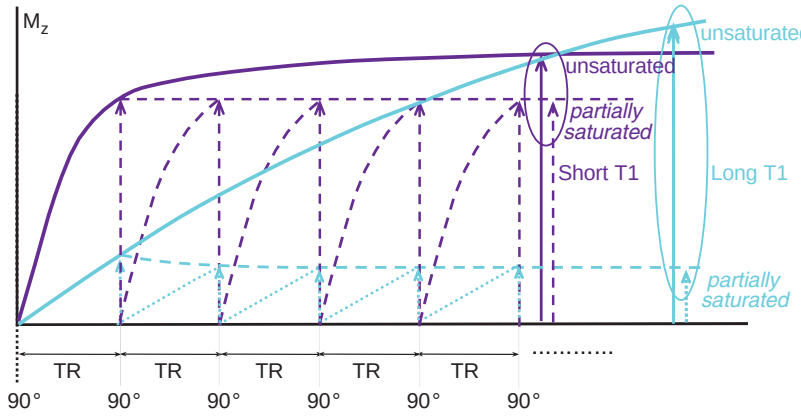

■ **FIGURE 12-21** Partial saturation of tissues occurs because the repetition time between excitation pulses does not allow for full return to equilibrium, and the M_z amplitude for the next RF pulse is reduced. After the third excitation pulse, a steady-state equilibrium is reached, where the amount of longitudinal magnetization is the same from pulse to pulse, as is the transverse magnetization for a tissue with a specific T1 decay constant. Tissues with long T1 experience a greater partial saturation than do tissues with short T1 as shown above. Partial saturation is important in understanding contrast mechanisms and signal from unsaturated and saturated tissues.

Spin Echo

SE describes the excitation of the magnetized protons in a sample with a 90-degree RF pulse and production of a FID, followed by a refocusing 180-degree RF pulse to produce an echo. The 90-degree pulse converts M_z into M_{xy}, and creates the largest phase coherent transverse magnetization that immediately begins to decay at a rate described by T2* relaxation. The 180-degree RF pulse, applied at TE/2, inverts the spin system and induces phase coherence at TE, as depicted in the rotating frame in Figure 12-22. Inversion of the spin system causes the protons to experience external magnetic field variations opposite of that prior to TE/2, resulting in the cancellation of the extrinsic inhomogeneities and associated dephasing effects. In the rotating frame of reference, the echo magnetization vector reforms in the opposite direction from the initial transverse magnetization vector.

Subsequent 180-degree RF pulses during the TR interval (Fig. 12-23) produce corresponding echoes with peak amplitudes that are reduced by intrinsic T2 decay of the tissues, and are immune from extrinsic inhomogeneities. Digital sampling and acquisition of the signal occurs in a time window symmetric about TE, during the evolution and decay of each echo.

Spin Echo Contrast Weighting

Contrast is proportional to the difference in signal intensity between adjacent pixels in an image, corresponding to different voxels in the patient. The details of signal localization and image acquisition in MRI are discussed in Section 12.6. Here, the signal intensity variations for different tissues based upon TR and TE settings are described without consideration of spatial localization.

Ignoring the signal due to moving protons (e.g., blood flow), the signal intensity produced by an MR system for a specific tissue using a SE sequence is

$$S \propto r_H \left[1 - e^{TR/T1}\right] e^{-TE/T2}$$

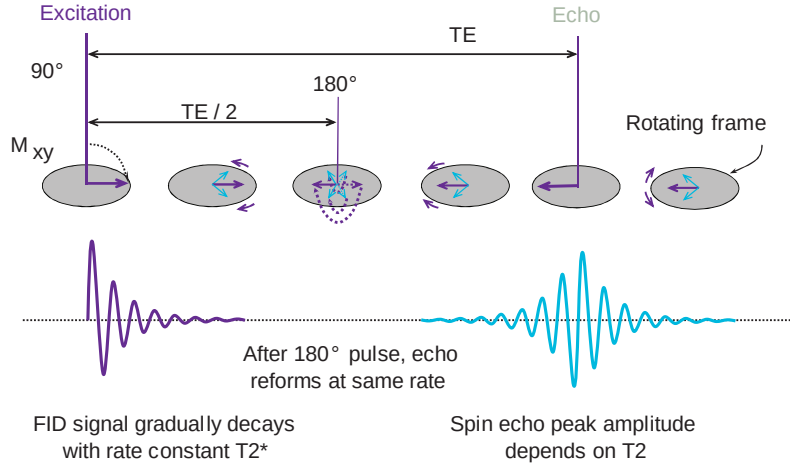

■ **FIGURE 12-22** The SE pulse sequence starts with a 90-degree pulse and produces an FID that decays according to T2* relaxation. After a delay time TE/2, a 180-degree RF pulse inverts the spins that re-establishes phase coherence and produces an echo at a time TE. Inhomogeneities of external magnetic fields are canceled, and the peak amplitude of the echo is determined by T2 decay. The rotating frame shows the evolution of the echo vector in the opposite direction of the FID. The sequence is repeated for each repetition period, TR.

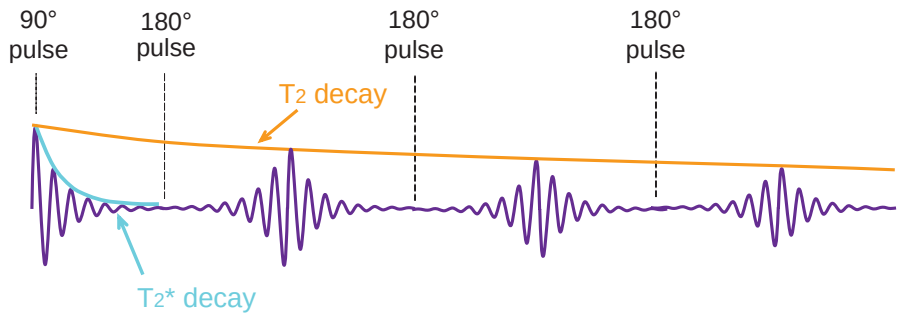

■ **FIGURE 12-23** "True" T2 decay is determined from multiple 180-degree refocusing pulses acquired during the repetition period. While the FID envelope decays with the T2* decay constant, the peak amplitudes of subsequent echoes decay exponentially according to the T2 decay constant, as extrinsic magnetic field inhomogeneities are cancelled.

where ρ_H is the proton density, *T1* and *T2* are physical properties of tissue, and *TR* and *TE* are pulse sequence timing parameters. For the same pulse sequence, different values of T1, T2, and ρ_H change the signal intensity S, and generate contrast amongst different tissues. Importantly, by changing the pulse sequence parameters TR and TE, the contrast dependence can be weighted toward T1, proton density, or T2 characteristics of the tissues.

T1 Weighting

A "T1-weighted" SE sequence is designed to produce contrast chiefly based on the T1 characteristics of tissues, with de-emphasis of T2 and proton density contributions to the signal. This is achieved by using a relatively short TR to maximize the differences in longitudinal magnetization recovery during the return to equilibrium, and a short TE to minimize T2 decay during signal acquisition. In Figure 12-24, on the left is the graph of longitudinal recovery in steady-state partial saturation after a 90-degree RF excitation at time t = 0, depicting four tissues (CSF, gray matter, white matter, and fat). The next 90-degree RF pulse occurs at the selected TR interval, chosen to create the largest signal difference between the tissues based upon their respective T1 recovery values, which is shown to be about 600 ms (the red vertical line). At this instant in time, all M_z recovered for each tissue is converted to M_{xy}, with respective signal amplitudes projected over to the transverse magnetization graph on the right. Decay immediately occurs, t = 0, at a rate based upon respective T2 values of the tissues. To minimize T2 decay and to maintain the differences in signal amplitude due to T1 recovery, the TE time is kept short (red vertical line). Horizontal projections from the TE intersection with each of the curves graphically illustrate the relative signal amplitudes acquired according to tissue type. Fat, with a short T1, has a large signal, because there is greater recovery of the M_z vector over the TR period. White and gray matter have intermediate T1 values with intermediate signal amplitude, and CSF, with a long T1, has the lowest signal amplitude. A short TE preserves the T1 signal differences by not allowing any significant transverse (T2) decay.

T1-weighted SE contrast therefore requires a short TR and a short TE. A T1-weighted axial image of the brain acquired with TR = 500 ms and TE = 8 ms is illustrated in Figure 12-25. Fat is the most intense signal, followed by white matter, gray matter, and CSF. Typical SE T1-weighting machine parameters are TR = 400 to 600 ms and TE = 3 to 10 ms.

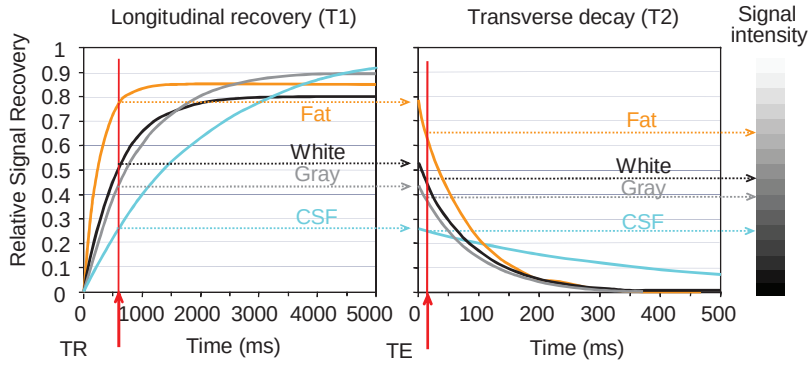

■ **FIGURE 12-24** T1-weighted contrast: Longitudinal recovery (**left**) and transverse decay (**right**) diagrams (note the values of the x-axis time scales) show four brain tissues and T1 and T2 relaxation constants. T1-weighted contrast requires the selection of a TR that emphasizes the differences in the T1 characteristics of the tissues (e.g., TR = ~ 500 *ms*), and reduces the T2 characteristics by using a short TE so that transverse decay is reduced (e.g., TE ≤ 15 *ms*).

Proton Density Weighting

Proton density contrast weighting relies mainly on differences in the number of magnetized protons per unit volume of tissue. At equilibrium, tissues with a large proton density, such as lipids, fats, and CSF, have a corresponding large M_z compared to other soft tissues. Contrast based on proton density differences is achieved by reducing the contributions of T1 recovery and T2 decay. T1 differences are reduced by selecting a long TR value to allow substantial recovery of M_z. T2 differences of the tissues are reduced by selecting a short TE value. Longitudinal recovery and transverse decay graphs for proton density weighting, using a long TR and a short TE, are illustrated in Figure 12-26. Contrast is generated from variations in proton density (CSF > fat > gray matter > white matter). Figure 12-27 shows a proton

■ **FIGURE 12-25** T1 contrast weighting, TR=500 ms, TE=8 ms. Short TR (400 to 600 ms) generates T1 relaxation-dependent signals. Signals with short T1 have high signal intensity (fat and white matter), while signals with long T1 have low signal intensity (CSF). Short TE (less than 15 ms) preserves the T1 tissue differences by not allowing significant T2 decay to occur.

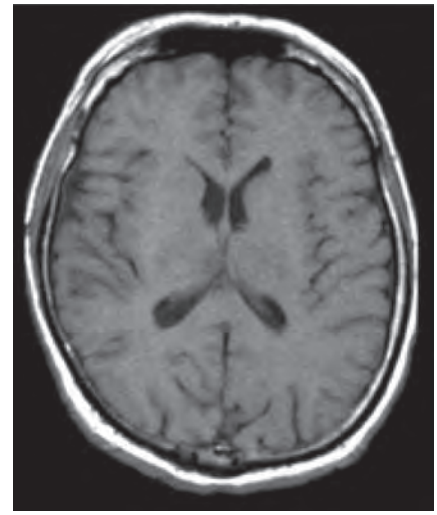

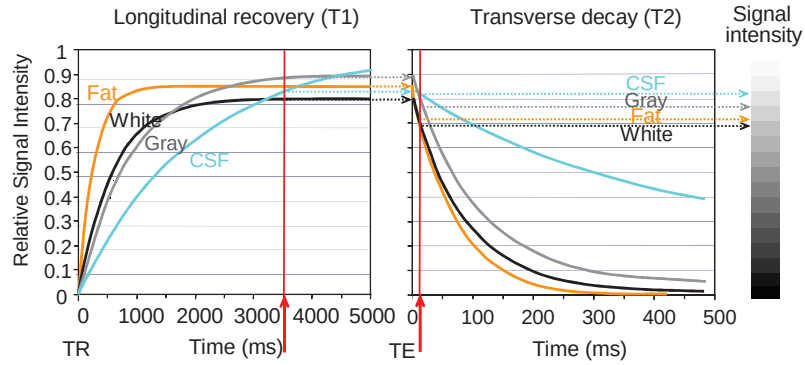

■ **FIGURE 12-26** Proton density weighting: Proton (spin) density weighted contrast requires the use of a long TR (e.g., greater than 2,000 *ms*) to reduce T1 effects, and a short TE (e.g., less than 35 *ms*) to reduce T2 influence in the acquired signals. Note that the average overall signal intensity is higher.

density-weighted image with TR = 2,400 ms and TE = 30 ms. Fat and CSF display as a relatively bright signal, and a slight contrast inversion between white and gray matter occurs. A typical proton density-weighted image has a TR between 2,000 and 4,000 ms (see footnote in Table 12.5) and a TE between 3 and 30 ms. The proton density SE sequence achieves the highest overall signal intensity and the largest signal-to-noise ratio (SNR); however, the image contrast is relatively low, and therefore the contrast-to-noise ratio is not necessarily larger than achievable with T1 or T2 contrast weighting.

T2 Weighting

T2 contrast weighting follows directly from the proton density-weighting sequence: reduce T1 differences in tissues with a long TR, and emphasize T2 differences with a *long* TE. The T2-weighted signal is generated from the second echo produced by a

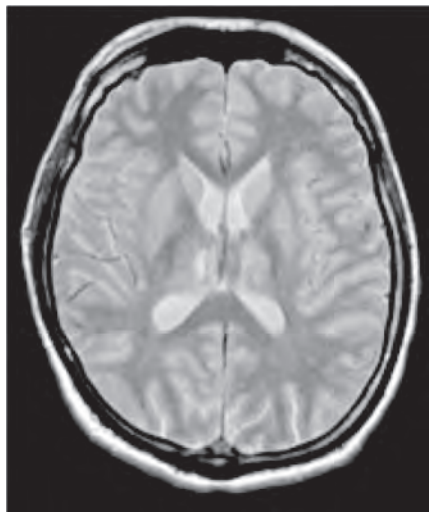

■ **FIGURE 12-27** Proton density contrast weighting, TR=2400 ms, TE=30 ms.. Long TR minimizes T1 relaxation differences of the tissues. Signals with large proton density have higher signal intensity (CSF). Short TE preserves the proton density differences without allowing significant T2 decay. This sequence produces a high peak SNR, even though the contrast differences are less than a T2-weighted image.

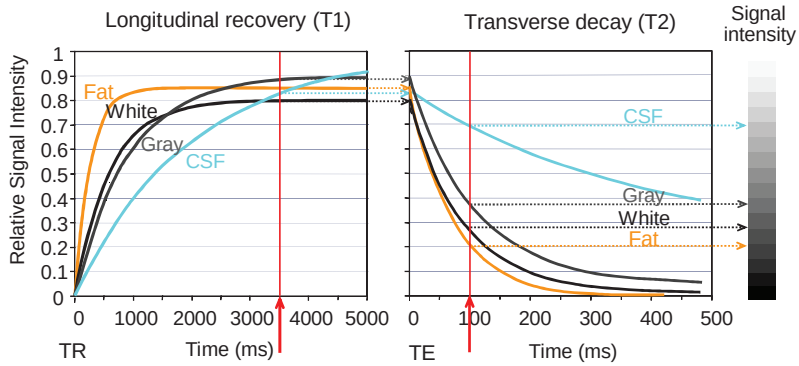

FIGURE 12-28 T2 weighted contrast requires the use of a long TR (e.g., greater than 2,000 ms) to reduce T1 influences, and a long TE (e.g., greater than 80 ms) to allow for T2 decay to evolve. Compared to the proton density weighting, the difference is with longer TE.

second 180-degree pulse of a long TR spin echo pulse sequence, where the first echo is proton density weighted, with short TE. T2 contrast differences are manifested by allowing M_{xy} signal decay as shown in Figure 12-28. Compared with a T1-weighted image, inversion of tissue contrast occurs in the image where CSF is bright, and gray and white matter are reversed in intensity.

A T2-weighted image (Fig. 12-29) demonstrates high tissue contrast, compared with either the T1-weighted or proton density-weighted images. As TE is increased, more T2-weighted contrast is achieved, but at the expense of less M_{xy} signal and greater image noise. However, even with low signal amplitudes, image processing with *window width* and *window level* adjustments can remap the signals over the full range of the display, so that the overall average brightness is similar for all images. The typical T2-weighted sequence uses a TR of approximately 2,000 to 4,000 ms and a TE of 80 to 120 ms.

FIGURE 12-29 T2 contrast weighting. Long TR minimizes T1 relaxation differences of the tissues. Long TE allows T2 decay differences to be manifested. A second echo provides time for T2 decay to occur, so a T2 W image is typically acquired in concert with a PD W image. While this sequence has high contrast, the signal decay reduces the overall signal and therefore the SNR.

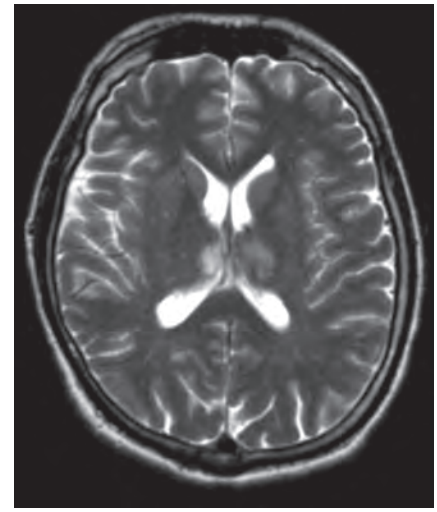

TABLE 12-5 SE PULSE SEQUENCE CONTRAST WEIGHTING PARAMETERS

PARAMETER	T1 CONTRAST	PROTON DENSITY CONTRAST[a]	T2 CONTRAST
TR (ms)	400–600	2,000–4,000	2,000–4,000
TE (ms)	5–30	5–30	60–150

[a]Strictly speaking, SE images with TR less than 3,000 ms are not proton density with respect to the CSF; because of its long T1, only 70% of the CSF magnetization recovery will have occurred and will not appear as bright as for a true PD image. True PD image intensities can be obtained with fast spin echo methods (Chapter 13) with longer TR (e.g., 8,000 ms).
TE, time of echo; TR, time of repetition.

Spin Echo Parameters

Table 12-5 lists typical contrast-weighting values of TR and TE for SE imaging. For conventional SE sequences, both proton density and T2-weighted contrast signals are acquired during each TR by acquiring two echoes with a short TE and a long TE (Fig. 12-30).

Inversion Recovery

IR emphasizes T1 relaxation times of the tissues by extending the amplitude of the longitudinal recovery by a factor of two. An initial 180-degree RF pulse inverts M_z to $-M_z$. After a programmed delay, the time of inversion—TI, a 90-degree RF (readout) pulse rotates the recovered fraction of M_z into the transverse plane to generate the FID. A second 180-degree pulse (or gradient polarity reversal, see next section, GE) at TE/2 produces an echo at TE (Fig. 12-31); in this situation, the sequence is called *inversion recovery spin echo* (IR SE). The TR for IR is the time between 180-degree initiation pulses. Partial saturation of the protons and steady-state equilibrium of the longitudinal magnetization is achieved after the first three excitations in the sequence. The echo amplitude associated with a given tissue depends on TI, TE, TR, and magnitude (positive or negative) of M_z.

The signal intensity at a location (x,y) in the image matrix for an IR SE acquisition with nonmoving anatomy is approximated as

$$S \propto \rho_H (1 - 2e^{-TI/T1}) (1 - e^{-(TR-TI)/T1}) (e^{-TE/T2})$$

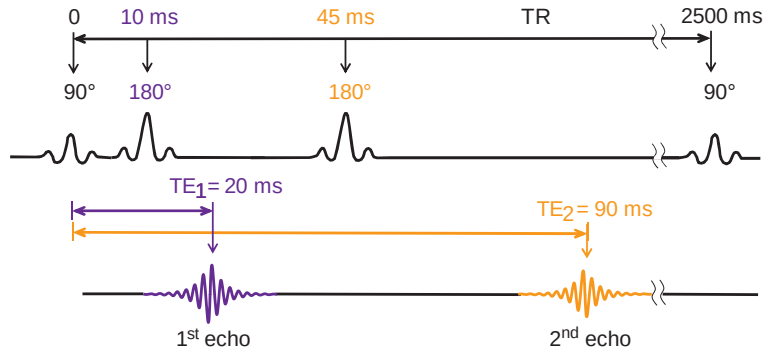

■ **FIGURE 12-30** SE with two 180-degree refocusing pulses after the initial 90-degree excitation pulse. The early echo contains information related to proton density of the tissues, and the longer echo provides T2 weighting. This double echo method is used for providing proton density content and T2 weighted content independently during the same TR interval, and used to fill two separate k-space repositories that are used in producing the final proton density and T2 weighted images.

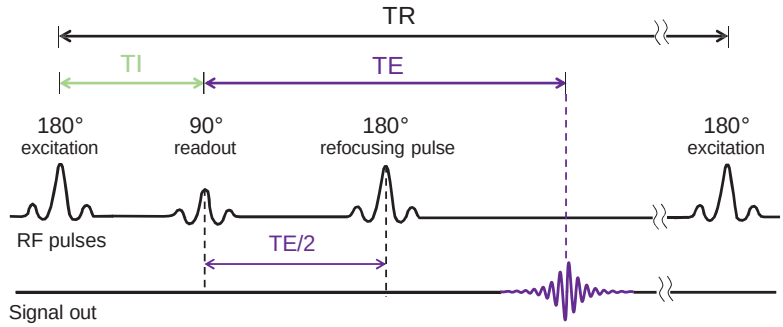

■ **FIGURE 12-31** Inversion-recovery SE sequence is shown. The initial 180-degree excitation pulse inverts the longitudinal magnetization, and thus requires a factor of two times recovery of the longitudinal magnetization over time. The "inversion time" (TI) is the delay between the excitation pulse and conversion to transverse magnetization of the recovered longitudinal magnetization. Subsequently, a second 180-degree pulse is applied at TE/2, which refocuses the transverse magnetization as an echo at time TE. The signal strength is chiefly a function of the T1 characteristics of the tissues, as the TE values are kept short.

where the factor of 2 in the first part of the equation arises from the longitudinal magnetization recovery from $-M_z$ to M_z, and all other parameters are as previously described. For the TI to control contrast between tissues, it follows that TR must be relatively long and TE short. The RF sequence is shown in Figure 12-31.

The IR sequence produces "negative" longitudinal magnetization that results in negative (in phase) or positive (out of phase) transverse magnetization when short TI is used. The actual signals are acquired as magnitude (absolute values) such that M_z values are positive.

Short Tau Inversion Recovery

Short Tau Inversion Recovery, or STIR, is a pulse sequence that uses a very short TI and magnitude signal processing, where M_z signal amplitude is always positive (Fig. 12-32).

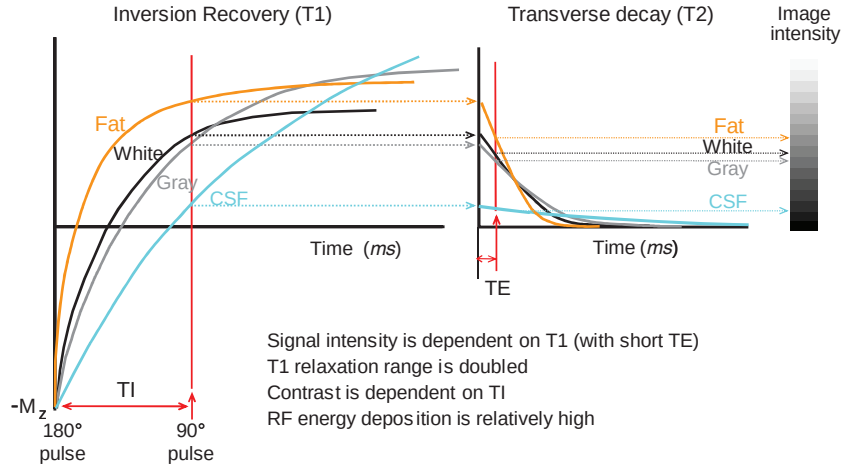

■ **FIGURE 12-32** The IR longitudinal recovery diagram shows the 2 × M_z range provided by the 180-degree excitation pulse. A 90-degree readout pulse at a time TI and a 180-degree refocusing pulse at a time TE/2 from the readout pulse forms the echo at time TE. The time scale is not explicitly indicated on the x-axis. A short TE is used to reduce T2 contrast characteristics.

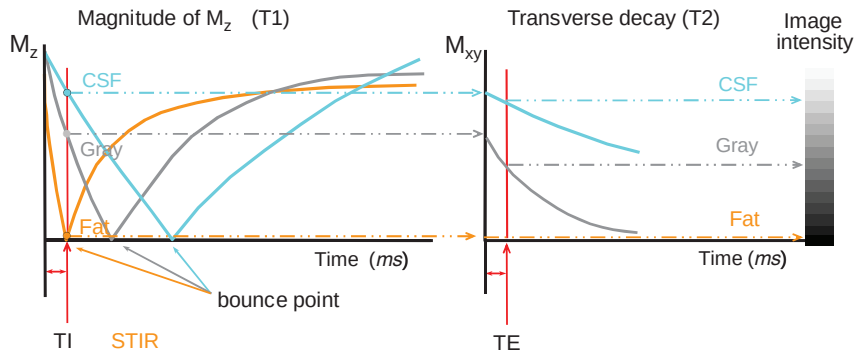

■ **FIGURE 12-33** IR longitudinal magnetization as a function of time, with magnitude signal processing. All tissues go through a null (the bounce point) at a time dependent on T1. The inversion time (TI) is adjusted to select a time to null a certain tissue type. Shown above is the STIR (Short Tau IR) used for suppressing the signal due to fat tissues, achieved with TI = approximately 150 ms (0.693 × 260 ms).

In this situation, materials with short T1 have a lower signal intensity (the reverse of a standard T1-weighted image), and all tissues at some point during recovery have $M_z = 0$. This is known as the *bounce point* or tissue null. Selection of an appropriate TI can thus suppress tissue signals (e.g., fats/lipids, CSF) depending on their T1 relaxation times. The signal null ($M_z = 0$) occurs at TI = $ln(2) \times T1$, where *ln* is the natural log and $ln(2) = 0.693$. Since T1 for fat at 1.5T is approximately 260 ms, TI is selected as 0.693 × 260 ms = 180 ms. A typical STIR sequence uses TI of 140 to 180 ms and TR of approximately 2,500 ms. Compared with a T1-weighted examination, STIR reduces distracting fat signals (Fig. 12-33) and chemical shift artifacts (explained in Chapter 13) (Fig. 12-34).

Fluid Attenuated Inversion Recovery

The signal levels of CSF and other tissues with long T1 relaxation constants can be overwhelming in the magnitude IR image. Fluid attenuated IR, the *FLAIR* sequence,

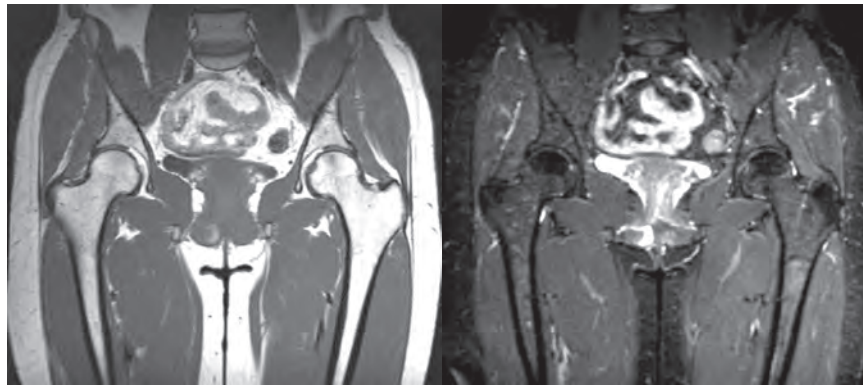

T1 STIR

■ **FIGURE 12-34** SE T1-weighting versus STIR technique. **Left**. T1 W with TR = 750 ms, TE = 13 ms. **Right**. STIR with TR = 5,520 ms, TI = 150 ms, TE = 8 ms. The fat is uniformly suppressed in the STIR image, providing details of nonfat structures otherwise difficult to discern.

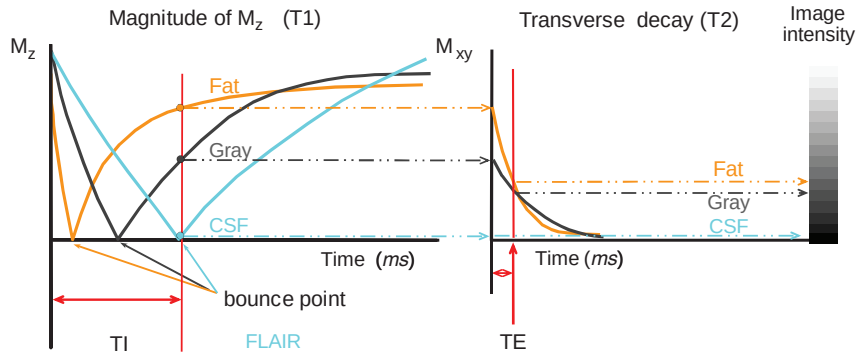

■ **FIGURE 12-35** Shown above is the FLAIR acquisition, with the TI set to the null of CSF, which reduces the large CSF signals and allows the visualization of subtle details otherwise hidden. TE is short to not allow T2 "contamination" of the signals.

reduces CSF signal and other water-bound anatomy in the MR image by using a TI selected at or near the bounce point of CSF to permit better evaluation of the surrounding anatomy as shown in Figure 12-35. Reducing the CSF signal (T1 ≈ 2,500 ms @ 1.5 T) requires TI = 0.693 × 2,500 ms, or ≈ 1,700 ms. A comparison of T1, T2, and FLAIR sequences demonstrates the contrast differences achievable by reducing signals of one tissue to be able to visualize another (see Fig. 12-36).

Summary, Spin Echo Sequences

MR contrast schemes for clinical imaging use the SE or an IR variant of the SE pulse sequences for many examinations. SE and IR SE sequences are less sensitive to magnetic field inhomogeneities, magnetic susceptibilities, and generally give high SNR and CNR. The downsides are the relatively long TR and corresponding long acquisition times.

Gradient Echo

The *GE* technique uses a magnetic field gradient applied in one direction and then reversed to induce the formation of an echo, instead of the 180-degree

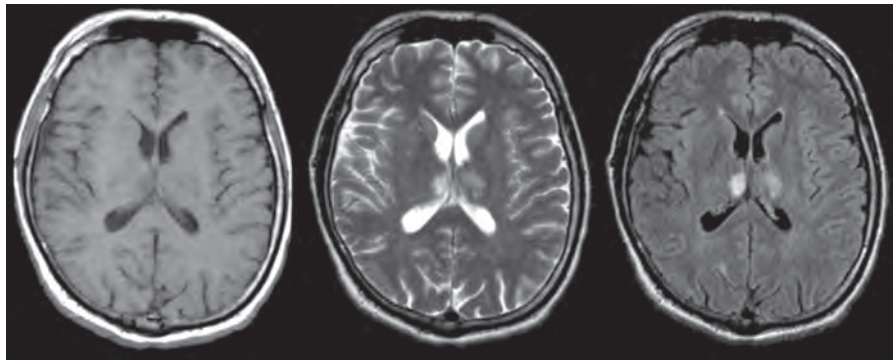

T1 T2 FLAIR

■ **FIGURE 12-36** **Left.** T1-weighted spin-echo axial brain image (TR = 549 ms, TE = 11 ms); Middle: T2 weighted spin-echo image (TR = 2,400 ms, TE = 90 ms); **Right.** FLAIR image (TR = 10,000 ms, TI = 2,400 ms, TE = 150 ms).

inversion pulse. For a FID signal generated under a linear gradient, the transverse magnetization dephases rapidly as the gradient is applied. After a predetermined time, the nearly instantaneous reversal of the GE polarity will rephase the protons and produce a *GE* that occurs when the opposite gradient polarity of equal strength has been applied for the same time as the initial gradient. The induced GE signal is acquired just before and after the peak amplitude, as illustrated in Figure 12-37.

The GE is not a true SE but a purposeful dephasing and rephasing of the FID. Magnetic field (B_0) inhomogeneities and tissue susceptibilities caused by paramagnetic or diamagnetic tissues or contrast agents are emphasized in GE imaging. This is because the dephasing and rephasing of the FID signals occur in the same direction relative to the main magnetic field. In this situation, unlike a 180-degree refocusing RF pulse, the external magnetic field variations are not cancelled. Compare Figures 12-22 and 12-37 and the direction of the M_{xy} vector in the rotating frame. For SE techniques, the FID and echo vectors form in opposite directions, whereas with GE, the FID and echo form in the same direction. Significant sensitivity to field nonuniformity and magnetic susceptibility agents thus occurs, as M_{xy} decay is a strong function of T2*, which is much shorter than the "true" T2 achieved in SE sequences. Timing of the gradient echo is controlled either by inserting a time delay between the negative and positive gradients or by reducing the amplitude of the reversed gradient, thereby extending the time for the rephasing process to occur.

A major variable determining tissue contrast in GE sequences is the flip angle. Depending on the desired image contrast, flip angles of a few degrees to more than 90 degrees are used, a majority of which are small angles much less than 60 degrees. In the realm of very short TR, smaller flip angles require less time and create more transverse magnetization compared to larger flip angles. A plot of M_{xy} signal amplitude versus TR as a function of flip angle (Fig. 12-38) shows that smaller flip angles produce more M_{xy} signal than larger flip angles when TR is less than 200 ms.

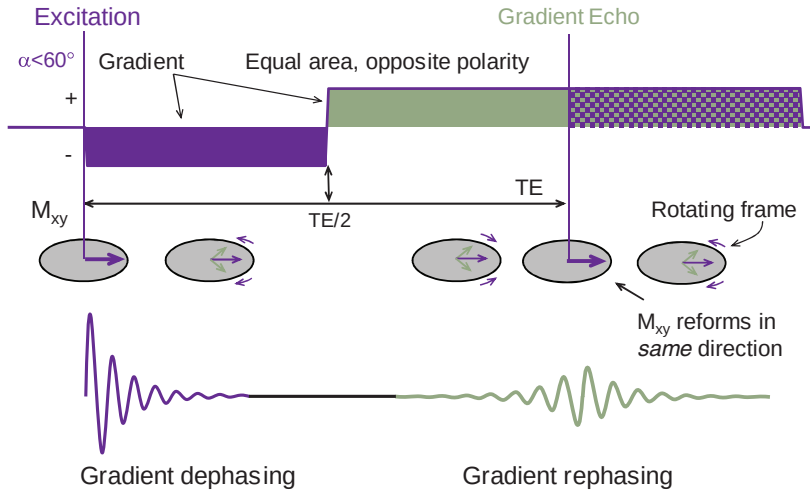

■ **FIGURE 12-37** A magnetic field gradient induces the formation of an "echo" (instead of a 180-degree RF pulse). Transverse magnetization spins are dephased with an applied gradient of one polarity and rephased with the gradient reversed in polarity; this produces a "gradient echo." Note that the rotating frame depicts the magnetic moment vector of the echo in the *same direction* as the FID relative to the main magnetic field, and therefore extrinsic inhomogeneities are not cancelled.

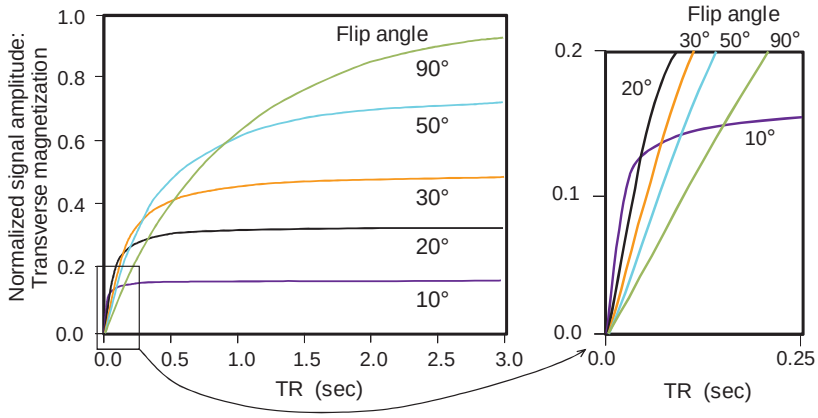

■ **FIGURE 12-38** Transverse magnetization as a function of TR and the flip angle is shown. For small flip angles and very short TR, the transverse magnetization is higher for small flip angles compared to larger flip angles. Detail is shown on the right.

Ultimately, tissue contrast in GE pulse sequences depends on TR, TE, and flip angle along with specialized manipulation of the acquisition sequence.

Gradient Echo Sequences with Long TR

For GE sequences with "long" TR (greater than 200 ms) and flip angles greater than 45 degrees, contrast behavior is similar to that of SE sequences. The major difference is image contrast that is based on T2* rather than T2, because external magnetic field inhomogeneities are not cancelled. As for clinical interpretation, the mechanisms of contrast based on T2* are different from those based on T2, particularly for MRI contrast agents. A relatively long TE tends to emphasize the differences between T2* and T2, rather than improve T2 contrast, as would be expected in an SE sequence. T1 weighting is achieved with a short TE (5 to 10 ms). In most situations, however, GE imaging is not useful with long TR, except when contrast produced by magnetic susceptibility differences is desired.

Gradient Echo Sequences with short TR, less than 50 ms

Reducing the repetition period below 50 ms does not allow for transverse decay (T2*) to fully occur, and a steady-state equilibrium of longitudinal and transverse magnetization from pulse to pulse exists. The persistent transverse magnetization is produced from previous RF excitations, and multiple signals are generated: (1) the FID signal generated at the end of the current RF pulse, and once rephased, contains T2* or T1 information depending on the TE; (2) a stimulated echo generated from the previous RF pulse acting on the persistent transverse magnetization accruing from the RF pulse twice displaced. The stimulated echo contains T2 and T2* weighting. This is schematically shown in Figure 12-39 for a train of RF pulses and the generated signals.

Given the nature of the overlapping signals, there are generic GE acquisitions termed coherent, incoherent, and steady-state free precession (SSFP) that provide differential tissue contrast weighting.

Coherent GE

The coherent GE sequence is shown in Figure 12-40, indicating the timing of the RF pulse with the dephasing and rephasing implemented by reversal of gradient

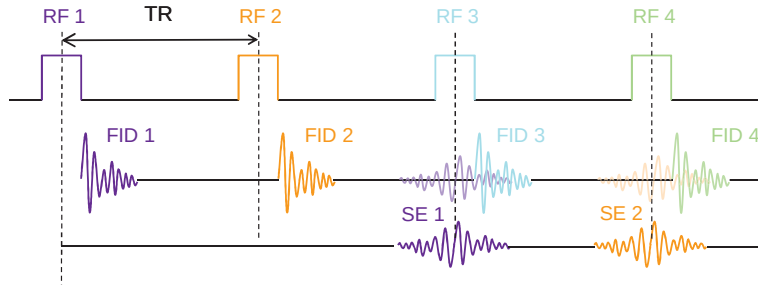

■ **FIGURE 12-39** GE acquisition with short TR less than 50 ms and flip angles upto 45 degrees produces two signals: (1) the FID from the current RF pulse and (2) stimulated echo from the previous RF pulse resulting from persistent transverse magnetization. These signals overlap, but are shown distinct in the illustration for clarity. Resultant image contrast is due to the ratio of T1 to T2 in a tissue because of the mixed signals generated by the combined FID (chiefly T1 and T2* contrast) and SE (chiefly T2 and T2* contrast) in the digitized signal. With the train of RF excitation pulses, RF pulse 2 stimulates the echo formation of the FID produced from RF pulse 1, which appears during RF pulse 3 and superimposes on the current (RF pulse 3) FID. While this is a conceptual illustration, in fact, the actual situation is much more complicated, as there are many higher order stimulated and gradient echoes that contribute to the observed signal.

polarity to generate an echo at a selectable time TE for the frequency encode gradient (FEG), where identification of proton position based upon frequency is performed. (Note: the various encoding gradients used to localize the protons are discussed in the next section of this chapter.) Also involved in this sequence is the phase encode gradient (PEG), which is applied and incrementally changed for each TR to identify proton position in the direction perpendicular to the FEG based upon phase changes of the protons after the PEG is turned off. A "rewinder PEG" of the same strength but opposite polarity is applied after the echo to realign the phase prior to the next RF pulse. The combined FID and simulated echo signals are generated during the GE, and produce tissue contrast dependent on flip angle, TR, and TE. With moderate flip angles of 30 to 60 degrees, the differences in tissue contrast are primarily based upon T2/T1 ratios. Since most tissues with a long

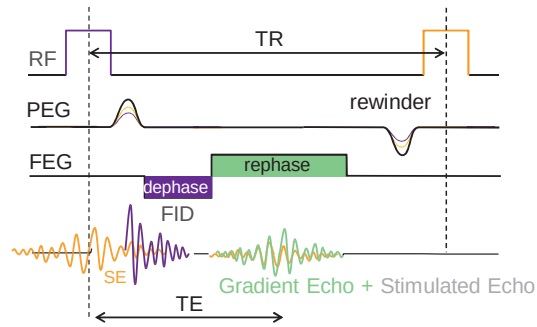

■ **FIGURE 12-40** Coherent GE: Multiple gradients are used for localizing the protons, including the PEG and the FEG. In addition to localizing protons, these gradients are intrinsic to the manipulation of the signals in the coherent GE acquisition. As shown above, the PEG is applied after the RF pulse but prior to the FEG, to determine location in one direction by adding a known phase to the protons based on location per TR interval. Subsequently, a rewinder gradient of the same strength but opposite polarity resets the phase prior to the next TR excitation. The FEG is the gradient that generates the echo from the FID plus the stimulated echo from the previous RF pulse.

TABLE 12-6 GRADIENT RECALLED ECHO WEIGHTING (STEADY-STATE)

PARAMETER	T1	T2/T1	T2	T2*	PROTON DENSITY
Flip angle (degrees)	45–90	30–50	5–15	5–15	5–30
TR (ms)	200–400	10–50	200–400	100–300	100–300
TE (ms)	3–15	3–15	30–50	10–20	5–15

T2 also have a long T1 and vice versa, there is very little tissue contrast generated. In certain applications such as MR angiography, this is a good outcome, so that anatomical contrast differences that would otherwise compete with the bright blood when displayed by image processing techniques (described in Chapter 13) would reduce the image quality.

This acquisition technique is described by the acronyms GRASS (*g*radient *r*ecalled *a*cquisition in the *s*teady *s*tate), FISP (*f*ast *i*maging with *s*teady-state *p*recession), FAST (*F*ourier *a*cquired *s*teady *s*tate), and other acronyms coined by MRI equipment manufacturers. Table 12-6 indicates typical parameter values for contrast desired in steady-state and GE acquisitions. The steady-state sequences with coherent echoes produce T2* and proton density contrast. A GRASS/FISP sequence using TR = 35 ms, TE = 3 ms, and flip angle = 20 degrees shows unremarkable contrast, but blood flow shows up as a bright signal (Fig. 12-41). This technique enhances vascular contrast, from which MR angiography sequences can be reconstructed.

Incoherent, "Spoiled" Gradient Echo Techniques

With very short TR steady-state acquisitions, T1 weighting *cannot* be achieved to any great extent, owing to either a small difference in longitudinal magnetization with small flip angles or dominance of the T2* effects for larger flip angles produced

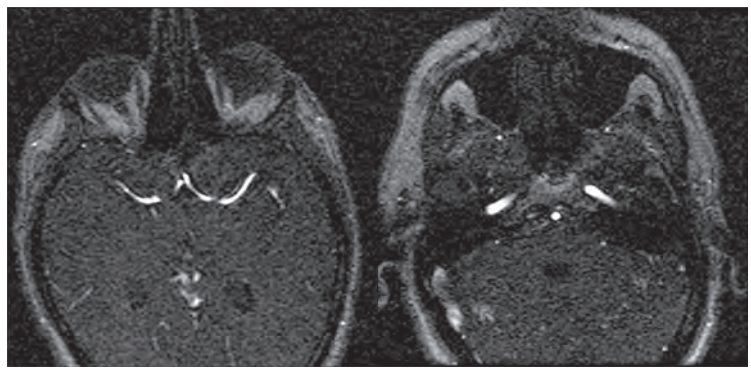

TR=35 *ms*, TE=3 *ms*, flip angle=20

■ **FIGURE 12-41** A *steady-state* gradient recalled echo (GRASS) sequence (TR = 24 *ms*, TE = 4.7 *ms*, flip angle = 50 degrees) of two slices out of a volume acquisition is shown. Contrast is unremarkable for white and gray matter because of a T2-/T1-weighting dependence. Blood flow appears as a relatively bright signal. MR angiography (see Chapter 13) depends on pulse sequences such as these to reduce the contrast of the anatomy relative to the vasculature.

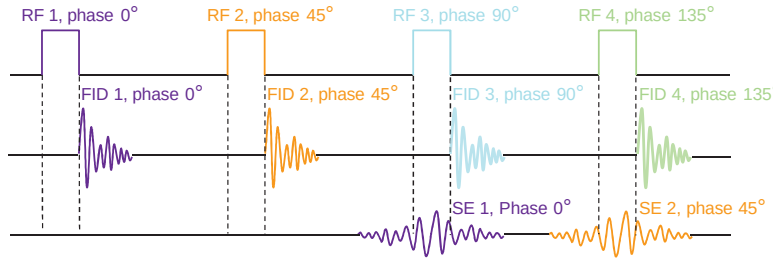

■ **FIGURE 12-42** Incoherent (spoiled) GE acquisition: Persistent transverse magnetization is dephased by each RF pulse; the superposition of the FID from the current RF pulse with a stimulated-echo from the previous RF pulse is separable, because of differences in the phase of the generated signals. In an actual sequence with TR of 5 to 6 ms, several of stimulated echoes will contribute to the signal, along with the FID. Particular angles of phase increment (typically 117 or 123 degrees) have been determined empirically to cause cancellation by destructive interference of the magnetization from the different coherence pathways to eliminate the signal, leaving only the signal from the FID. T1 contrast can be preferentially generated without contamination of the signals due to the T2 characteristics of the tissues.

by persistent residual transverse magnetization created by stimulated echoes. The T2* influence can be reduced by using a long TR (usually not an option), or by "spoiling" the steady-state transverse magnetization by introducing incoherent phase differences from pulse to pulse. The latter is achieved by adding a phase shift to successive RF pulses during the excitation of protons. Both the RF transmitter and RF receiver are phase locked, so that the receiver discriminates the phase of the GE from the SE generated by the previous RF pulse, now out of phase, as shown in Figure 12-42. Mostly, T1-weighted contrast is obtained, with short TR, short TE, and moderate to large flip angle. Spoiled transverse magnetization gradient recalled echo (SPGR) is often used in three-dimensional volume acquisitions because of the extremely short acquisition time allowed by the short TR of the GE sequence and the good contrast rendition of the anatomy provided by T1 weighting (Fig. 12-43).

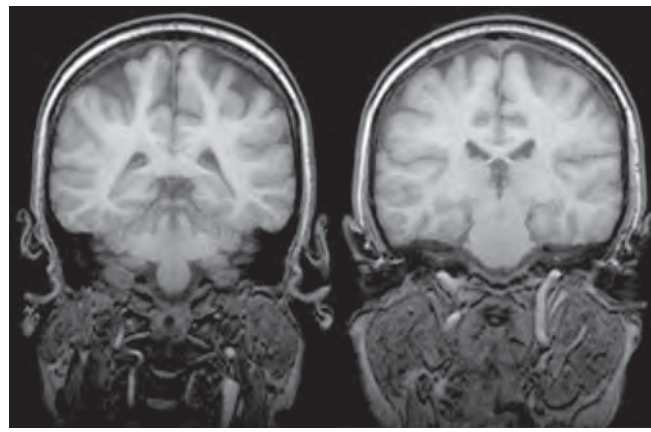

TR=8 *ms*, TE=1.9 *ms*, flip angle=20°
Note T1 contrast and high blood vessel signal

■ **FIGURE 12-43** Incoherent (spoiled) GE images. The ability to achieve T1 contrast weighting is extremely useful for rapid three-dimensional volume imaging. Bright blood (lower portion of each image) and magnetic susceptibility artifacts are characteristic of this sequence. TR = 8 *ms*, TE = 1.9 *ms*, flip angle = 20 degrees.

MR contrast agents (e.g., gadolinium) produce greater contrast with T1-weighted SPGR than with a comparable T1-weighted SE sequence because of the greater sensitivity to magnetic susceptibility. The downsides of spoiled GE techniques are the increased sensitivity to other artifacts such as chemical shift and magnetic field inhomogeneities, as well as lower SNR.

Steady-State Free Precession

In GE sequences with short TR (less than 50 ms), the TE is not long enough to generate any T2 contrast, and GE rephasing is inefficient and dominated by T2* effects. The SSFP sequence emphasizes acquisition of only the stimulated echo, which arises from the previous RF pulse and appears during the next RF pulse at a time equal to 2 × TR (see Fig. 12-39). To reposition the stimulated echo to an earlier time in the TR interval for signal acquisition, a rewinder gradient is applied, which speeds up the rephasing process initiated by the RF pulse, so that it reforms and decays just before the next RF pulse. In the SSFP sequence, there are two TE values: one is the *actual TE*, the time between the peak stimulated echo amplitude and the *next* excitation pulse, and the other is the *effective TE*, the time from the echo and the RF pulse that created its FID. The effective TE is thus longer than the TR and is calculated as: effective TE = 2 × TR-actual TE. So for TR = 50 ms and TE = 5 ms, the effective TE is 95 ms, which means that the stimulated echo has had 95 ms to manifest T2 weighting. SSFP sequences provide true T2 contrast weighting, are useful for brain and joint imaging, and can be used with three-dimensional volumetric acquisitions (as discussed in Chapter 13) (Figs. 12-44 and 12-45). "Balanced" SSFP sequences generate accumulated gradient echo (FID) and stimulated echo signals with the use of symmetrical gradients in 3 spatial directions, which null phase shifts induced by flow. Balanced SSFP provides T2/T1 contrast and high speed acquisitions, particularly useful for cardiac imaging (Chavan, et.al., 2008).

Summary, Gradient Echo contrast

For GE acquisition in the realm of short TR, persistent transverse magnetization produces two signals: (1) the FID produced from the RF pulse just applied and

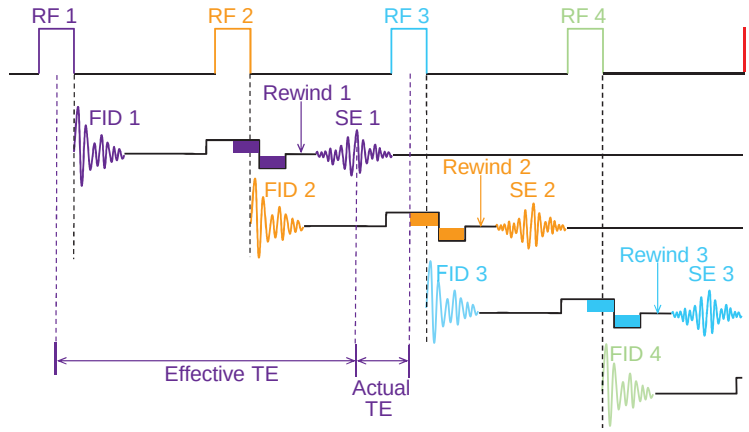

■ **FIGURE 12-44** SSFP uses a rewinder gradient to position each stimulated echo so that it appears just before the next excitation pulse, and is acquired separately from the FID. Since rephasing of the stimulated echo is initiated by an RF pulse rather than a gradient, more T2 rather than T2* weighting occurs. The *actual* TE is the time from the peak echo amplitude to the center of the next RF pulse. The *effective* TE is 2 × TR−actual TE (This is shown in the lower left of the figure).

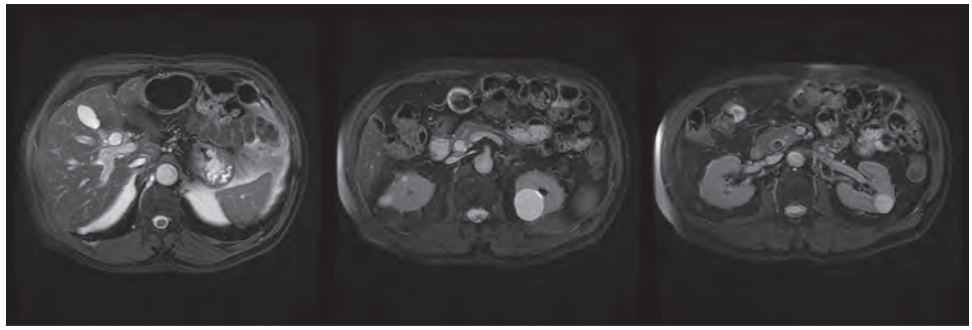

■ **FIGURE 12-45** Three abdominal post gadolinium contrast axial images are part of a breath-hold dataset using a "balanced SSFP" acquisition, which simultaneously accumulates the FID and the stimulated echo with contrast varying according to the T2/T1 ratio (TR: 3.34 ms, TE: 1.2 milliseconds, Flip angle 70 degrees, matrix size 192 × 320). Each image is acquired in approximately 700 milliseconds, making this sequence useful for reducing voluntary and involuntary patient motion in contrast enhanced abdominal and cardiac imaging.

(2) the stimulated echo from the residual transverse magnetization. From these two generated signals, coherent, incoherent, or SSFP sequences are used in order to generate different contrast-weighting schemes. Coherent GE uses the combined FID and SE signals and produces contrast mainly depending on the ratio of T2/T1 or T2*/T1; incoherent (or spoiled) GE produces contrast mainly based on T1, and SSFP samples the SE signal only, thus producing signals that are more T2 weighted. Figure 12-46 shows the signals and the timing of acquisition for these three scenarios. Note that these are generic, not fully inclusive, and do not include specific sequences implemented by the major manufacturers that do not fit into this simplified categorization. Additionally the term SSFP is used differently by the manufacturers. One should consult the specific applications manuals and descriptions of the specific models and pulse sequence implementations for more detailed information (Also see Chapter 13, Table 1 for a brief comparison of GE sequences). Details of GE techniques are reviewed in an article by Chavhan, et.al. (2008).

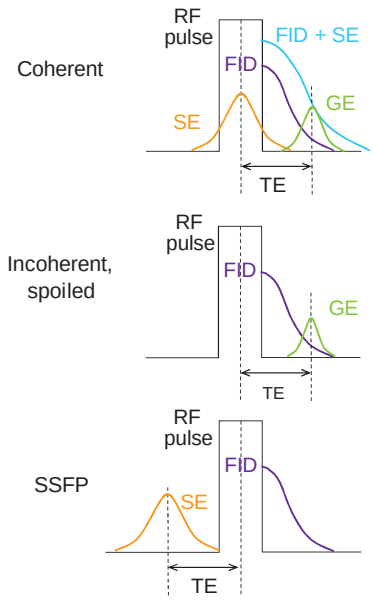

■ **FIGURE 12-46** A schematic summary of the three major GE sequences (RF, RadioFrequency; FID, Free Induction Decay; GE, Gradient Echo; SE, Stimulated or Spin Echo; TE, Time of Echo) are shown. Coherent GE uses signals from the FID and the SE to produce the image, typically with contrast dependent on T2/T1 weighting, and low contrast. Incoherent GE eliminates the detection of the SE, thus, providing a means to generate T1-weighted contrast from the FID signal. SSFP uses the SE signal, which provides mainly T2-weighted contrast. Balanced SSFP uses both the gradient and stimulated echo to produce a T2/T1 weighting with symmetrically applied gradients in three dimensions.

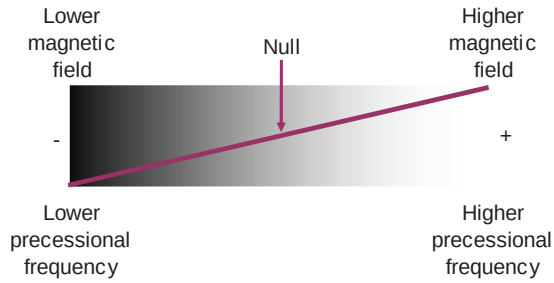

■ **FIGURE 12-47** The gradient magnetic field creates a net positive and negative magnetic environment that adds to and subtracts from the main magnetic field. Associated with the local change in magnetic field is a positionally dependent change in precessional frequencies, per the Larmor equation. The precessional frequencies directly vary across the field in proportion to the applied gradient strength.

12.6 MR Signal Localization

Spatial localization is essential for creating MR images and determining the location of discrete sample volumes for MR spectroscopy. This is achieved by superimposing linear magnetic field variations on the main (B_0) field to generate corresponding position-dependent variations in precessional frequency of the protons (Fig. 12-47). Simultaneous application of an RF excitation (B_1 pulse) excites only those protons in resonance within the frequency bandwidth (BW) of the B_1 RF pulse by absorbing energy.

Magnetic Field Gradients

Inside the magnet bore, three sets of gradients reside along the logical coordinate axes—x, y, and z—and produce a magnetic field variation determined by the magnitude of the applied current in each coil set (Fig. 12-48). When independently energized, the three coils (x, y, z) can produce a linearly variable magnetic field in

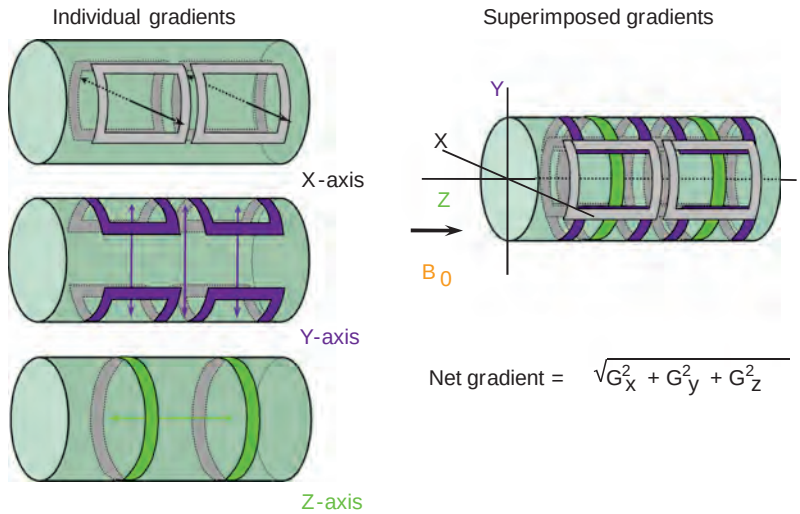

■ **FIGURE 12-48** Within the large stationary magnetic field, field gradients are produced by three separate coil pairs placed within the central core of the magnet, along the *x, y,* or *z* directions. In modern systems, the current loops are distributed across the cylinders for the x-, y- and z- gradients, which generates a lower, but more uniform gradient field. Magnetic field gradients of arbitrary direction are produced by the vector addition of the individual gradients turned on simultaneously. Any gradient direction is possible by superimposition of magnetic fields generated by the three-axis gradient system.

any direction, where the net gradient is equal to $\sqrt{G_x^2 + G_y^2 + G_z^2}$. Gradient polarity reversals (positive to negative and negative to positive changes in magnetic field strength) are achieved by reversing the current direction in the gradient coils.

Two important properties of magnetic gradients are: (1) The *gradient field strength* is determined by its peak amplitude and slope (change over distance), and typically ranges from 1 to 50 mT/m. (2) The *slew rate* is the time to achieve the peak magnetic field amplitude. Typical slew rates of gradient fields are from 5 to 250 mT/m/ms. As the gradient field is turned on, *eddy currents* are induced in nearby conductors such as adjacent RF coils and the patient, which produce magnetic fields that oppose the gradient field and limit the achievable slew rate. Actively shielded gradient coils and compensation circuits can reduce problems caused by eddy currents.

In a gradient magnetic field, protons maintain precessional frequencies corresponding to local magnetic field strength. At the middle of the gradient, called the *null*, there is no change in the field strength or precessional frequency. With a linear gradient, the magnetic field increases and decreases linearly from the null, as does the precessional frequency (Fig. 12-47 and Table 12-7). In the rotating frame of reference, incremental changes of frequency occur symmetrically about the null, and the positions of protons are encoded by frequency and phase. The frequency BW is the range of frequencies over the FOV, and the frequency BW per pixel is the BW divided by the number of discrete samples. Gradient amplitude can also be expressed in frequency per distance. For instance, a 10-mT/m gradient can be expressed as 10 mT/m × 42.58 MHz/T × 1 T/1,000 mT = 0.4258 MHz/m, which is equivalent to 425.8 kHz/m or 425.8 Hz/mm. The relationship of gradient strength and frequency BW across the FOV is independent of the main magnet field strength.

Localization of protons in the three-dimensional volume requires the application of three distinct gradients during the pulse sequence: slice select, frequency encode, and phase encode. These gradients are sequenced in a specific order, depending on the pulse sequences employed. Often, the three gradients overlap partially or completely during the scan to achieve a desired spin state, or to leave protons in their original phase state after the application of the gradient(s).

TABLE 12-7 PRECESSIONAL FREQUENCY VARIATION AT 1.5 T ALONG AN APPLIED GRADIENT

Gradient field strength	3 mT/m = 127.74 Hz/mm
Main magnetic field strength	1.5 T
FOV	0.15 m = 150 mm
Linear gradient amplitude over FOV	0.45 mT; from −0.225 mT to +0.225 mT
Maximum magnetic field (frequency)	1.500225 T (63.8795805 MHz)
Unchanged magnetic field at null	1.500000 T (63.8700000 MHz)
Minimum magnetic field	1.499775 T (63.8604195 MHz)
Net frequency range across FOV[a]	0.019161 MHz = 19.2 kHz = 19,161 Hz
Frequency range across FOV (1,278 Hz/cm)[b]	127.74 Hz/mm × 150 mm = 19,161 Hz
Frequency BW per pixel (256 samples)	19,161 Hz/256 = 74.85 Hz/pixel

[a]Calculated using the absolute precessional frequency range: 63.8796–63.8604 MHz.
[b]Calculated using the gradient strength expressed in Hz/mm.

Slice Select Gradient

RF transmitters cannot spatially direct the RF energy to a specific region in the body; rather the RF pulse, when turned on during the application of the slice select gradient (SSG), determines the slice location of protons in the tissues that absorb energy. For axial MR images, the SSG is applied along the long (cranial-caudal) axis of the body. Under the influence of the gradient field, the proton precessional frequencies in the volume are incrementally increased or decreased dependent on their distance from the null. A selective, narrow band RF frequency pulse of a known duration and amplitude delivers energy to the total volume, but only those protons with precessional frequencies matching the RF BW frequencies will absorb energy within a defined slice of tissues as shown in Figure 12-49 (red vertical line indicates energy absorbed due to resonance). If the center frequency of the RF pulse is increased, then a different slab of protons absorbs energy (blue vertical line).

Slice thickness is chiefly determined by the frequency BW of the RF pulse and the gradient strength across the FOV. For a fixed gradient strength, the RF pulse with a narrow BW excites protons within a thin slice, and a wide BW excites a thick slice (Fig. 12-50A). For a fixed RF BW, a high gradient strength produces a large range of frequencies across the FOV and decreases the slice thickness, whereas a low gradient strength produces a small range of frequencies and produces an increase in the slice thickness (Fig. 12-50B).

A combination of a narrow BW and a low gradient strength or a wide BW and a high gradient strength can result in the same slice thickness. Decisions depend chiefly on the SNR and the propensity for "chemical shift" artifacts. SNR is inversely proportional to the receiver BW: $\text{SNR} \propto \frac{1}{\sqrt{\text{BW}}}$; therefore narrow BW and low gradient strength are preferred; however, artifacts due to *chemical shift* (see Chapter 13, Section 13.5, Chemical Shift Artifacts) can be problematic. Consequently, trade-offs in image quality must be considered when determining the optimal RF BW and SSG field strength combinations.

After the SSG is turned off, the protons revert to the precessional frequency of the main magnetic field, but phase coherence is lost. To reestablish the original phase of all stationary protons, a gradient of opposite polarity equal to one-half of the

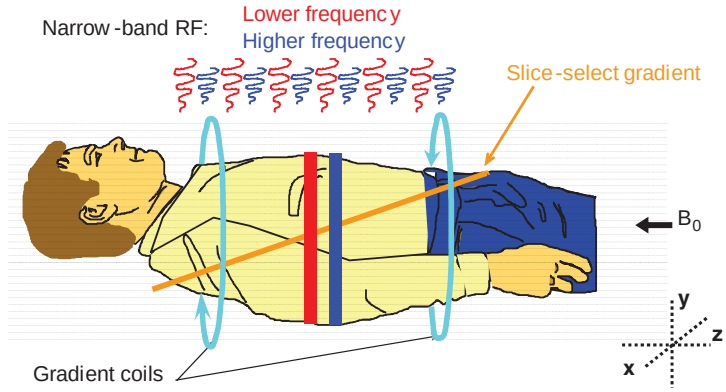

■ **FIGURE 12-49** The *SSG* disperses the precessional frequencies of the protons in a known way along the gradient. A narrow band RF pulse excites only a selected volume (slice) of tissues, determined by frequency, BW, and SSG strength. In the example above, two narrow-band RF pulses with different center frequencies irradiate the whole body during the application of the gradient, and only those protons at the same frequencies as the RF pulses will absorb energy. Note that the higher frequency slice is shifted towards the positive pole of the applied gradient.

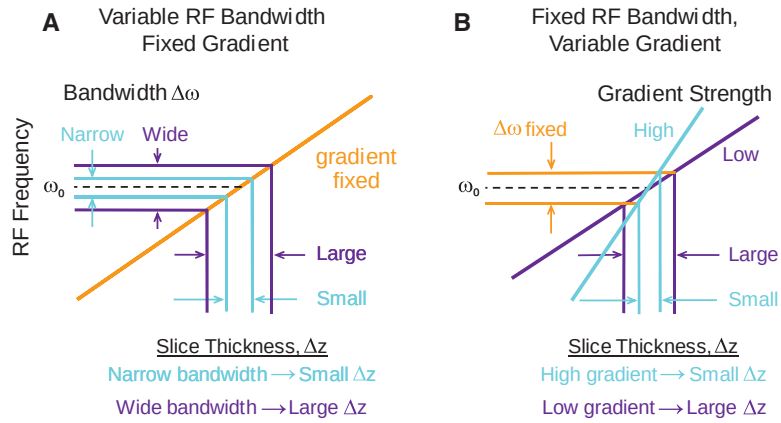

■ **FIGURE 12-50** Slice thickness is dependent on RF BW and gradient strength. **A.** For a fixed gradient strength, the RF BW determines the slice thickness. **B.** For a fixed RF BW, gradient strength determines the slice thickness.

area of the original SSG is applied (Fig. 12-51). For 180-degree RF excitations, the rephasing gradient is not necessary, as all protons maintain their phase relationships because of the symmetry of the RF pulse and spin inversion.

To summarize, the SSG is applied simultaneously with a RF pulse of a known BW to create proton excitation in a single plane with a known slice thickness, and to localize signals orthogonal to the gradient. It is the first of three gradients applied to the volume.

Frequency Encode Gradient

The *FEG*, also known as the *readout gradient*, is applied in a direction perpendicular to the SSG, along the "logical" x-axis, during the evolution and decay of the induced echo. Net changes in precessional frequencies are distributed symmetrically from 0 at the null to $+f_{max}$ and $-f_{max}$ at the edges of the FOV (Fig. 12-52) under the applied FEG. The composite signal is amplified, digitized, and processed by the Fourier transform to convert frequency into spatial position (Fig. 12-53). A spatial "projection" is created by integrating the resultant Fourier transformed signal amplitudes perpendicular to the direction of the applied gradient at corresponding spatial positions.

The SSG in concert with an incremental rotation of the FEG direction about the object can produce data projections through the object as a function of angle, as shown in Figure 12-54. With a sufficient number of projections, filtered back-projection can be used for reconstructing a tomographic image (see Chapter 11 on

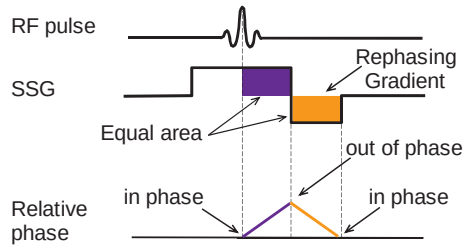

■ **FIGURE 12-51** SSG rephasing. At the peak of the RF pulse, all protons in the slice are in phase, but the SSG causes the spins to become dephased after the gradient is turned off. To reestablish phase coherence, a reverse polarity gradient is applied equal to one-half the area of the original SSG. At the next pulse, the relative phase will be identical.

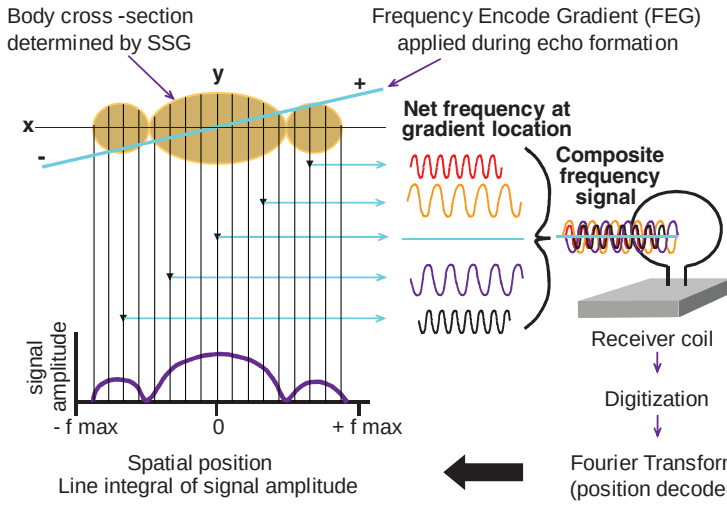

■ **FIGURE 12-52** The *FEG* is applied in an orthogonal direction to the SSG, and confers *a spatially dependent variation* in the precessional frequencies of the protons. Acting only on those protons in a slice determined by the SSG excitation, the composite signal is acquired, digitized, demodulated (Larmor frequency removed), and Fourier transformed into frequency and amplitude information. A one-dimensional array represents a *projection* of the slice of tissue (amplitude and position) at a specific angle. (Demodulation into net frequencies occurs *after* detection by the receiver coil; this is shown in the figure for clarity only.)

CT Reconstruction). In fact, this is how some of the first MR images were reconstructed from individual projections, using a rotating FEG. However, inefficient acquisition and data handling, in addition to motion artifacts, has led to near-universal acquisition with phase encoding techniques.

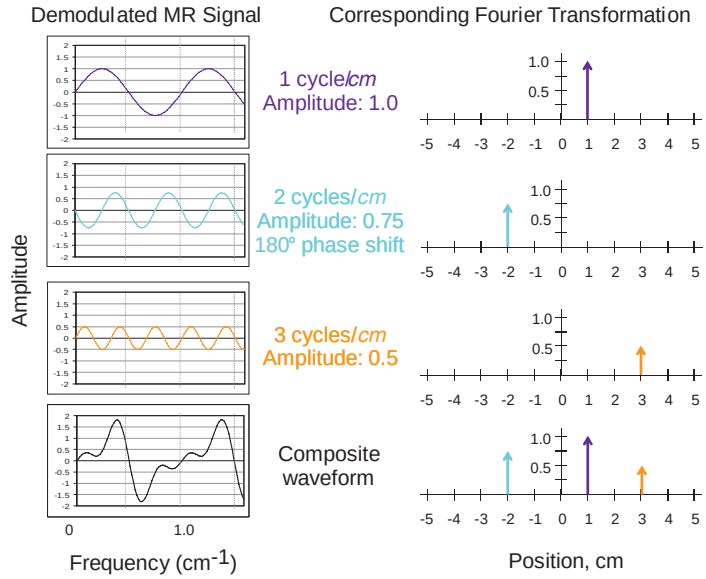

■ **FIGURE 12-53** Spatial frequency signals (cycles/cm) and their Fourier transforms (spatial position) are shown for three simple sinusoidal waveforms with a specific amplitude and phase. The Fourier transform decodes the frequency, phase and amplitude variations in the spatial frequency domain into a corresponding position and amplitude in the spatial domain. A 180-degree phase shift (second from the top) is shifted in the negative direction from the origin. The composite waveform (a summation of all waveforms, lower left) is decoded by Fourier transformation into the corresponding positions and amplitudes (lower right).

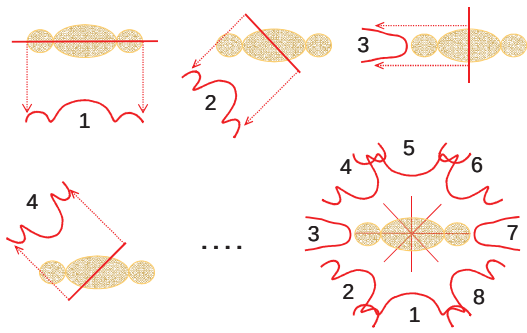

■ **FIGURE 12-54** A rotating FEG in the x-y plane allows the acquisition of individual projections as a function of angle, by repeating the SSG – FEG sequence with incremental change of the FEG direction. This example shows eight projections; to have sampling sufficient for high SNR and resolution would require hundreds of projections about the object.

Phase Encode Gradient

Position of the protons in the third orthogonal dimension is determined with a PEG, which is applied after the SSG but before the FEG, along the third orthogonal axis. Phase in this context represents a linear variation in the starting point of sinusoidal waves that precess at the same frequency. Phase changes are purposefully introduced by the application of a short duration PEG within each data acquisition (DAQ) interval. Prior to the PEG, all protons have the same phase, and turning on the PEG introduces a linear variation in the precessional frequency of the protons according to their position along the gradient. After a brief interval, the PEG is turned off, all protons revert to the Larmor frequency, and linear phase shifts are manifested by a specific gradient strength and polarity. Incremental positive phase change is introduced for protons under the positive pole, negative phase change under the negative pole, and no phase change occurs for protons at the null of the PEG. Throughout the acquisition sequence, the PEG strength and polarity is incrementally changed to introduce specific known phase changes as a function of position across the FOV for each acquisition interval (Fig. 12-55). Spatial encoding is determined by the amount of phase shift that has occurred. Protons located at the center

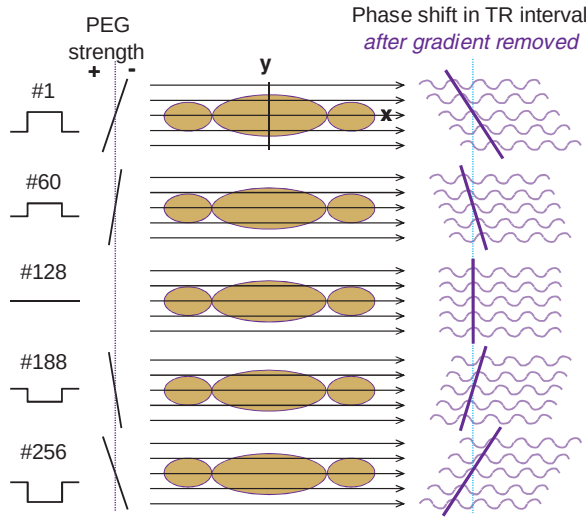

■ **FIGURE 12-55** The PEG is applied *before* the FEG and *after* the SSG. The PEG produces a spatially dependent variation in angular frequency of the excited spins for a brief duration, and generates a spatially dependent variation in phase when the spins return to the Larmor frequency. Incremental changes in the PEG strength for each TR interval spatially encodes the phase variations: protons at the null of the PEG do not experience any phase change, while protons in the periphery experience a large phase change dependent on their distance from the null. The incremental variation of the PEG strength can be thought of as providing specific "views" of the volume because the SSG and FEG remain fixed throughout the acquisition.

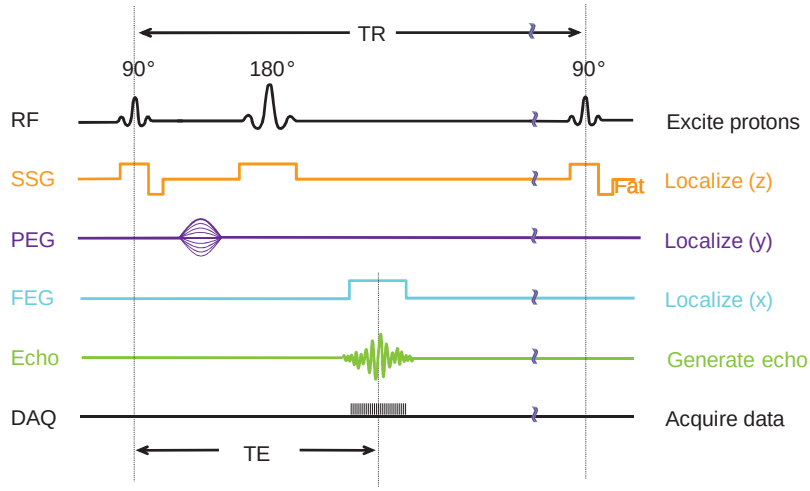

■ **FIGURE 12-56** A typical spin-echo pulse sequence diagram indicates the timing of the SSG, PEG, and FEG during the repetition time (TR) interval, synchronized with the RF pulses and the DAQ when the echo appears. Each TR interval is repeated with a different PEG strength (this appears as multiple lines in the illustration, but only one PEG strength is applied per TR as indicated by the bold line in this figure).

of the FOV, the PEG null, do not exhibit a phase shift. Protons located at the edges of the FOV exhibit the largest positive to negative (or negative to positive) phase shifts. Protons located at intermediate distances from the null experience intermediate phase shifts (positive or negative). Each location along the phase encode axis is spatially encoded by the amount of phase shifts experienced by the protons. For sequential acquisition sequences, each sample in the PEG direction is separated in time by the TR interval.

Gradient Sequencing

An acquisition of an *SE* pulse sequence is illustrated in Figure 12-56, showing the timing of the SSG in conjunction with the 90-degree RF excitation pulse, the application of a short duration PEG at a known strength, followed by a 180-degree refocusing RF pulse at TE/2, and the echo envelope with the peak amplitude occurring at TE. This sequence is repeated with slight incremental changes in the PEG strength to define the three dimensions in the image over the acquisition time.

12.7 "K-Space" Data Acquisition and Image Reconstruction

MR data are initially stored in the k-space matrix, the "frequency domain" repository (Fig. 12-57). K-space describes a two-dimensional matrix of positive and negative spatial frequency values, encoded as complex numbers (e.g., $a + bi$, $i = \sqrt{-1}$). The matrix is divided into four quadrants, with the origin at the center representing frequency = 0. Frequency domain data are encoded in the k_x direction by the FEG, and in the k_y direction by the PEG in most image sequences. The lowest spatial frequency increment (the fundamental frequency) is the BW across each pixel (see Table 12-7). The maximum useful frequency (the Nyquist frequency) is equal to ½ frequency range across the k_x or k_y directions, as the frequencies are encoded from $-f_{max}$ to $+f_{max}$. The periodic nature of the frequency domain has a built-in symmetry described by "symmetric" and "antisymmetric" functions (e.g., cosine and sine waves). "Real," "imaginary," and "magnitude" describe specific phase and amplitude characteristics of the composite MR frequency waveforms. Partial acquisitions are

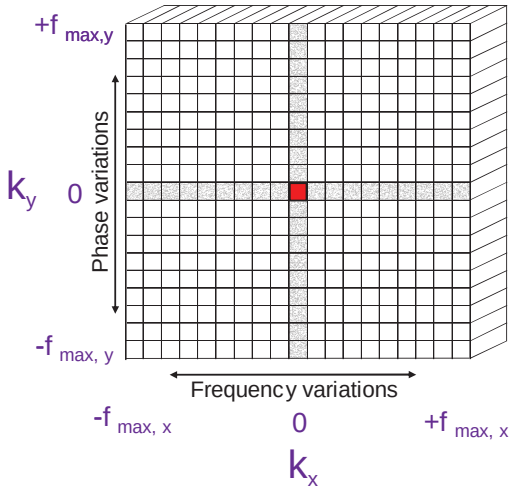

■ **FIGURE 12-57** The k-space matrix is the repository for spatial frequency signals acquired during the evolution and decay of the echo. The k_x axis (along the rows) and the k_y axis (along the columns) have units of cycles/unit distance. Each axis is symmetric about the center of k-space, ranging from $-f_{max}$ to $+f_{max}$ along the rows and the columns. The matrix is filled one row at a time in a conventional acquisition with the FEG induced frequency variations mapped along the k_x axis and the PEG induced phase variations mapped along the k_y axis.

possible (e.g., one-half of the k-space matrix plus one line) with complex conjugate symmetry filling the remainder (See Chapter 13, Section 1, "Data Synthesis").

Two-Dimensional Data Acquisition

MR data are acquired as a complex, composite frequency waveform. With methodical variations of the PEG during each excitation, the k-space matrix is filled to produce the desired variations across the frequency and phase encode directions as shown in Figure 12-58.

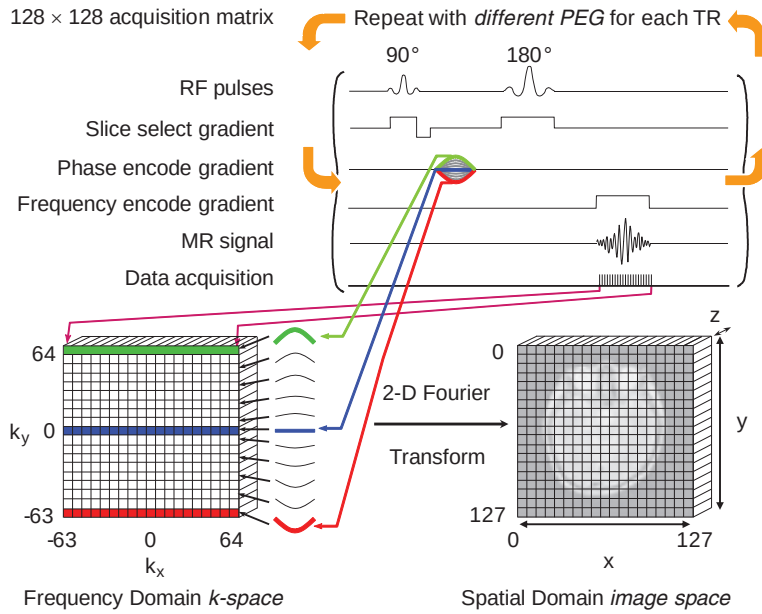

■ **FIGURE 12-58** MR data are acquired into k-space matrix, where each row in k-space represents spatially dependent frequency variations under a fixed FEG strength, and each column represents spatially dependent phase shift variations under an incrementally varied PEG strength. Data are placed in a specific row determined by the PEG strength for each TR interval. The grayscale image is constructed from the two-dimensional Fourier transformation of the k-space matrix by sequential application of one-dimensional transforms along each row, and then along each column of the intermediate transformed data. The output image matrix is arranged with the image coordinate pair, x = 0, y = 0 at the upper left of the image matrix.

A summary description of the two-dimensional spin-echo image acquisition steps follows.

1. A narrow band RF excitation pulse simultaneously applied with the SSG causes a specific slab of tissues with protons at the same frequency to absorb energy. Transverse magnetization, M_{xy}, is produced with amplitude dependent on the saturation of the protons and the angle of excitation. A 90-degree flip angle produces the largest M_{xy}.
2. A PEG is applied for a brief duration, which introduces a phase difference among the protons along the phase encode direction to produce a specific "view" of the data along the k_y axis, corresponding to the strength of the PEG,
3. A refocusing 180-degree RF pulse is delivered at TE/2 to invert and reestablish the phase coherence of the transverse magnetization at time TE.
4. During the evolution and decay of the echo signal, the FEG is applied orthogonal to both the SSG and PEG directions, generating spatially dependent changes in the precessional frequencies of the protons.
5. Data sampling and acquisition of the complex signal occurs simultaneous to the FEG. A one-dimensional inverse Fourier transform converts the digital data into discrete frequency values and corresponding amplitudes to determine position along the k_x (readout) direction.
6. Data are deposited in the k-space matrix at a row location specifically determined by the strength of the PEG. For each TR, an incremental variation of the PEG strength sequentially fills each row. In some sequences, the phase encode data are acquired in nonsequential order to fill portions of k-space more pertinent to the requirements of the exam (e.g., in the low-frequency, central area of k-space). Once filled, the k-space matrix columns contain positionally dependent variations in phase change along the k_y (phase encode) direction.
7. After all rows are filled, an inverse Fourier transform decodes the frequency domain variations in phase for each of the columns of k-space to produce the spatial domain representation.
8. The final image is scaled and adjusted to represent the proton density, T1, T2, and flow characteristics of the tissues using a grayscale range, where each pixel represents a voxel.

The bulk of image information representing the lower spatial frequencies is contained in the center of k-space, whereas the higher spatial frequencies are contained in the periphery, as shown in Figure 12-59, representing a grayscale rendition of k-space for a sagittal slice of a brain MR image acquisition. The innermost areas represent the bulk of the anatomy, while the outer areas of *k-space* contain the detail and resolution components of the anatomy, as shown by reconstructed images.

Two-Dimensional Multiplanar Acquisition

Direct axial, coronal, sagittal, or oblique planes can be obtained by energizing the appropriate gradient coils during the image acquisition, as shown in Figure 12-60. The SSG determines the orientation of the slices: axial uses z-axis coils; coronal uses y-axis coils; and sagittal uses x-axis coils for selection of the slice orientation. Oblique plane acquisition depends on a combination of the x-, y-, and z-axis coils energized simultaneously. SSG, PEG, and FEG applications are perpendicular to each other, and acquisition of data into the k-space matrix remains the same, with the FEG along the k_x axis and the PEG along the k_y axis.

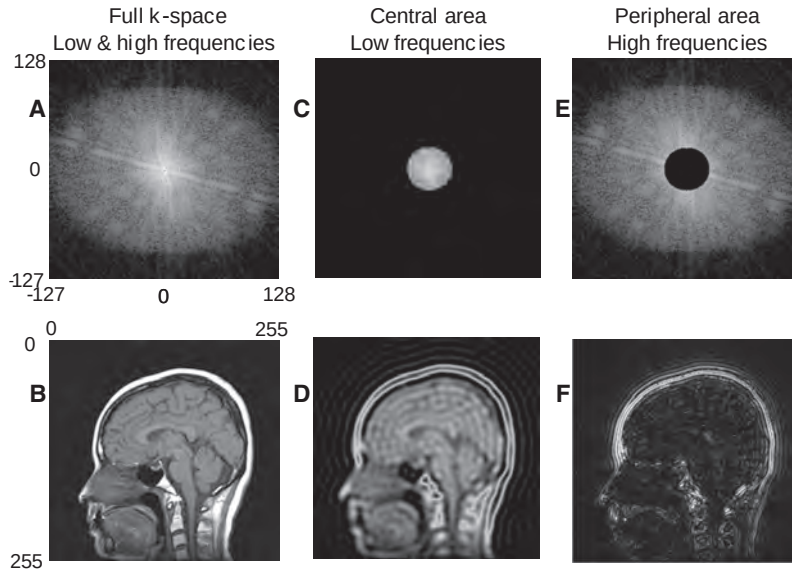

■ **FIGURE 12-59** **A.** Image representations of *k-space* segmentation show a concentration of information around the origin (the k-space images are logarithmically amplified for display of the lowest amplitude signals). **B.** Inverse two-dimensional Fourier transformation converts the data into a visible image. **C.** Segmenting a radius of 25 pixels out of 128 in the central area and zeroing out the periphery extracts a majority of the low-frequency information. **D.** The corresponding image demonstrates the majority of the image content is in the center of k-space. **E.** Zeroing out the central portion and leaving the peripheral areas isolates the higher spatial frequency signals. **F.** The resulting image is chiefly comprised of high frequency detail and resolution. Ringing that is visible in the image is due to the sharp masking transition from the image data to zero.

12.8 Summary

The basics of magnetic resonance are covered in this chapter, including the simplest descriptions of magnetism, magnetic characteristics of the elements, and magnetization of tissue samples. Important is the description of the intrinsic decay constants T1, T2, T2*, and proton density in terms of tissue-specific structures and variation in the intrinsic and extrinsic local magnetic fields. Contrast between tissues is determined by pulse sequences including SE, IR, GE, and their associated parameters

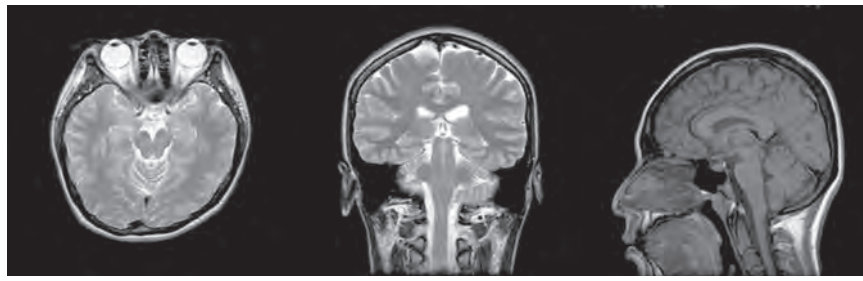

■ **FIGURE 12-60** Direct acquisitions of axial, coronal, and sagittal tomographic images are possible by electronically energizing the magnetic field gradients in a different order without moving the patient. Oblique planes can also be obtained. PEG (k_y axis) and FEG (k_x axis) are perpendicular to the SSG.

TR, TE, TI, and flip angle. In addition to generating contrast, the ability to spatially localize the protons and create a two-dimensional image is as important, so that the differences can be appreciated in a grayscale rendition of the anatomy. The concepts of the frequency domain description of the signals and the k-space acquisition matrix are integral to the discussion, as well as the Fourier transform and the conversion of frequency to spatial domain representations of the data, necessary for visualization. In the next chapter, more details are given for image acquisition time, various pulse sequence designs, how image acquisition time is shortened, and characteristics of the image in terms of SNR, CNR, and artifacts. Unique capabilities for noninvasive "biopsy" of tissues, quality control, equipment, MR safety, and biological effects are also discussed.

REFERENCES AND SUGGESTED READINGS

Bottomley PA, Foster TH, Argersinger RE, Pfeifer LM. A review of normal tissue hydrogen NMR relaxation mechanisms from 1-100 MHz: dependence on tissue type, NMR frequency, temperature, species, excision, and age. *Med Phys* 1984;11:425–448.

Chavhan GB, Babyn PS, Jankharia BG, Cheng HM,Shroff MM. Steady-State MR Imaging Sequences: Physics, Classification, and Clinical Applications. *Radiographics* 2008;28:1147–1160.

Fullerton GD, Potter JL, Dornbluth NC. NMR relaxation of protons in tissues and other macromolecular water solutions. *Magn Reson Imaging* 1982; 1:209–228.

NessAiver M. *All you really need to know about MRI physics.* Baltimore, MD: Simply Physics, 1997.

Pooley RA. AAPM/RSNA physics tutorial for residents: fundamental Physics of MR imaging. *Radiographics* 2005;25:1087–1099.

Westbrook C, Kaut-Roth C, Talbot J. *MRI in practice*. 3rd ed. Malden, MA: Blackwell Publishing, 2005.

CHAPTER 13

Magnetic Resonance Imaging: Advanced Image Acquisition Methods, Artifacts, Spectroscopy, Quality Control, Siting, Bioeffects, and Safety

The essence of magnetic resonance imaging (MRI) in medicine is the acquisition, manipulation, display, and archive of datasets that have clinical relevance in the context of making a diagnosis or performing research for new applications and opportunities. There are many advantages and limitations of MRI and MR spectroscopy (MRS) as a solution to a clinical problem. Certainly, as described previously (note that this chapter assumes a working knowledge of Chapter 12 content), the great advantages of MR are the ability to generate images with outstanding tissue contrast and good resolution, without resorting to ionizing radiation. Capabilities of MR extend far beyond those basics, into fast acquisition sequences, perfusion and diffusion imaging, MR angiography (MRA), tractography, spectroscopy, and a host of other useful or potentially useful clinical applications. Major limitations of MR are also noteworthy, including extended acquisition times, MR artifacts, patient claustrophobia, tissue heating, and acoustic noise to name a few. MR safety, often ignored, is also of huge concern to the safety of the patient.

In this second of two MR chapters, advanced pulse sequences and fast image acquisition methods, dedicated radiofrequency (RF) coils, methods for perfusion, diffusion, and angiography imaging, image quality metrics, common artifacts, spectroscopy, MR equipment and siting, as well as MR safety issues are described and discussed with respect to the underlying physics.

The concepts of image acquisition and timing issues for standard and advanced pulse sequences into k-space is discussed first, with several methods that can be used to reduce acquisition times and many of the trade-offs that must be considered.

13.1 Image Acquisition Time

A defining character of MRI is the tremendous range of acquisition time needed to image a patient volume. Times ranging from as low as 50 ms to tens of minutes are commonly required depending on the study, pulse sequence, number of images in the dataset, and desired image quality. When MR was initially considered to be a potential diagnostic imaging modality in the late 1970s, the prevailing conventional wisdom gave no chance for widespread applicability because of the extremely long times required to generate a single slice from a sequentially acquired dataset, which

required several minutes or more per slice. Breakthroughs in technology, equipment design, RF coils, the unique attributes of the k-space matrix, and methods of acquiring data drastically shortened acquisition times (or effective acquisition times) quickly, and propelled the rapid adoption of MRI in the mid-1980s. By the early 1990s, MRI established its clinical value that continues to expand today.

Acquisition Time, Two-Dimensional Fourier Transform Spin Echo Imaging

The time to acquire an image is determined by the data needed to fill the fraction of k-space that allows the image to be reconstructed by Fourier transform methods. For a standard spin echo sequence, the relevant parameters are the TR, number of phase encoding steps, and number of excitations (NEX) used for averaging identical repeat cycles, as

$$\textbf{Acquisition time} = \textbf{TR} \times \#\ \textbf{PEG Steps} \times \textbf{NEX}$$

Even though there may be multiple echoes as illustrated in Figure 13-1, there is also the same number of k-space repositories to capture the data in a specific, single row of k-space defined by the strength of the PEG, as shown for the first echo with proton density weighting and second echo with T2 weighting for this double echo acquisition. Thus, effective imaging time can be reduced by producing two (or more) images of the same slice within the TR interval. In addition, the matrix size that defines k-space is often not square (e.g., 256 × 256, 128 × 128), but

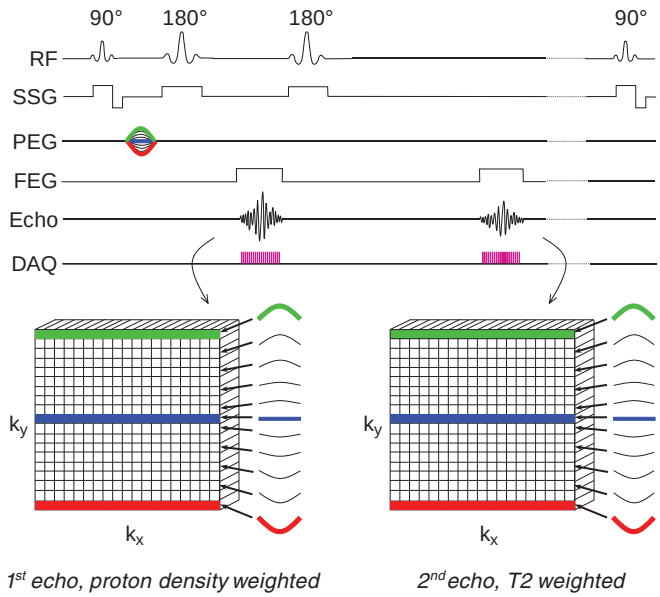

■ **FIGURE 13-1** Standard spin echo pulse sequence is shown with two echoes per TR interval to encode proton density contrast (short TE, first echo), and T2 contrast (long TE, second echo). In this acquisition, two separate images are acquired independently by storing in a designated k-space matrix according to echo time. A single PEG strength is momentarily applied to induce phase variations to encode the row to be filled in each of the matrices (see the *red* PEG encoding for the last row in k-space, for instance). The full k-space matrix requires the sequence to be repeated with incremental variations in the PEG strength until each k-space row is fully populated. If averaging is desired, then an identical sequence (without incrementing the PEG) is repeated and averaged in the same row.

rectangular (e.g., 256 × 192, 256 × 128) where the small matrix dimension is most frequently along the phase encode direction to minimize the number of incremental PEG strength applications during the acquisition. A 256 × 192 image matrix and two averages (NEX) per phase encode step with a TR = 600 ms (for T1 weighting) requires imaging time of 0.6 s × 192 × 2 = 230.4 s = 3.84 min for a single slice! For a proton density and T2-weighted double echo sequence with TR = 2,500 ms (Fig. 13-1), this increases to 16 min, although two images are created in that time. Of course, a simple first-order method would be to eliminate the number of averages (NEX), which reduces the time by a factor of 2; however, the downsides are an increase in the statistical variability of the data, which decreases the image signal-to-noise ratio (SNR) and makes the image appear "noisy." Methods to reduce acquisition time and/or time per slice are crucial to making MR exam times reasonable, as described by various methods below.

Multislice Data Acquisition

The average acquisition time per reconstructed image slice in a single-slice spin echo sequence is clinically unacceptable. However, the average time per slice is significantly reduced using multislice acquisition methods, where several slices within the tissue volume are selectively excited in a sequential timing scheme during the TR interval to fully utilize the dead time waiting for longitudinal recovery in an adjacent slice, as shown in Figure 13-2. This requires cycling all of the gradients and tuning the RF excitation pulse many times during the TR interval. The total number of slices that can be acquired simultaneously is a function of TR, TE, and machine limitations:

$$\text{Total Number of Slices} = \text{TR}/(\text{TE} + \text{C}),$$

where C is a constant dependent on the MR equipment capabilities (computer speed; gradient capabilities; sequence options; additional pulses, e.g., spoiling pulses in standard SE; use of spatial saturation; and chemical shift, among others). Each slice and each echo, if multiecho, requires its own k-space repository to store data as it is acquired. Long TR acquisitions such as proton density and T2-weighted sequences

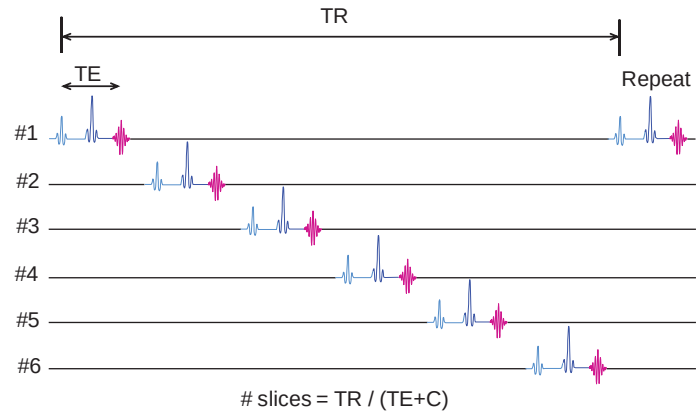

■ **FIGURE 13-2** Multislice two-dimensional image acquisition is accomplished by discretely exciting different slabs of tissue during the TR period; appropriate changes of the RF excitation bandwidth, SSG, PEG, and FEG parameters are necessary. Because of diffuse excitation profiles, RF irradiation of adjacent slices leads to partial saturation and loss of contrast. The number of slices (volume) that can be obtained is a function of the TR, TE, and C, the latter representing the capabilities of the MR system and type of pulse sequence.

can produce a greater number of slices over a given volume than T1-weighted sequences with a short TR. The chief trade-off is a loss of tissue contrast due to *cross-excitation* of adjacent slices due to nonsquare excitation profiles, causing undesired proton saturation as explained in Section 13.5 on artifacts.

Data Synthesis

Data "synthesis" takes advantage of the symmetry and redundant characteristics of the frequency domain signals in k-space. The acquisition of as little as one-half the data plus one row of k-space allows the mirroring of "complex conjugate" data to fill the remainder of the matrix (Fig. 13-3). In the phase encode direction, "half Fourier," "½ NEX," or "phase conjugate symmetry" (vendor-specific names) techniques effectively reduce the number of required TR intervals by one-half plus one line, and thus can reduce the acquisition time by nearly one-half. In the frequency encode direction, "fractional echo" or "read conjugate symmetry" refers to reading a fraction of the echo. While there is no scan time reduction when all the phase encode steps are acquired, there is a significant echo time reduction, which can reduce motion-related artifacts, such as dephasing of blood. However, the penalty for either half Fourier or fractional echo techniques is a reduction in the SNR (caused by a reduced NEX or

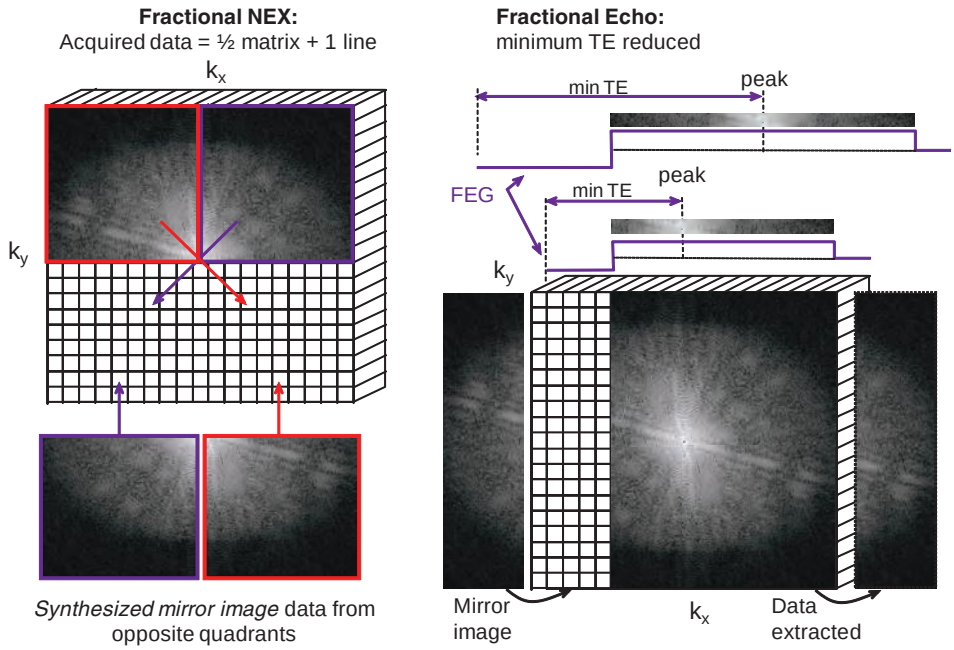

■ **FIGURE 13-3** Fractional NEX and Fractional Echo. **Left**. Data synthesis uses the redundant characteristics of the frequency domain. This is an example of phase conjugate symmetry, in which ½ of the PEG views +1 extra are acquired, and the complex conjugate of the data is reflected in the symmetric quadrants. Acquisition time is thus reduced by approximately $\sqrt{2}\left(\sim 40\%\right)$, although image noise is increased by approximately $\sqrt{2}$. Right: Fractional echo acquisition is performed when only part of the echo is read during the application of the FEG. Usually, the peak of the echo is centered in the middle of the readout gradient, and the echo signals prior to the peak are identical mirror images after the peak. With fractional echo, the echo is no longer centered, and the sampling window is shifted such that only the peak echo and the dephasing part of the echo are sampled. As the peak of the echo is closer to the RF excitation pulse, TE can be reduced, which can improve T1 and proton density weighting contrast. A larger number of slices can also be obtained with a shorter TE in a multislice acquisition (see Fig. 13-2).

data sampling in the volume) and the potential for artifacts if the approximations in the complex conjugation of the signals are not accurate. Other inaccuracies result from inhomogeneities of the magnetic field, imperfect linear gradient fields, and the presence of magnetic susceptibility agents in the volume being imaged.

Fast Pulse Sequences

Fast Spin Echo (FSE) techniques use multiple PEG steps in conjunction with multiple 180-degree refocusing RF pulses to produce an echo train length (ETL) with corresponding digital data acquisitions per TR interval, as illustrated in Figure 13-4. Multiple k-space rows are filled during each TR equal to the ETL, which is also the reduction factor for acquisition time. "Effective echo time" is determined when the central views in k-space are acquired, which are usually the first echoes, and subsequent echoes are usually spaced apart via increased PEG strength with the same echo spacing time. *"Phase re-ordering"* optimizes SNR by acquiring the low-frequency information with the early echoes (lowest amount of T2 decay), and the high-frequency, peripheral information with late echoes, where the impact on overall image SNR is lower. The FSE technique has the advantage of spin echo image acquisition, namely immunity from external magnetic field inhomogeneities, with 4×, 8×, to 16× faster acquisition time. However, each echo experiences different amounts of intrinsic T2 decay, which results in image contrast differences when compared with conventional spin echo images of similar TR and TE. Lower signal levels in the later echoes produce less SNR, and fewer images can be acquired in the image volume during the same acquisition. A T2-weighted spin echo image (TR = 2,000 ms, 256 phase encode steps, one average) requires approximately 8.5 min, while a corresponding FSE with an ETL of 4 (Fig. 13-4) requires about 2.1 min.

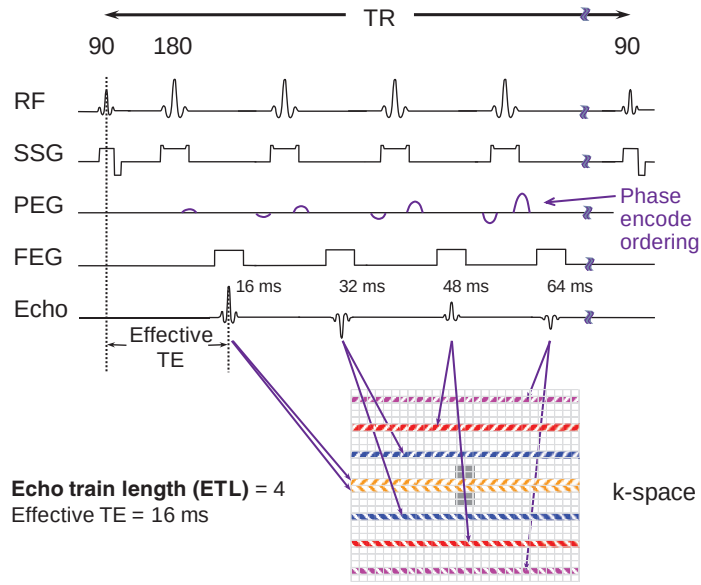

■ **FIGURE 13-4** Conventional FSE uses multiple 180-degree refocusing RF pulses per TR interval with incremental changes in the PEG to fill several views in k-space (the ETL). This example illustrates an ETL of four, with an "effective" TE equal to 16 *ms*. Total time of the acquisition is reduced by the ETL factor. The reversed polarity PEG steps reestablish coherent phase before the next gradient application. Slightly different PEG strengths are applied to fill the center of k-space first, and then the periphery with later echoes, continuing until all views are recorded. As shown, data can be mirrored using conjugate symmetry to reduce the overall time by another factor of two.

Longer TR values allow for a greater ETL, which will offset the longer TR in terms of overall acquisition time, and will also allow more proton density weighting. Specific FSE sequences for T2 weighting and multiecho FSE are employed with variations in phase reordering and data acquisition. FSE is also known as "turbo spin echo" or "RARE" (rapid acquisition with refocused echoes).

A Gradient Echo (GE) Acquisition pulse sequence is similar to a standard spin echo sequence with a readout gradient reversal substituting for the 180-degree pulse (Fig. 13-5). Repetition of the acquisition sequence occurs for each PEG step and with each average. With small flip angles and gradient reversals, a considerable reduction in TR and TE is possible for fast image acquisition; however, the ability to acquire multiple slices is compromised. A PEG rewinder pulse of opposite polarity is applied to maintain phase relationships from pulse to pulse in the coherent image acquisition. Spoiler gradients are used to eliminate persistent transverse magnetization from stimulated echoes for incoherent GE (see Chapter 12, Section 12.5).

Acquisition times are calculated in the same way as spin echo; a GE sequence for a 256 × 192 image matrix, two averages, and a TR = 30 ms, results in an imaging time equal to 192 × 2 × 0.03 s = 15.5 s. A conventional spin echo requires 3.84 min for a TR = 600 ms. Trade-offs for fast acquisition speed include SNR losses, magnetic susceptibility artifacts, and less immunity from magnetic field inhomogeneities. There are several acronyms for GE sequences, including GRASS, FISP, Spoiled GRASS, FLASH, SSFP, etc., depending on the manufacturer of the equipment. Table 13-1 describes a partial list of the different GE sequences and their method of data acquisition.

Echo Planar Image (EPI) Acquisition is a technique that provides extremely fast imaging time. Spin Echo (SE-EPI) and Gradient Echo (GE-EPI) are two methods used for acquiring data, and a third is a hybrid of the two, GRASE (Gradient and Spin Echo). Single-shot (all of the image information is acquired within 1 TR interval) or multishot EPI has been implemented with these methods. For single-shot SE-EPI,

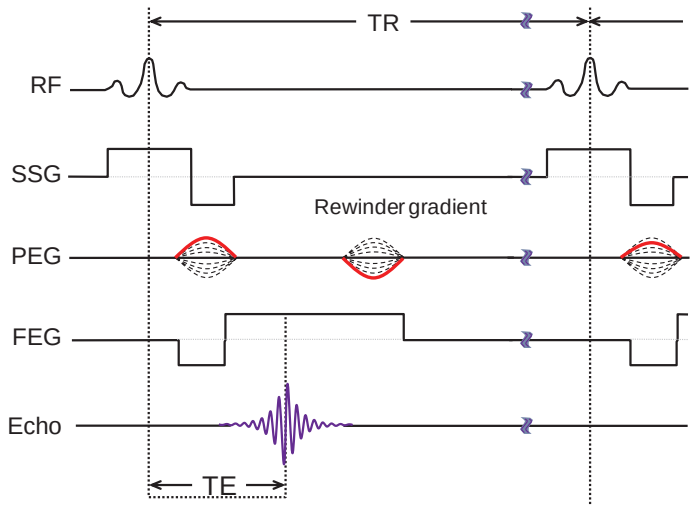

■ **FIGURE 13-5** Coherent GE pulse sequence uses a small flip angle (30 to 40 degrees) RF pulse simultaneous to the SSG. Phase and frequency encode gradients are applied shortly afterward (with a TE of less than 3 *ms* in certain sequences). A PEG "rewinder" (reverse polarity) reestablishes the phase conditions prior to the next pulse, simultaneous with the extended FEG duration.

TABLE 13-1 COMPARISON OF MANUFACTURER-NAMED ACRONYMS FOR GE SEQUENCES

SEQUENCE	GENERAL ELECTRIC	PHILIPS	SIEMENS	TOSHIBA
Coherent GE	GRASS, FGR FMPGR	FFE	FISP	Field echo
Incoherent GE (RF spoiled)	SPGR, FSPGR	T1 FFE		Field echo
Incoherent GE (Gradient spoiled)	MPGR		FLASH	Field echo
Steady-state free precession	SSFP, DE FGR	T2 FFE	PSIF	
SSFP: balanced sequence / true FISP	FIESTA	Balanced FFE	True FISP	True SSFP

Note: Not all manufacturers are listed in this table, nor are all GE sequences. (Blank areas indicate particular sequence is not performed (at time of publication).

image acquisition typically begins with a standard 90-degree flip, then a PEG/FEG gradient application to initiate the acquisition of data in the periphery of the k-space, followed by a 180-degree echo-producing RF pulse. Immediately after, an oscillating readout gradient and phase encode gradient "blips" are continuously applied to stimulate echo formation and rapidly fill k-space in a stepped "zig-zag" pattern (Fig. 13-6). The "effective" echo time occurs at a time TE, when the maximum amplitude of the induced GEs occurs. Acquisition of the data must proceed in a period less than T2* (around 50 ms), placing high demands on the sampling rate, the gradient coils (shielded coils are required, with low induced "eddy currents"), the RF transmitter/receiver, and RF energy deposition limitations. For GE-EPI, a similar acquisition strategy is implemented but without a 180 degrees refocusing RF pulse, allowing for faster acquisition time. SE-EPI is generally longer, but better image quality is achieved; on the other hand, larger RF energy deposition to the patient occurs. EPI acquisition can

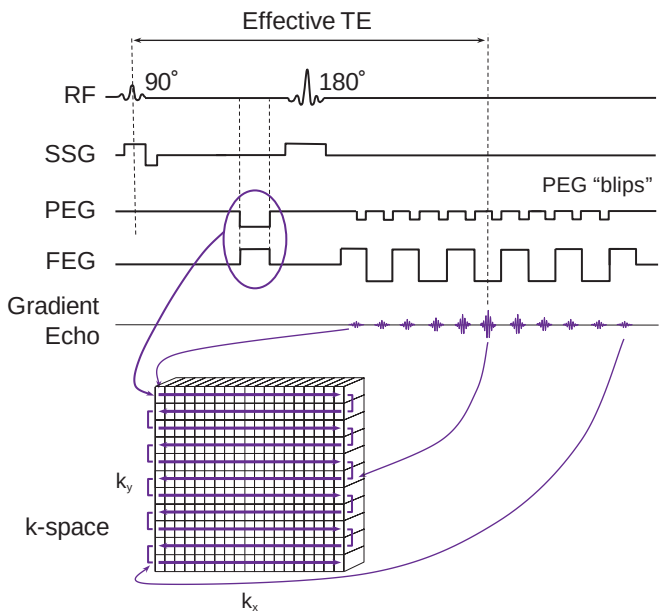

■ **FIGURE 13-6** Single shot Echo Planar Spin Echo image (SE-EPI) acquisition sequence. Data is deposited in k-space, initially positioned by a simultaneous PEG and FEG application to locate the initial row and column position (in this example, the upper left), followed by phase encode gradient "blips" simultaneous to FEG oscillations, to fill *k-space* line by line by introducing 1-row phase changes in a zig-zag pattern. Image matrix sizes of 64 × 64 and 128 × 64 are common.

be preceded with any type of RF pulse, for instance FLAIR (EPI-FLAIR), which will produce images much faster than the corresponding conventional FLAIR sequence.

The GRASE (Gradient and Spin Echo) sequence combines the initial spin echo with a series of GEs, followed by an RF rephasing (180 degrees) pulse, and the pattern is repeated until k-space is filled. This hybrid sequence achieves the benefits of both types of rephasing: the speed of the gradient and the ability of the RF pulse to compensate for T2* effects, providing significant improvements in image quality compared to the standard EPI methods. A trade-off is a longer acquisition time (e.g., greater than 100 ms) and much greater energy deposition from the multiple 180 degrees RF pulses.

EPI acquisitions typically have poor SNR, low resolution (matrices of 64 × 64 or 128 × 64 are typical), and many artifacts, particularly of chemical shift and magnetic susceptibility origin. Nevertheless, EPI offers real-time "snapshot" image capability with 50 ms total acquisition time. EPI is emerging as a clinical tool for studying time-dependent physiologic processes and functional imaging. Concerns of safety with EPI, chiefly related to the rapid switching of gradients and possible nerve stimulation of the patient, the associated acoustic noise, image artifacts, distortion, and chemical shift are components that will limit use for many imaging procedures.

Other K-Space Filling Methods

Methods to fill k-space in a nonsequential way can enhance signal, contrast, and achieve rapid scan times as shown in Figure 13-7. ***Centric k-space filling*** has been discussed with FSE imaging (above), where the lower strength phase encode gradi-

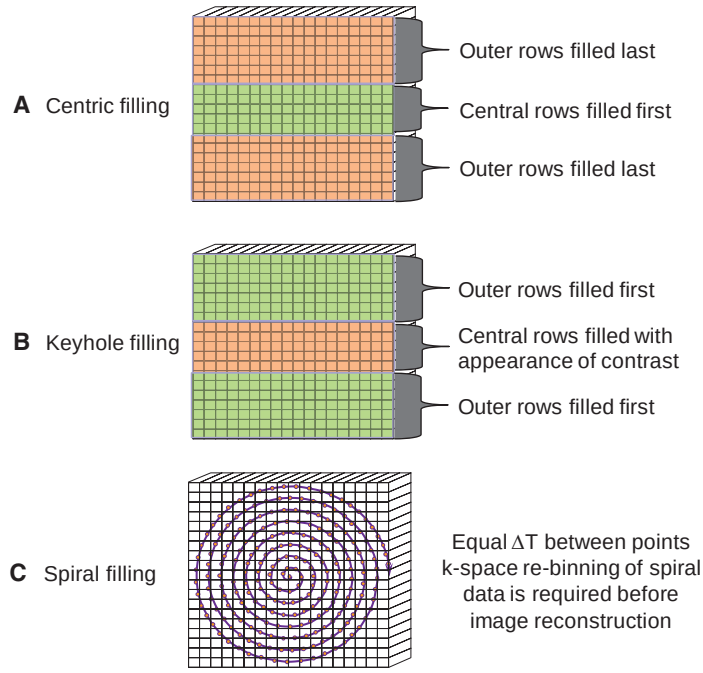

■ **FIGURE 13-7** Alternate methods of filling k-space. **A.** Centric filling applies the lower strength PEG's first to maximize signal and contrast from the earliest echoes of a FSE or GE sequence. **B.** Keyhole filling applies PEG's of higher strength first to fill the outer portions of k-space, and the central lines are filled only during a certain part of the sequence, such as with arrival of contrast signal. **C.** Spiral data acquisition occurs with sinusoidal oscillation of the X and Y gradients 90 degrees out of phase with each other, with samples beginning in the center of k-space and spiraling out to the periphery. Interpolating the data into the k_x, k_y matrix is required in order to apply 2DFT image reconstruction.

ents are applied first, filling the center of k-space when the echoes have their highest amplitude. This type of filling is also important for fast GE techniques, where the image contrast and the SNR fall quickly with time from the initial excitation pulse.

Keyhole filling methods fill k-space similarly to centric filling, except the central lines are filled when important events occur during the sequence, in situations such as contrast-enhanced angiography. Outer areas of k-space are filled first, and when gadolinium appears in the imaging volume, the center areas are filled. At the end of the scan, the outer and central k-space regions are meshed to produce an image with both good contrast and resolution.

Spiral filling is an alternate method of filling k-space radially, which involves the simultaneous oscillation of equivalent encoding gradients to sample data points during echo formation in a spiral, starting at the origin (the center of the k-space) and spiraling outward to the periphery in the prescribed acquisition plane. The same contrast mechanisms are available in spiral sequences (e.g., T1, T2, proton density weighting), and spin or GEs can be obtained. After acquisition of the signals, an additional post-processing step, re-gridding, is necessary to convert the spiral data into the rectilinear matrix for two-dimensional Fourier transform (2DFT). Spiral scanning is an efficient method for acquiring data and sampling information in the center of k-space, where the bulk of image information is contained.

A variant of radial sampling with enhanced filling of the center of k-space is known generically as "blade" imaging, and commonly as ***propeller***: Periodically Rotated Overlapping Parallel Lines with Enhanced Reconstruction, where a rectangular block of data is acquired and then rotated about the center of k-space. Redundant information concentrated in the center of k-space is used for improvement of SNR or for the identification of times during the scan in which the patient may have moved, so that those blocks of data can be processed with a phase-shifting algorithm to eliminate the movement effect on the data during the reconstruction process and to mitigate motion artifacts to a great extent. Filling of k-space for this method is shown in Figure 13-8.

Parallel Imaging

Parallel imaging is a technique that fills k-space by using the response of multiple receive RF coils that are coupled together with independent channels, so that data can be acquired simultaneously. Specific hardware and software are necessary for the electronic orchestration of this capability. Typically, 2, 4, 5, 7, 8, 16, 18 (or more) coils are arranged around the area to be imaged; if a 4-coil configuration is used, then during each TR period, each coil acquires a view of the data as the acquisition sequence proceeds. Lines in k-space are defined only after the processing of linear combinations of the signals that are received by all of the coils. Since 4 views of the data are acquired per TR interval, scan time can be decreased by a factor of 4 (known as the *reduction factor*). However, the acquisition of the signals have gaps, and the FOV in the phase direction is reduced to one-quarter of its original size. This results in a known aliasing of the information (a wrapped image—see section on Artifacts), that is rectified by using the measured sensitivity profile of each coil to calculate from where the signal is coming. This sensitivity profile determines the position of the signal based on its amplitude, where the signal near the coil has a higher amplitude than that farthest away. As a result of the process, commonly known as SENSE (SENSitivity Encoding—there are several acronyms coined by the manufacturers), the image can be unwrapped and combined with the unwrapped images from each of the other coils. A simple two-coil example is shown in Figure 13-9 for a breast image application of SENSE, in which improved resolution is desired over reduced scan time.

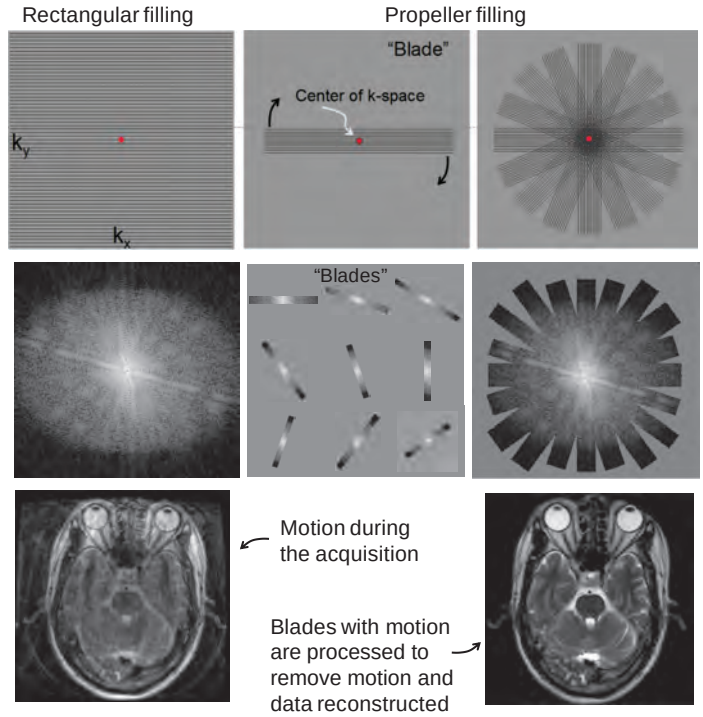

■ **FIGURE 13-8** The propeller data acquisition compared to a rectangular filling of k-space is shown above. Instead of acquiring single lines of information to fill k-space consecutively as shown in the upper left and middle left, a rectangular data acquisition at a specific angle (e.g., 0 degree) is acquired encompassing several lines of k-space, which represents a "blade" of information. The partial acquisition is rotated about the center of k-space at angular increments, which provides a dense sampling of data at the center of k-space and less in the periphery as shown by the schematic (upper right illustration). If the patient moves during a portion of the examination (lower left image), the blades in which the motion occurred can be identified, reprocessed, and the image reconstructed without the motion artifacts (lower right image).

■ **FIGURE 13-9** Parallel imaging with two RF coils. **Top**. A single coil acquisition of a breast MR exam over the full FOV. **Middle**. Individual coils with every-other row of k-space being filled represent ½ FOV, with image overlap caused by aliasing. **Bottom**. After SENSE processing, images are combined to deliver twice the spatial resolution in the left/right (Phase) direction, with the same imaging time.

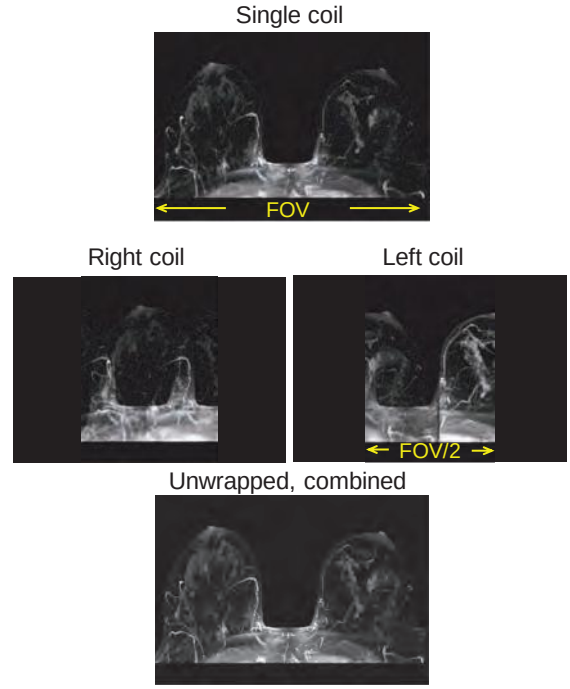

Parallel imaging can be used to either reduce scan times or improve resolution. It also can be used with most pulse sequences. There are obvious benefits in terms of scan times and/or resolution, but there is a slight loss of SNR due to the manipulation of the signals, and chemical shift artifacts (explained in the Artifacts section) may increase. Patient motion can also cause misalignment between the undersampled data and the reference scans of the coils.

Three-Dimensional Fourier Transform Image Acquisition

Three-dimensional image acquisition (volume imaging) requires the use of a broadband, nonselective, or "slab-selective" RF pulse to excite a large volume of protons simultaneously. Two phase gradients are discretely applied in the slice encode and phase encode directions, prior to the frequency encode (readout) gradient (Fig. 13-10). The image acquisition time is equal to

$$\text{TR} \times \#\ \text{Phase Encode Steps (z-axis)} \times \#\ \text{Phase Encode Steps (y-axis)} \times \#\ \text{Signal Averages}$$

A three-dimensional Fourier transform (three one-dimensional Fourier transforms) is applied for each column, row, and depth axis in the image matrix "cube." Volumes obtained can be either isotropic, the same size in all three directions, or anisotropic, where at least one dimension is different in size. The advantage of the former is equal resolution in all directions; reformations of images from the volume do not suffer from degradations of larger sample size from other directions. After the spatial domain data are obtained, individual two-dimensional slices in any arbitrary plane are extracted by interpolation of the cube data.

When using a standard TR of 600 ms with one average for a T1-weighted exam, a 128 × 128 × 128 cube requires 163 min or about 2.7 h! Obviously, this is unacceptable for standard clinical imaging. GE pulse sequences with TR of 50 ms acquire the same image volume in about 15 min. Another shortcut is with anisotropic voxels, where the phase encode steps in one dimension are reduced, albeit with a loss of resolution. A major benefit to isotropic three-dimensional acquisition is the uniform resolution

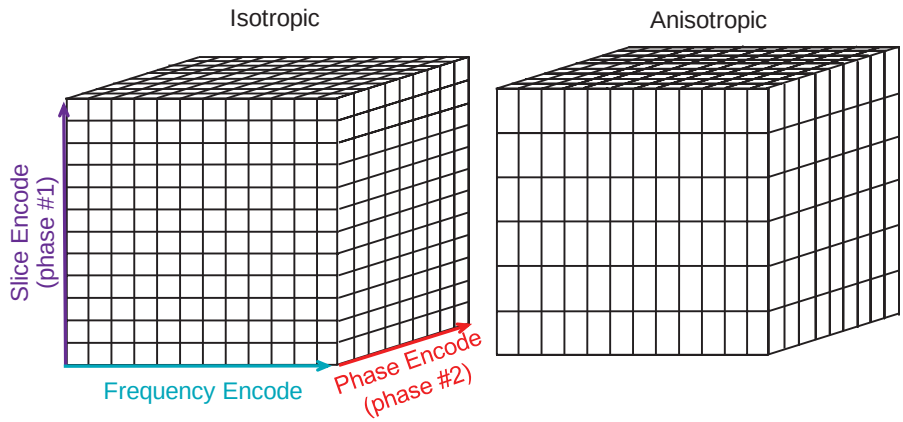

■ **FIGURE 13-10** Three-dimensional image acquisition requires the application of a broadband RF pulse to excite all of the protons in the volume simultaneously, followed by a phase encode gradient along the slice encode direction, a phase encode gradient along the phase encode direction, and a frequency encode gradient in the readout direction. Spatial location is decoded sequentially by the Fourier transform along each encode path, storing intermediate results in the three-dimensional k-space matrix.

in all directions when extracting any two-dimensional image from the matrix cube. In addition, high SNR is achieved compared to a similar two-dimensional image, allowing reconstruction of very thin slices with good detail (less partial volume averaging) and high SNR. A downside is the increased probability of motion artifacts and increased computer hardware requirements for data handling and storage.

13.2 MR Image Characteristics

Spatial Resolution and Contrast Sensitivity

Spatial resolution, contrast sensitivity, and SNR parameters form the basis for evaluating the MR image characteristics. The spatial resolution is dependent on the FOV, which determines pixel size, the gradient field strength, which determines the FOV, the receiver coil characteristics (head coil, body coil, and various surface coil designs), the sampling bandwidth, and the image matrix. Common image matrix sizes are 128 × 128, 256 × 128, 256 × 192, and 256 × 256, with 512 × 256, 512 × 512, and 1,024 × 512 becoming prevalent. In general, MR provides spatial resolution approximately equivalent to that of CT, with pixel dimensions on the order of 0.5 to 1.0 mm for a high-contrast object and a reasonably large FOV (greater than 250 mm). A 250 mm FOV and a 256 × 256 matrix will have a pixel size on the order of 1 mm. In small FOV acquisitions with high gradient strengths and with surface coil receivers, the effective pixel size can be smaller than 0.1 to 0.2 mm (of course, with a limited FOV of 25 to 50 mm. Slice thickness in MRI is usually 5 to 10 mm and represents the dimension that produces the most partial volume averaging.

Spatial resolution can be improved with higher field strength magnets due to a larger SNR, which allows thinner slice acquisition, and/or higher sampling rates (smaller pixels) for a given acquisition. However, with higher B_0, increased RF absorption, artifact production, and a lengthening of T1 relaxation occur. The latter decreases T1 contrast sensitivity because of increased saturation of the longitudinal magnetization.

Contrast sensitivity is the major attribute of MR. The spectacular contrast sensitivity of MR enables the exquisite discrimination of soft tissues and contrast due to blood flow. This sensitivity is achieved through differences in the T1, T2, proton density, and flow velocity characteristics. Contrast, which is dependent upon these parameters, is achieved through the proper application of pulse sequences, as discussed previously. MR contrast materials, usually susceptibility agents that disrupt the local magnetic field to enhance T2 decay or provide a relaxation mechanism for shorter T1 recovery time (e.g., bound water in hydration layers), are becoming important enhancement agents for differentiation of normal and diseased tissues. The absolute contrast sensitivity of the MR image is ultimately limited by the SNR and presence of image artifacts.

Signal-to-Noise Ratio, SNR

There are numerous dependencies on the ultimate SNR achievable by the MR system. The intrinsic signal intensity based on T1, T2, and proton density parameters has been discussed; to summarize, the TR, TE, and flip angle will have an impact on the magnitude of the signal generated in the image. While there are many mitigating factors, a long TR increases the longitudinal magnetization recovery and increases the SNR; a long TE increases the transverse magnetization decay and reduces the SNR; a smaller flip angle (reduced from 90 degrees) reduces the SNR. Therefore, spin echo pulse sequences with large flip angle, long TR, short TE, coarse matrix,

large FOV, thick slices, and many averages will generate the best SNR; however, the resultant image may not be clinically relevant or desirable. While SNR is important, it's not everything.

For a given pulse sequence (TR, TE, flip angle), the SNR of the MR image is dependent on a number of variables, as shown in the equation below for a two-dimensional image acquisition:

$$\text{SNR} \propto I \times \text{voxel}_{x,y,z} \times \frac{\sqrt{\text{NEX}}}{\sqrt{\text{BW}}} \times \text{f(QF)} \times \text{f(B)} \times \text{f(slice gap)} \times \text{f(reconstruction)}$$

where I is the intrinsic signal intensity based on pulse sequence, $\text{voxel}_{x,y,z}$ is the voxel volume, determined by FOV, image matrix, and slice thickness, NEX is the number of excitations, determined by the number (or fractional number) of repeated signal acquisitions into the same voxels. BW is the frequency bandwidth of the RF receiver, f(QF) is the function of the coil quality factor parameter (tuning the coil), f(B) is the function of magnetic field strength, B, f(slice gap) is the function of interslice gap effects, and f(reconstruction) is the function of the reconstruction algorithm.

Other factors in the above equation are explained briefly below.

Voxel Volume

The voxel volume is equal to

$$\text{Volume} = \frac{\text{FOV}_x}{\text{No. of pixels, } x} \times \frac{\text{FOV}_y}{\text{No. of pixels, } y} \times \text{Slice thickness, } z$$

SNR is linearly proportional to the voxel volume. Thus, by reducing the image matrix size from 256 × 256 to 256 × 128 over the same FOV, the effective voxel size increases by a factor of two, and therefore increases the SNR by a factor of two for the same image acquisition time (e.g., 256 phase encodes with one average versus 128 phase encodes with two averages).

Signal Averages

Signal averaging (also known as number of excitations, NEX) is achieved by averaging sets of data acquired using an identical pulse sequence (same PEG strength). The SNR is proportional to the square root of the number of signal averages. A 2-NEX acquisition requires a doubling (100% increase) of the acquisition time for a 40% increase in the SNR $\left(\sqrt{2} = 1.4\right)$ Doubling the SNR requires 4 NEX. In some cases, less than 1 average (e.g., ½ or ¾ NEX) can be selected. Here, the number of phase encode steps is reduced by ½ or ¼, and the missing data are synthesized in the k-space matrix. Imaging time is therefore reduced by a similar amount; however, a loss of SNR accompanies the shorter imaging times by the same square root factor.

RF Bandwidth

The receiver bandwidth defines the range of frequencies to which the detector is tuned during the application of the readout gradient. A narrow bandwidth (a narrow spread of frequencies around the center frequency) provides a higher SNR, proportional to $\frac{1}{\sqrt{\text{BW}}}$. A twofold reduction in RF bandwidth—from 8 to 4 kHz,

for instance—increases the SNR by 1.4 × (40% increase). This is mainly related to the fact that the white noise, which is relatively constant across the bandwidth, does not change, while the signal distribution changes with bandwidth. In the spatial domain, bandwidth is inversely proportional to the sample dwell time, ΔT to sample the signal: BW = 1/ΔT. Therefore, a narrow bandwidth has a longer dwell time, which increases the signal height (Fig. 13-11), compared to the shorter dwell time for the broad bandwidth signal, thus spreading the signal over a larger range of frequencies. The SNR is reduced by the square root of the dwell time. However, any decrease in RF bandwidth must be coupled with a decrease in gradient strength to maintain the sampling across the FOV, which might be unacceptable if chemical shift artifacts are of concern (see Artifacts, below). Narrower bandwidths also require a longer time for sampling, and therefore affect the minimum TE time that is possible for an imaging sequence. Clinical situations that can use narrow bandwidths are with T2-weighted images and long TEs that allow the echo to evolve over an extended period, particularly in situations where fat saturation pulses are used to reduce the effects of chemical shift in the acquired images. Use of broad bandwidth settings is necessary when very short TEs are required, such as in fast GE imaging to reduce the sampling time.

RF Coil Quality Factor

The coil quality factor is an indication of RF coil sensitivity to induced currents in response to signals emanating from the patient. Coil losses that lead to lower SNR are caused by patient "loading" effects and eddy currents, among other factor. Patient loading refers to the electric impedance characteristics of the body, which to a certain extent acts like an antenna. This effect causes a variation in the magnetic field that is different

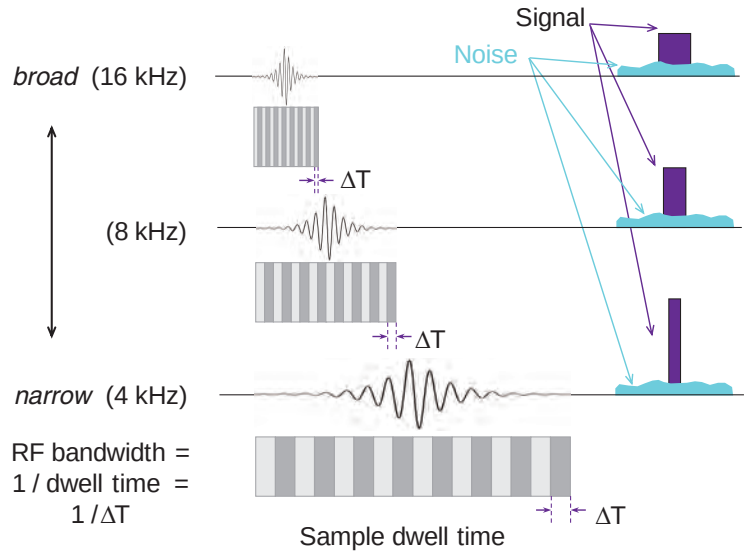

■ **FIGURE 13-11** RF Receiver Bandwidth is determined by the FEG strength, the FOV, and sampling rate. This figure illustrates the spatial domain view of SNR and corresponding sample dwell time. Evolution of the echo in the broad bandwidth situation occurs rapidly with minimal dwell time, which might be needed in situations where very short TE is required, even though the SNR is reduced. On the other hand, in T2 weighted images requiring a long TE, narrow bandwidth can improve SNR.

for each patient, and must be measured and corrected for. Consequently, tuning the receiver coil to the resonance frequency is mandatory before image acquisition. Eddy currents are signals that are opposite of the induced current produced by transverse magnetization in the RF coil, and reduce the overall signal. Quadrature coils increase the SNR as two coils are used in the reception of the signal; phased array coils increase the SNR even more when the data from several coils are added together (see Parallel Imaging, Section 13.1). The proximity of the receiver coil to the volume of interest affects the coil quality factor, but there are trade-offs with image uniformity. Positioning of the coil with respect to the direction of the main magnetic field is also an issue that occurs with air core (horizontal B_0) to solid core (vertical B_0) magnets. Body receiver coils positioned in the bore of the magnet have a moderate quality factor, whereas surface coils have a high quality factor. With the body coil, the signal is relatively uniform across the FOV; however, with surface coils, the signal falls off abruptly near the edges of the field, limiting the useful imaging depth and resulting in nonuniform brightness across the image.

Magnetic Field Strength

Magnetic field strength influences the SNR of the image by a factor of $B^{1.0}$ to $B^{1.5}$. Thus, one would expect a three- to fivefold improvement in SNR with a 1.5 T magnet over a 0.5 T magnet. Although the gains in the SNR are real, other considerations mitigate the SNR improvement in the clinical environment, including longer T1 relaxation times and greater RF absorption, as discussed previously.

Cross-Excitation

Cross-excitation occurs from the nonrectangular RF excitation profiles in the spatial domain and the resultant overlap of adjacent slices in multislice image acquisition sequences. This saturates the protons and reduces contrast and the contrast-to-noise ratio. To avoid cross-excitation, interslice gaps or interleaving procedures are necessary (see Artifacts section, below).

Image Acquisition and Reconstruction Algorithms

Image acquisition and reconstruction algorithms have a profound effect on SNR. The various acquisition/reconstruction methods that have been used in the past and those used today are, in order of increasing SNR, point acquisition methods, line acquisition methods, two-dimensional Fourier transform acquisition methods, and three-dimensional Fourier transform volume acquisition methods. In each of these techniques, the volume of tissue that is excited is the major contributing factor to improving the SNR and image quality. Reconstruction filters and image processing algorithms will also affect the SNR. High-pass filtration methods that increase edge definition will generally decrease the SNR, while low-pass filtration methods that smooth the image data will generally increase the SNR at the cost of reduced resolution.

Summary, Image Quality

The best possible image quality is always desirable, but not always achievable because of the trade-off between SNR, scan speed, and spatial resolution. To increase one of these three components of image quality involves the consideration of reducing one or both of the other two. It is thus a balancing act that is chosen by the operator, the protocol, and the patient in order to acquire images with the best diagnostic yield.

MR parameters that may be changed include TR, TE, TI, ETL, Matrix Size, Slice Thickness, Field of view, and NEX. Working with these parameters in the optimization of acquisition protocols to achieve high image quality is essential.

13.3 Signal from Flow

The appearance of moving fluid (vascular and cerebrospinal fluid [CSF]) in MR images is complicated by many factors, including flow velocity, vessel orientation, laminar versus turbulent flow patterns, pulse sequences, and image acquisition modes. Flow-related mechanisms combine with image acquisition parameters to alter contrast. Signal due to flow covers the entire gray scale of MR signal intensities, from "black blood" to "bright blood" levels, and flow can be a source of artifacts. The signal from flow can also be exploited to produce MR angiographic images.

Low signal intensities (flow voids) are often a result of *high-velocity signal loss* (HVSL), in which protons in the flowing blood move out of the slice during echo reformation, causing a lower signal. *Flow turbulence* can also cause flow voids, by causing a dephasing of protons in the blood with a resulting loss of the tissue magetization in the area of turbulence. With HVSL, the amount of signal loss depends on the velocity of the moving fluid. Pulse sequences to produce "black blood" in images can be very useful in cardiac and vascular imaging. A typical black blood pulse sequence uses a "double inversion recovery" method, whereby a nonselective 180-degree RF pulse is initially applied, inverting all protons in the body, and is followed by a selective 180-degree RF pulse that restores the magnetization in the selected slice. During the inversion time, blood outside of the excited slice with inverted protons flows into the slice, producing no signal; therefore, the blood appears dark.

Flow-Related Enhancement

Flow-related enhancement is a process that causes increased signal intensity due to flowing protons; it occurs during imaging of a volume of tissues. *Even-echo rephasing* is a phenomenon that causes flow to exhibit increased signal on even echoes in a multiple-echo image acquisition. Flowing protons that experience two subsequent 180-degree pulses (even echoes) generate higher signal intensity due to a constructive rephasing of protons during echo formation. This effect is prominent in slow laminar flow (e.g., veins show up as bright structures on even-echo images).

Flow enhancement in GE images is pronounced for both venous and arterial structures, as well as CSF. The high intensity is caused by the wash-in (between subsequent RF excitations) of fully unsaturated protons into a volume of partially saturated protons due to the short TR used with gradient imaging. During the next excitation, the signal amplitude resulting from the moving unsaturated protons is about 10 times greater than that of the nonmoving saturated protons. With GE techniques, the degree of enhancement depends on the velocity of the blood, the slice or volume thickness, and the TR. As blood velocity increases, unsaturated blood exhibits the greatest signal. Similarly, a thinner slice or decreased repetition time results in higher flow enhancement. In arterial imaging of high-velocity flow, it is possible to have bright blood throughout the imaging volume of a three-dimensional acquisition if unsaturated blood can penetrate into the volume prior to experiencing an RF pulse.

Signal from blood is dependent on the relative saturation of the surrounding tissues and the incoming blood flow in the vasculature. In a multislice volume,

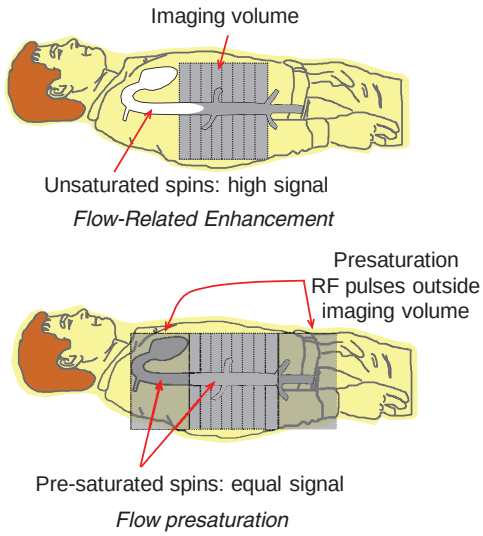

■ **FIGURE 13-12** The repeated RF excitation within an imaging volume produces partial saturation of the tissue magnetization (**top** figure, **gray** area). Unsaturated protons flowing into the volume generate a large signal difference that is bright relative to the surrounding tissues. Bright blood effects can be reduced by applying pre-saturation RF pulses adjacent to the imaging volume, so that protons in inflowing blood will have a similar partial saturation (**bottom** figure; note no blood signal).

repeated excitation of the tissues and blood causes a partial saturation of the protons, dependent on the T1 characteristics and the TR of the pulse sequence. Blood outside of the imaged volume does not interact with the RF excitations, and therefore these unsaturated protons may enter the imaged volume and produce a large signal compared to the blood within the volume. This is known as flow-related enhancement. As the pulse sequence continues, the unsaturated blood becomes partially saturated and the protons of the blood produce a similar signal to the tissues in the inner slices of the volume (Fig. 13-12). In some situations, flow-related enhancement is undesirable and is eliminated with the use of "presaturation" pulses applied to volumes just above and below the imaging volume. These same saturation pulses are also helpful in reducing motion artifacts caused by adjacent tissues outside the imaging volume.

MR Angiography

Exploitation of blood flow enhancement is the basis for MRA. Two techniques to create images of vascular anatomy include time-of-flight and phase contrast angiography.

Time-of-Flight Angiography

The time-of-flight technique relies on the tagging of blood in one region of the body and detecting it in another. This differentiates moving blood from the surround stationary tissues. Tagging is accomplished by proton saturation, inversion, or relaxation to change the longitudinal magnetization of moving blood. The penetration of the tagged blood into a volume depends on the T1, velocity, and direction of the blood. Since the detectable range is limited by the eventual saturation of the tagged blood, long vessels are difficult to visualize simultaneously in a three-dimensional volume. For these reasons, a two-dimensional stack of slices is typically acquired, where even slowly moving blood can penetrate the region of RF excitation in thin slices (Fig. 13-13). Each slice is acquired separately, and blood moving in one direction (north or south, e.g., arteries versus veins) can be selected by delivering a presaturation pulse on an adjacent slab superior or inferior to the slab of data acquisition. Thin slices are also helpful in preserving resolution of the flow pattern. Often used for the two-dimensional

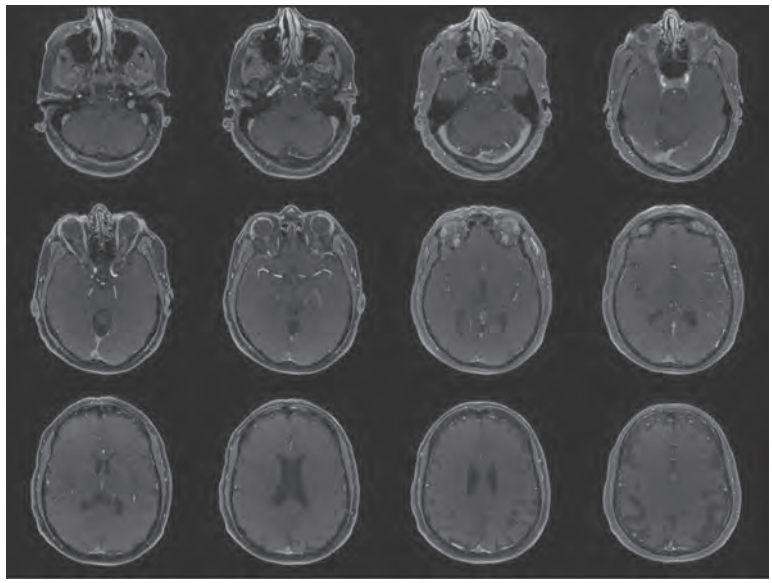

■ **FIGURE 13-13** The *time of flight* MRA acquisition collects each slice separately with a sequence to enhance blood flow. Exploitation of blood flow is achieved by detecting unsaturated protons moving into the volume, producing a bright signal. A coherent GE image acquisition pulse sequence is shown, TR = 24 ms, TE = 3.1 ms, Flip Angle = 20 degrees. Every 10th image in the stack is displayed above, from left to right and top to bottom.

image acquisition is a "GRASS" or "FISP" GE technique that produces relatively poor anatomic contrast, yet provides a high-contrast "bright blood" signal. Magnetization transfer contrast sequences (see below) are also employed to increase the contrast of the signals due to blood by reducing the background anatomic contrast.

Two-dimensional TOF MRA images are obtained by projecting the content of the stack of slices at a specific angle through the volume. A maximum intensity projection (MIP) algorithm detects the largest signal along a given ray through the volume and places this value in the image (Fig. 13-14). The superimposition of residual

■ **FIGURE 13-14** A simple illustration shows how the MIP algorithm extracts the highest (maximum) signals in the two-dimensional stack of images along a specific direction in the volume, and produces projection images with maximum intensity variations as a function of angle.

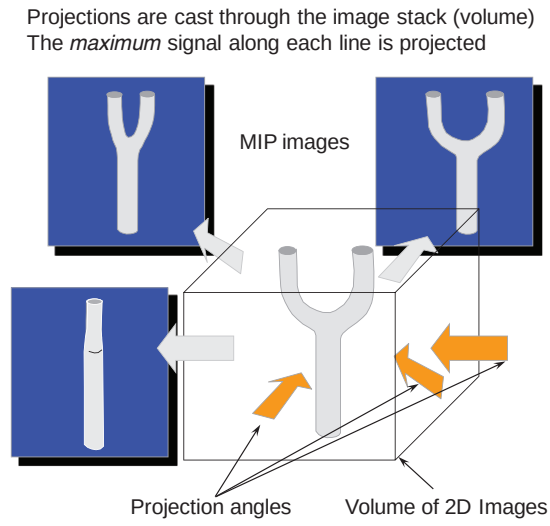

stationary anatomy often requires further data manipulation to suppress undesirable signals. This is achieved in a variety of ways, the simplest of which is setting a window threshold. Another method is to acquire a dataset without contrast, and subtract the noncontrast MIP from the contrast MIP to reduce background signals. Clinical MRA images show the three-dimensional characteristics of the vascular anatomy from several angles around the volume stack (Fig. 13-15) with some residual signals from the stationary anatomy. Time-of-flight angiography often produces variation in vessel intensity dependent on orientation with respect to the image plane, a situation that is less than optimal.

Phase Contrast Angiography

Phase contrast imaging relies on the phase change that occurs in moving protons such as blood. One method of inducing a phase change is dependent on the application of a bipolar gradient (one gradient with positive polarity followed by a second gradient with negative polarity, separated by a delay time ΔT). In a second acquisition of the same view of the data (same PEG), the polarity of the bipolar gradients is reversed, and moving protons are encoded with negative phase, while the stationary protons exhibit no phase change (Fig. 13-16). Subtracting the second excitation from the first cancels the magnetization due to stationary protons but enhances magnetization due to moving protons. Alternating the bipolar gradient polarity for each subsequent excitation during the acquisition provides phase contrast image information. The degree of phase shift is directly related to the velocity encoding (VENC) time, ΔT, between the positive and negative lobes of the bipolar gradients and the velocity of the protons within the excited volume. Proper selection of the VENC time

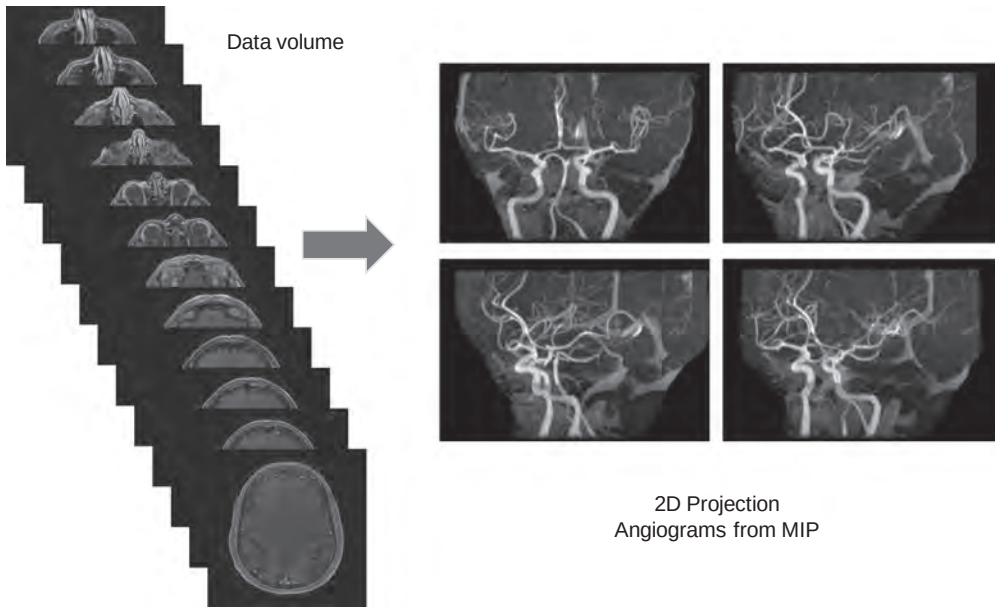

■ **FIGURE 13-15** A volume stack of bright blood images (left) is used with MIP processing to create a series of projection angiograms at regular intervals; the three-dimensional perspective is appreciated in a stack view, with virtual rotation of the vasculature.

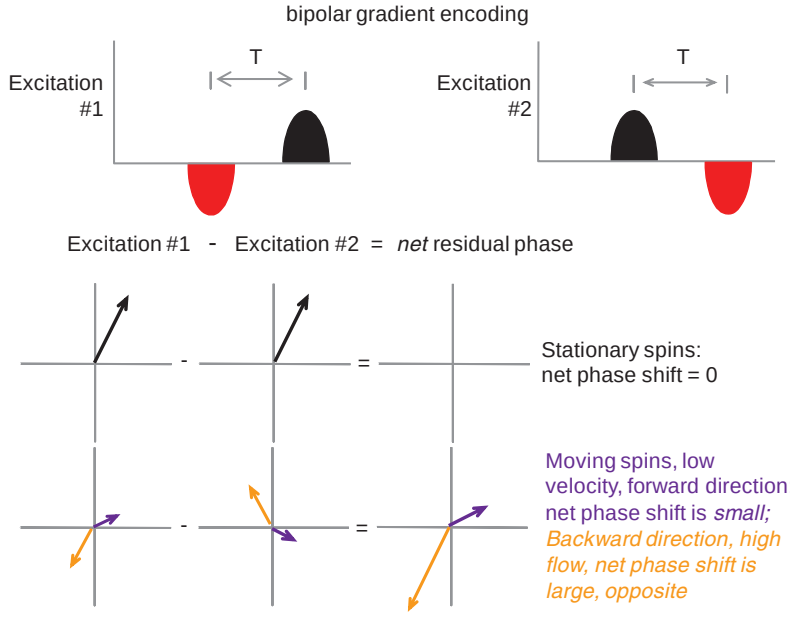

■ **FIGURE 13-16** Phase Contrast Angiography uses consecutive excitations that have a bipolar gradient encoding with the polarity reversed between the first and second excitation, as shown in the top row. Magnetization vectors (lower two rows) illustrate the effect of the bipolar gradients on stationary and moving spins for the first and second excitations. Subtracting the two will cancel stationary tissue magnetization and enhance phase differences caused by the velocity of moving blood.

is necessary to avoid phase wrap error (exceeding 180-degree phase change) and to ensure an optimal phase shift range for the velocities encountered. Intensity variations are dependent on the amount of phase shift, where the brightest pixel values represent the largest forward (or backward) velocity, a mid-scale value represents 0 velocity, and the darkest pixel values represent the largest backward (or forward) velocity. Figure 13-17 shows a representative magnitude and phase contrast image of the cardiac vasculature. Unlike the time-of-flight methods, the phase contrast image

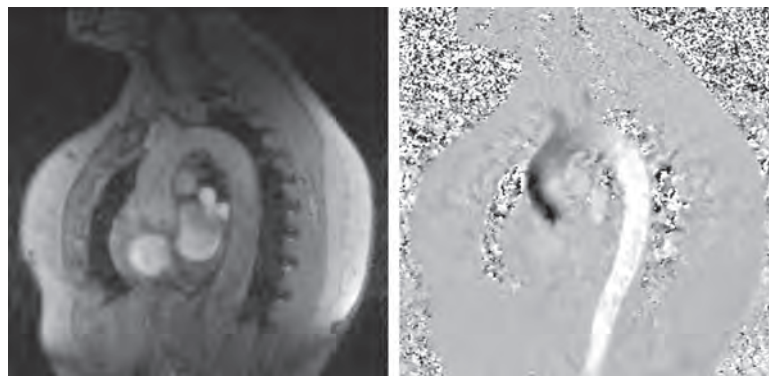

■ **FIGURE 13-17** Magnitude (**left**) and phase (**right**) images provide contrast of flowing blood. Magnitude images are sensitive to flow, but not to direction; phase images provide direction and velocity information. The blood flow from the heart shows forward flow in the ascending aorta (*dark* area) and forward flow in the descending aorta at this point in the heart cycle for the phase image. Some bright flow patterns in the ascending aorta represent backward flow to the coronary arteries. Grayscale amplitude is proportional to velocity, where intermediate grayscale is 0 velocity.

is inherently quantitative, and when calibrated carefully, provides an estimate of the mean blood flow velocity and direction. Two- and three-dimensional phase contrast image acquisitions for MRA are possible.

Gradient Moment Nulling

In spin echo and gradient recalled echo imaging, the slice select and readout gradients are balanced, so that the uniform dephasing with the initial gradient application is rephased by an opposite polarity gradient of equal area. However, when moving protons are subjected to the gradients, the amount of phase dispersion is not compensated (Fig. 13-18). This phase dispersal can cause ghosting (faint, displaced copies of the anatomy) in images. It is possible, however, to rephase the protons by a gradient moment nulling technique. With constant velocity flow (first-order motion), all protons can be rephased using the application of a gradient triplet. In this technique, an initial positive gradient of unit area is followed by a negative gradient of twice the area, which creates phase changes that are compensated by a third positive gradient of unit area. The velocity compensated gradient (right graph in Fig. 13-18) depicts the evolution of the proton phase back to zero for both stationary and moving protons. Note that the overall applied gradient has a net area of zero—equal to the sum of the positive and negative areas. Higher order corrections such as second- or third-order moment nulling to correct for acceleration and other motions are possible, but these techniques require more complicated gradient switching. Gradient moment nulling can be applied to both the slice select and readout gradients to correct for problems such as motion ghosting as elicited by CSF pulsatile flow.

13.3 Perfusion and Diffusion Contrast Imaging

Perfusion of tissues via the capillary bed permits the delivery of oxygen and nutrients to the cells and removal of waste (e.g., CO_2) from the cells. Conventional perfusion measurements are based on the uptake and wash-out of radioactive tracers or other exogenous tracers that can be quantified from image sequences using well-characterized imaging equipment and calibration procedures. For MR perfusion images, exogenous

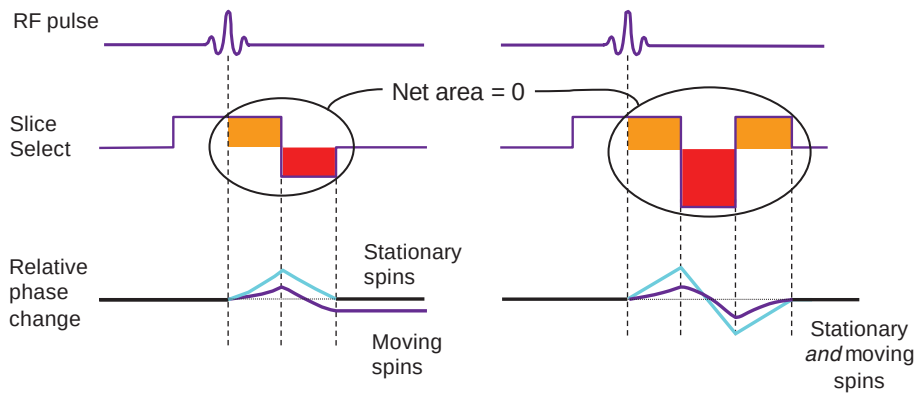

■ **FIGURE 13-18** **Left.** Phase dispersion of stationary and moving spins under the influence of an applied gradient (no flow compensation) as the gradient is inverted is shown. The stationary spins return to the original phase state, whereas the moving spins do not. **Right**. *Gradient moment nulling* of first order linear velocity (flow compensation) requires a doubling of the negative gradient amplitude followed by a positive gradient such that the total summed area is equal to zero. This will return both the stationary spins *and* the moving spins back to their original phase state.

and endogenous tracer methods are used. Freely diffusible tracers using nuclei such as ^{2}H (deuterium), ^{3}He, ^{17}O, and ^{19}F are employed in experimental procedures to produce differential contrast in the tissues. More clinically relevant are intravascular blood pool agents such as gadolinium–diethylenetriaminepentaacetic acid, which modify the relaxation of protons in the blood in addition to producing a shorter T2*. This produces signal changes that can be visualized in pre and post contrast images (Fig. 13-19). Endogenous tracer methods do not use externally added agents, but instead depend on the ability to generate contrast from specific excitation or diffusion mechanisms. For example, labeling of inflowing protons ("black blood" perfusion) uses protons in the blood as the contrast agent. Tagged (labeled) protons outside of the imaging volume perfuse into the tissues, resulting in a drop in signal intensity, a time course of events that can be monitored by quantitative measurements.

Functional MRI (fMRI) is based on the increase in blood flow to the local vasculature that accompanies neural activity in the specific areas of the brain, resulting in a local reduction of deoxyhemoglobin because the increase in blood flow occurs without an increase in oxygen extraction. As deoxyhemoglobin is a paramagnetic agent, it alters the T2*-weighted MRI image signal. Thus, this endogenous contrast enhancing agent serves as the signal for fMRI. Area voxels (represented by x-y coordinates and z slice thickness) of high metabolic activity resulting from a task-induced stimulus produce a correlated signal for Blood Oxygen Level Dependent (BOLD) acquisition techniques. A BOLD sequence produces multiple T2*-weighted images of the head before the application of the stimulus. The patient is repeatedly subjected to the stimulus and multiple BOLD images are acquired. Because the BOLD sequence produces images that are highly dependent on blood oxygen levels, areas of high metabolic activity will demonstrate a change in signal when the prestimulus image data set is subtracted, voxel by voxel, from post-stimulus image data set. Voxel locations defined by significant

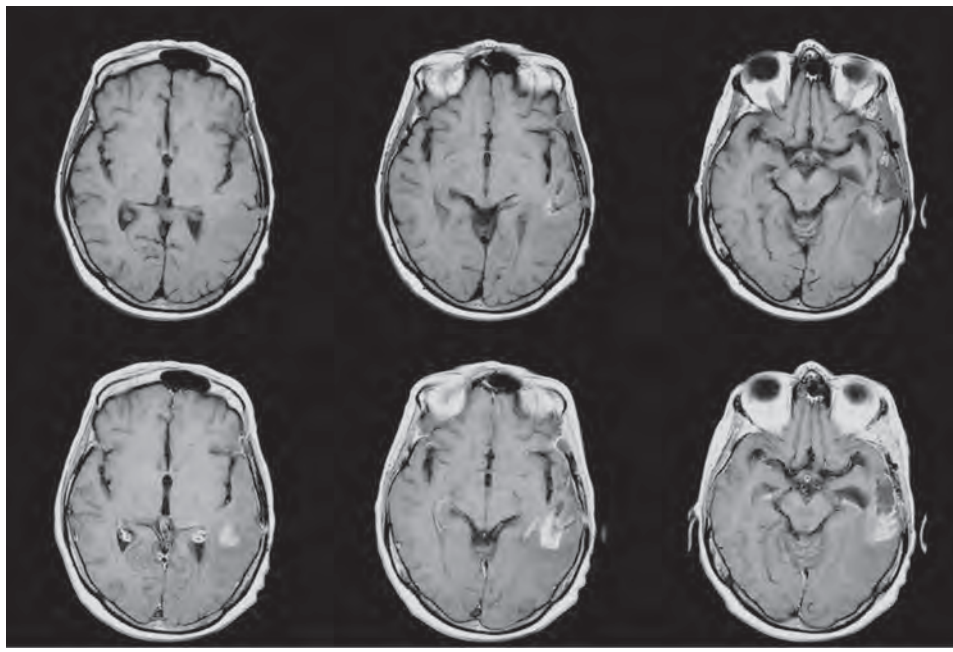

■ **FIGURE 13-19** Pre (**top row**) and post (**bottom row**) gadolinium contrast T1-weighted MR axial images of the brain illustrate the signal change that occurs with the appearance of gadolinium by shortening the T1 time of the perfused tissues.

signal changes indicate regions of the brain activated by a specific task. Stimuli in fMRI experiments can be physical (finger movement), sensory (light flashes or sounds), or cognitive (repetition of "good" or "bad" word sequences, complex problem solving), among others. To improve the SNR in the fMRI images, a stimulus is typically applied in a repetitive, periodic sequence, and BOLD images are acquired continuously, tagged with the timing of the stimulus. Regions in the brain that demonstrate time-dependent activity and correlate with the time-dependent application of the stimulus are statistically analyzed, and coded using a color scale, while voxels that do not show a significant intensity change are not colored. The resultant color map is overlaid onto a grayscale image of the brain for anatomic reference, as shown in Figure 13-20.

High-speed imaging and T2* weighting necessary for fMRI is typically achieved with EPI acquisition techniques that can be acquired in as little as 50 ms for a 64 × 64 acquisition matrix. Gradient Recalled Echo acquisitions using standard sequences are also employed with multiple contiguous slices (e.g., 16 slices, slice thickness 5 mm, TR = 3 s, TE = 60 ms, 90-degree flip angle) at 1.5 T, with 25 to 30 complete head acquisitions. The latter acquisition techniques provide better spatial resolution but rely on very cooperative subjects and a much longer exam time.

Diffusion Weighted Imaging

Diffusion relates to the random motion of water molecules in tissues. Interaction of the local cellular structure with the movement of water molecules produces anisotropic, directionally dependent diffusion (e.g., in the white matter of brain tissues).

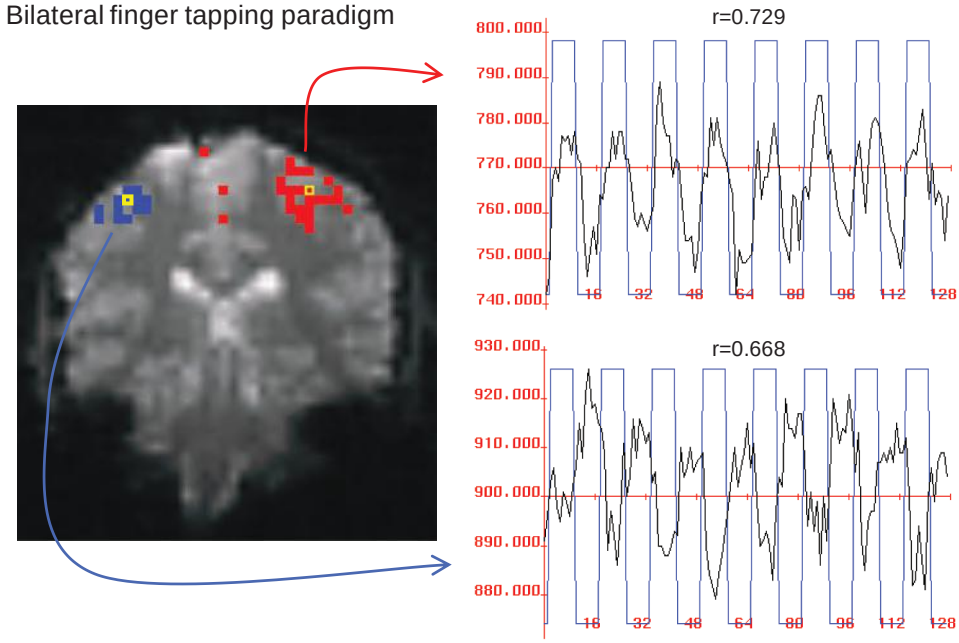

■ **FIGURE 13-20** Functional MR image bilateral finger tapping paradigm shows the areas of the brain activated by this repeated activity. The paradigm was a right finger tap alternated by a left finger tap (time sequence on the right side of the figure) and the correlated BOLD signals (*black traces*) derived from the echo planar image sequence. A voxel-by-voxel correlation of the periodic stimulus and MR signal is performed, and when exceeding a correlation threshold, a color overlay is added to the grayscale image. In this example, *red* indicates the right finger tap that excites the left motor cortex, which appears on the right side of the image, and blue the left finger tap. (Figure compliments of MH Buonocore, MD, PhD University of California Davis.)

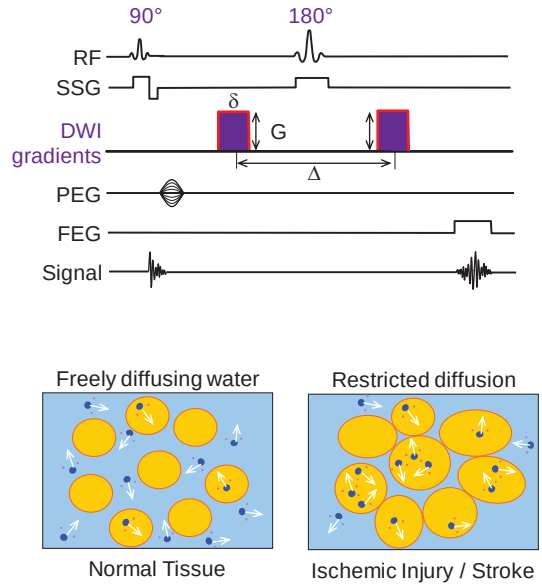

■ **FIGURE 13-21** The basic elements of a DWI pulse sequence are shown. The diffusion weighting gradients are of amplitude G, duration of the gradients δ and time between gradients is Δ.

Diffusion sequences use strong MR gradients applied symmetrically about the refocusing pulse to produce signal differences based on the mobility and directionality of water diffusion, as shown in Figure 13-21. Tissues with more water mobility (normal) have a greater signal loss than those of lesser water mobility (injury) under the influence of the diffusion weighted imaging (DWI) gradients.

The in vivo structural integrity of certain tissues (healthy, diseased, or injured) can be measured by the use of DWI, in which water diffusion characteristics are determined through the generation of apparent diffusion coefficient (ADC) maps. This requires two or more acquisitions with different DWI parameters. A low ADC corresponds to high signal intensity on a calculated image, which represents restricted diffusion (Fig. 13-22). ADC maps of the brain and the spinal cord have shown prom-

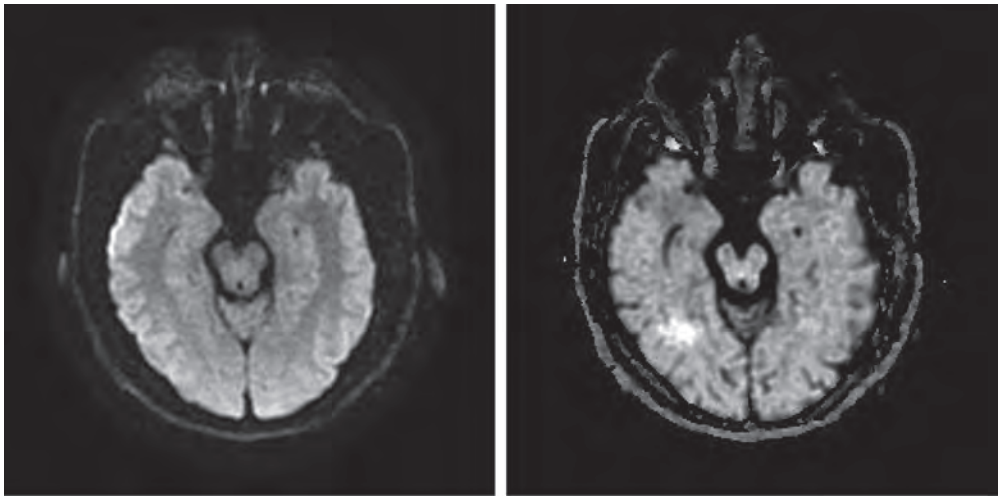

■ **FIGURE 13-22** **Left**. Diffusion weighted image. **Right**. Calculated ADC image, showing an area of increased brightness related to restricted mobility of water molecules.

ise in predicting and evaluating pathophysiology before it is visible on conventional T1- or T2-weighted images. DWI is also a sensitive indicator for early detection of ischemic injury. Areas of acute stroke show a drastic reduction in the diffusion coefficient compared with nonischemic tissues. Diagnosis of multiple sclerosis is a potential application, based on the measurements of the diffusion coefficients in three-dimensional space.

Various acquisition techniques are used to generate diffusion-weighted contrast. Standard spin echo and EPI pulse sequences with applied diffusion gradients of high strength are used. Challenges for DWI are the extreme sensitivity to motion of the head and brain, which is chiefly caused by the large pulsed gradients required for the diffusion preparation. Eddy currents are also an issue, which reduce the effectiveness of the gradient fields, so compensated gradient coils are necessary. Several strategies have been devised to overcome the motion sensitivity problem, including common electrocardiographic gating and motion compensation methods.

13.4 Magnetization Transfer Contrast

Magnetization transfer contrast is the result of selective observation of the interaction between protons in free water molecules and protons contained in the macromolecules of a protein. Magnetization exchange occurs between the two proton groups because of coupling or chemical exchange. Because the protons exist in slightly different magnetic environments, the selective saturation of the protons in the macromolecule can be excited separately from the bulk water by using narrow-band RF pulses (because the Larmor frequencies are different). A transfer of the magnetization from the protons in the macromolecule partially saturates the protons in bulk water, even though these protons have not experienced an RF excitation pulse (Fig. 13-23). Reduced signal from the

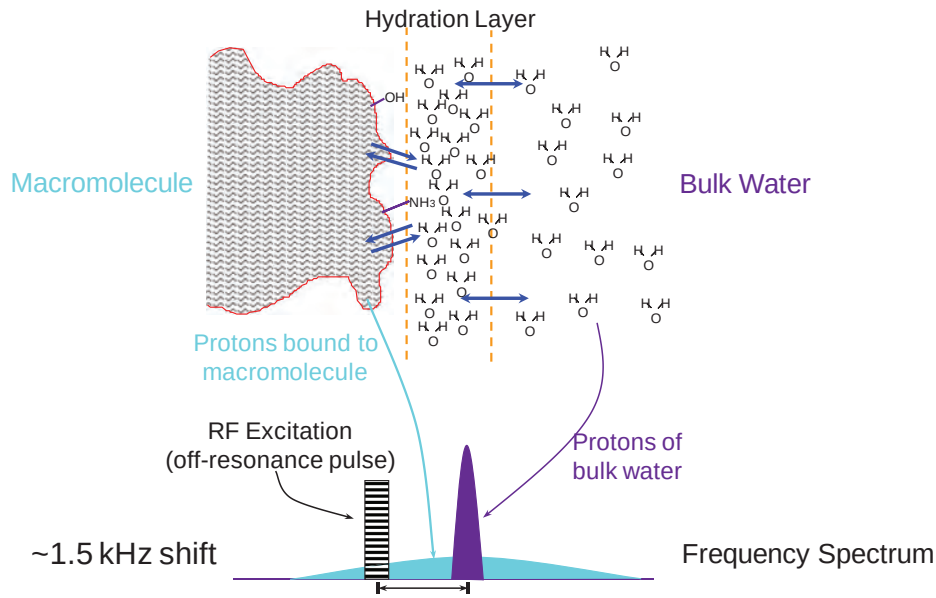

■ **FIGURE 13-23** Magnetization transfer contrast is implemented with an off-resonance RF pulse of about 1,500 Hz from the Larmor frequency. Excitation of hydrogen atoms on macromolecules is transferred via the hydration layer to adjacent "free-water" hydrogen atoms. A partial saturation of the tissues reduces the signals that would otherwise compete with signals from blood flow, making this useful for time-of-flight MRA.

adjacent free water protons by the saturation "label" affects only those protons having a chemical exchange with the macromolecules and improves local image contrast in many situations by decreasing the otherwise large signal generated by the protons in the bulk water. This technique is used for anatomic MRI of the heart, the eye, multiple sclerosis, knee cartilage, and general MRA. Tissue characterization is also possible, because the image contrast in part is caused by the surface chemistry of the macromolecule and the tissue-specific factors that affect the magnetization transfer characteristics.

Magnetization transfer contrast pulse sequences are often used in conjunction with MRA time-of-flight methods. Hydrogen atoms constitute a large fraction of macromolecules in proteins, are tightly bound to these macromolecules, and have a very short T2 decay with a broad range of resonance frequencies compared to protons in free water. Selective excitation of these protons is achieved with an off-resonance RF pulse of approximately 1,500 Hz from the Larmor frequency, causing their saturation. The protons in the hydration layer bound to these molecules are affected by the magnetization and become partially saturated themselves. MR signals from these tissues are suppressed, with an impact of reducing the contrast variation of the anatomy. As a result, the differential contrast of the flow-enhanced signals is increased, with overall better image quality angiographic sequence.

13.5 MR Artifacts

Artifacts manifest as positive or negative signal intensities that do not accurately represent the imaged anatomy. Although some artifacts are relatively insignificant and are easily identified, others can limit the diagnostic potential of the exam by obscuring or mimicking pathologic processes or anatomy. One must realize the impact of MR acquisition protocols and understand the etiology of artifact production to exploit the information they convey.

To minimize the impact of MR artifacts, a working knowledge of MR physics as well as image acquisition techniques is required. On the one hand, there are many variables and options available that complicate the decision-making process for MR image acquisition. On the other, the wealth of choices enhances the goal of achieving diagnostically accurate images. MR artifacts are classified into three broad areas—those based on the machine, on the patient, and on signal processing.

Machine-Dependent Artifacts

Magnetic field inhomogeneities are either global or focal field perturbations that lead to the mismapping of tissues within the image, and cause more rapid T2 relaxation. Distortion or misplacement of anatomy occurs when the magnetic field is not completely homogeneous. Proper site planning, self-shielded magnets, automatic shimming, and preventive maintenance procedures help to reduce inhomogeneities.

Focal field inhomogeneities arise from many causes. Ferromagnetic objects in or on the patient (e.g., makeup, metallic implants, prostheses, surgical clips, dentures) produce field distortions and cause protons to precess at frequencies different from the Larmor frequency in the local area. Incorrect proton mapping, displacement, and appearance as a signal void with a peripherally enhanced rim of increased signal are common findings. Geometric distortion of surrounding tissue is also usually evident. Even nonferromagnetic conducting materials (e.g., aluminum) produce field distortions that disturb the local magnetic environment. Partial compensation by the spin echo (180-degree RF) pulse sequence reduces these artifacts; on the other

hand, the gradient-refocused echo sequence accentuates distortions, since the protons always experience the same direction of the focal magnetic inhomogeneities within the patient.

Susceptibility Artifacts

Magnetic susceptibility is the ratio of the induced internal magnetization in a tissue to the external magnetic field. As long as the magnetic susceptibility of the tissues being imaged is relatively unchanged across the field of view, then the magnetic field will remain uniform. Any drastic changes in the magnetic susceptibility will distort the magnetic field. The most common susceptibility changes occur at tissue-air interfaces (e.g., lungs and sinuses), which cause a signal loss due to more rapid dephasing (T2*) at the tissue-air interface (Fig. 13-24). Any metal (ferrous or not) may have a significant effect on the adjacent local tissues due to changes in susceptibility and the resultant magnetic field distortions. Paramagnetic agents exhibit a weak magnetization and increase the local magnetic field causing an artifactual reduction in the surrounding T2* relaxation.

Magnetic susceptibility can be quite helpful in some diagnoses. Most notable is the ability to diagnose the age of a hemorrhage based on the signal characteristics of the blood degradation products, which are different in the acute, subacute, and chronic phases. Some of the iron-containing compounds (deoxyhemoglobin, methemoglobin, hemosiderin, and ferritin) can dramatically shorten T1 and T2 relaxation of nearby protons. The amount of associated free water, the type and structure of the iron-containing molecules, the distribution (intracellular versus extracellular), and the magnetic field strength all influence the degree of relaxation effect that may be seen. For example, in the acute stage, T2 shortening occurs due to the paramagnetic susceptibility of the organized deoxyhemoglobin in the local area, without any large effect on the T1 relaxation time. When red blood cells lyse during the subacute stage, the hemoglobin is altered into methemoglobin, and spin-lattice relaxation is enhanced with the formation of a hydration layer, which shortens T1 relaxation, leading to a much stronger signal

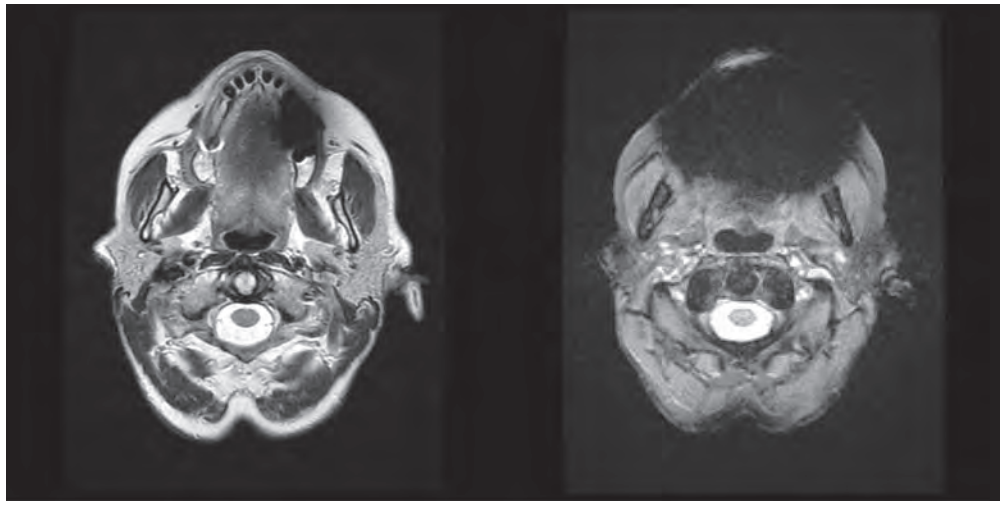

■ **FIGURE 13-24** Susceptibility artifacts due to dental fillings are shown in the same axial image slice. **Left.** Axial T2-weighted fast spin echo image illustrates significant suppression of susceptibility artifacts with 180-degree refocusing pulse. **Right.** Axial T2*-weighted gradient echo image illustrates significant image void exacerbated by the gradient echo, where external inhomogeneities are not canceled in the reformed echo.

on T1-weighted images. Increased signal intensity on T1-weighted images not found in the acute stage of hemorrhage identifies the subacute stage. In the chronic stage, hemosiderin, found in the phagocytic cells in sites of previous hemorrhage, disrupts the local magnetic homogeneity, causes loss of signal intensity, and leads to signal void, producing a characteristic dark rim around the hemorrhage site.

Gadolinium-based contrast agents (paramagnetic characteristics shorten T2 and hydration layer interactions shorten T1) are widely used in MRI. Tissues that uptake gadolinium contrast agents exhibit shortened T1 relaxation and demonstrate increased signal on T1-weighted images. Although focal inhomogeneities are generally considered problematic, there are certain physiologic and anatomic manifestations that can be identified and diagnostic information obtained.

Gradient Field Artifacts

Magnetic field gradients spatially encode the location of the signals emanating from excited protons within the volume being imaged. Proper reconstruction requires linear, matched, and properly sequenced gradients. The slice select gradient defines the volume (slice). Phase and frequency encoding gradients provide the spatial information in the other two dimensions.

Since the reconstruction algorithm assumes ideal, linear gradients, any deviation or temporal instability will be represented as a distortion. Gradient strength has a tendency to fall off at the periphery of the FOV. Consequently, anatomic compression occurs, especially pronounced on coronal and sagittal images having a large FOV, typically greater than 35 cm (Fig. 13-25). Minimizing the spatial distortion entails either reducing the FOV by lowering the gradient field strength or by holding the gradient field strength and number of samples constant while decreasing the frequency bandwidth. Of course, gradient calibration is part of a continuous quality control (QC) checklist, and geometric accuracy must be periodically verified.

Anatomic proportions may simulate abnormalities, so verification of pixel dimensions in the PEG and FEG directions are necessary. If the strength of the FEG and the strength of the largest PEG are different, the height or width of the pixels can become distorted and produce inaccurate measurements. Ideally, the phase and frequency encoding gradients should be assigned to the smaller and larger dimensions of the object, respectively, to preserve spatial resolution while limiting the number of phase encoding steps. In practice, this is not always possible, because motion artifacts or high-intensity

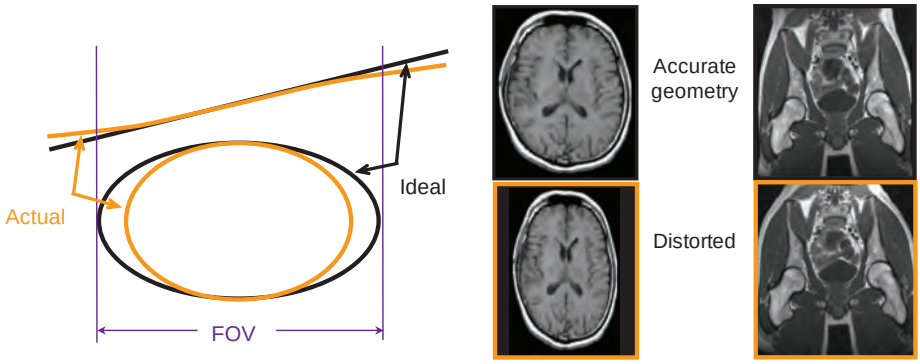

■ **FIGURE 13-25** Gradient nonlinearity causes image distortions by mis-mapping anatomy. In the above examples, the strength of the gradient at the periphery is less than the ideal (*orange line* versus *black line*). This results in a compression of the imaged anatomy, with inaccurate geometry (images with *orange* border). For comparison, images acquired with linear corrections are shown above.

signals that need to be displaced away from important areas of interest after an initial scan might require swapping the frequency and phase encode gradient directions.

RF Coil Artifacts

RF surface coils produce variations in uniformity across the image caused by RF excitation variability, attenuation, mismatching, and sensitivity falloff with distance. Proximal to the surface coil, receive signals are intense, and with distance, signal intensity is attenuated, resulting in grayscale shading and loss of brightness in the image. Nonuniform image intensities are the all-too-frequent result. Also, compensation for the disturbance of the magnetic field by the patient is typically compensated by an automatic shimming calibration. When this is not performed, or performed inadequately, a significant negative impact on image quality occurs. Examples of variable response are shown in Figure 13-26.

Other common artifacts from RF coils occur with RF quadrature coils (coils that simultaneously measure the signal from orthogonal views) that have two separate amplifier and gain controls. If the amplifiers are imbalanced, a bright spot in the center of the image, known as a center point artifact, arises as a "0 frequency" direct current offset. Variations in gain between the quadrature coils can cause ghosting of objects diagonally in the image. The bottom line for all RF coils is the need for continuous measurement and consistent calibration of their response, so that artifacts are minimized.

RF Artifacts

RF pulses and precessional frequencies of MRI instruments occupy the same frequencies of common RF sources, such as TV and radio broadcasts, electric motors, fluorescent lights, and computers. Stray RF signals that propagate to the MRI antenna can produce various artifacts in the image. Narrow-band noise creates noise patterns perpendicular to the frequency encoding direction. The exact position and spatial extent depends on the resonant frequency of the imager, applied gradient field strength, and bandwidth of the noise. A narrow band pattern of black/white

■ **FIGURE 13-26** Signal intensity variations occur when surface RF receive coils are too close to the skin, as exemplified by the MR breast image on the left. With inadequate shimming calibration, saturation pulses for adipose tissue in the breast is uneven, causing a significant variation in the uniformity of the reconstructed image. From Hendrick RE, *Breast MRI: fundamentals and technical aspects*. New York, NY: Springer, 2007. By permission.

alternating noise produces a "zipper" artifact. Broadband RF noise disrupts the image over a much larger area of the reconstructed image with diffuse, contrast-reducing "herringbone" artifacts. Appropriate site planning and the use of properly installed RF shielding materials (e.g., a Faraday cage) reduce stray RF interference to an acceptably low level. An example RF zipper artifact is shown in Figure 13-44.

RF energy received by adjacent slices during a multislice acquisition excite and saturate protons in adjacent slices, chiefly due to RF pulses without sharp off/on/off transitions. This is known as cross-excitation. On T2-weighted images, the slice-to-slice interference degrades the SNR; on T1-weighted images, the extra partial saturation reduces image contrast by reducing longitudinal recovery during the TR interval. A typical truncated "sinc" RF profile and overlap areas in adjacent slices are shown in Figure 13-27. Interslice gaps reduce the overlap of the profile tails, and pseudo-rectangular RF pulse profiles reduce the spatial extent of the tails. Important anatomic findings could exist within the gaps, so *slice interleaving* is a technique to mitigate cross-excitation by reordering slices into two groups with gaps. During the first half of the TR, the first slices are acquired (slices 1 to 5), followed by the second group of slices that are positioned in the gap of the first group (slices 6 to 10). This method reduces cross-excitation by separating the adjacent slice excitations in time. The most effective method is to acquire two independent sets of gapped multislice images, but the image time is doubled. The most appropriate solution is to devise RF pulses that approximate a rectangular profile; however, the additional time necessary for producing such an RF pulse can be prohibitive.

K-Space Errors

Errors in k-space encoding affect all areas of the reconstructed image, and cause the artifactual superimposition of wave patterns across the FOV. Each individual pixel value in k-space contributes to all pixel values in image space as a frequency harmonic with a signal amplitude. One bad pixel introduces a significant artifact, rendering the image suboptimal, as shown in Figure 13-28.

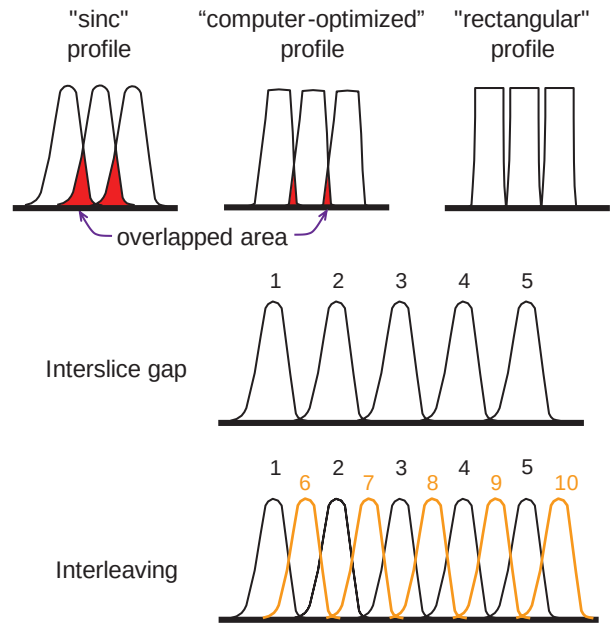

■ **FIGURE 13-27** **Top.** Poor pulse profiles are caused by truncated RF pulses, and resulting profile overlap causes unwanted partial saturation in adjacent slices, with a loss of SNR and CNR. Optimized pulses are produced by considering the tradeoff of pulse duration versus excitation profile. **Bottom.** Reduction of cross-excitation is achieved with interslice gaps, but anatomy at the gap location might be missed. An interleaving technique acquires the first half of the images with an interslice gap, and the second half of the images are positioned in the gaps of the first images. The separation in time reduces the amount of contrast reducing saturation of the adjacent slices.

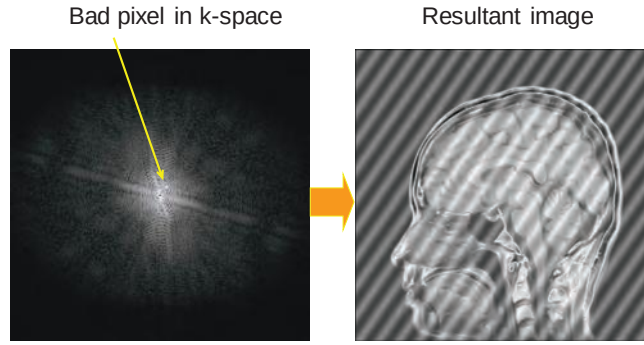

■ **FIGURE 13-28** A single bad pixel in k-space causes a significant artifact in the reconstructed image. The bad pixel is located at $k_x = 2$, $k_y = 3$, which produces a superimposed sinusoidal wave on the spatial domain image as shown above.

Motion Artifacts

The most ubiquitous and noticeable artifacts in MRI arise with patient motion, including voluntary and involuntary movement, and flow (blood, CSF). Although motion artifacts are not unique to MRI, the long acquisition time of certain MRI sequences increases the probability of motion blurring and contrast resolution losses. Motion artifacts occur mostly along the phase encode direction, as adjacent phase encoding measurements in k-space are separated by a TR interval that can last 3,000 ms or longer. Even very slight motion can cause a change in the recorded phase variation across the FOV throughout the MR acquisition sequence. Examples of motion artifacts are shown in Figure 13-29. The frequency encode direction is less affected, especially by periodic motion, since the evolution of the echo signal, frequency encoding, and sampling occur simultaneously over several milliseconds. Ghost images, which are faint copies of the image displaced along the phase encode direction, are the visual result of patient motion.

Several techniques can compensate for motion-related artifacts. The simplest technique transposes the PEG and FEG to relocate the motion artifacts out of the

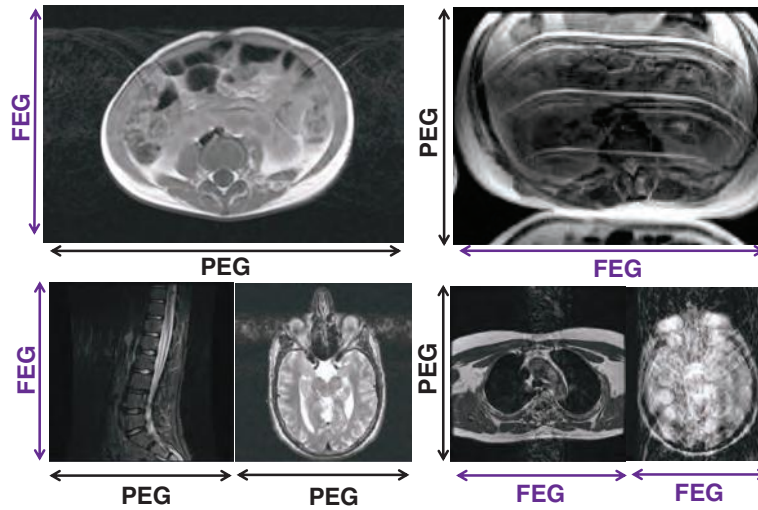

■ **FIGURE 13-29** Motion artifacts, particularly of flow patterns, are most always displayed in the phase encode gradient direction. Slight changes in phase produce multiple ghost images of the anatomy, since the variation in phase caused by motion can be substantial between excitations.

region of diagnostic interest with the same pulse sequences. This does not reduce the magnitude of the artifacts, however, and often there is a mismatch when placing the PEG along the long axis of a rectangular FOV (e.g., an exam of the thoracic spine) in terms of longer examination times or a significant loss of spatial resolution or of SNR.

There are other motion compensation methods:

1. Cardiac and respiratory gating—signal acquisition at a particular cyclic location synchronizes the phase changes applied across the anatomy (Fig. 13-30).
2. Respiratory ordering of the phase encoding projections based on location within the respiratory cycle. Mechanical or video devices provide signals to monitor the cycle.
3. Signal averaging to reduce artifacts of random motion by making displaced signals less conspicuous relative to stationary anatomy.
4. Short TE spin echo sequences (limited to proton density, T1-weighted scans, fractional echo acquisition, Fig. 13-3). Note: Long TE scans (T2 weighting) are more susceptible to motion.
5. Gradient moment nulling (additional gradient pulses for flow compensation) to help rephase protons that are dephased due to motion. Most often, these techniques require a longer TE and are more useful for T2-weighted scans (Fig. 13-18).
6. Presaturation pulses applied outside the imaging region to reduce flow artifacts from inflowing protons, as well as other patient motions that occur in the periphery (Fig. 13-12).
7. Multiple redundant sampling in the center of k-space (e.g., propeller) to identify and remove those sequences contributing to motion, without deleteriously affecting the image (Fig. 13-8).

Chemical Shift Artifacts of the First Kind

There are two types of chemical shift artifacts that affect the display of anatomy due to the precessional frequency differences of protons in fat versus protons in water. Chemical shift refers to the resonance frequency variations resulting from intrinsic

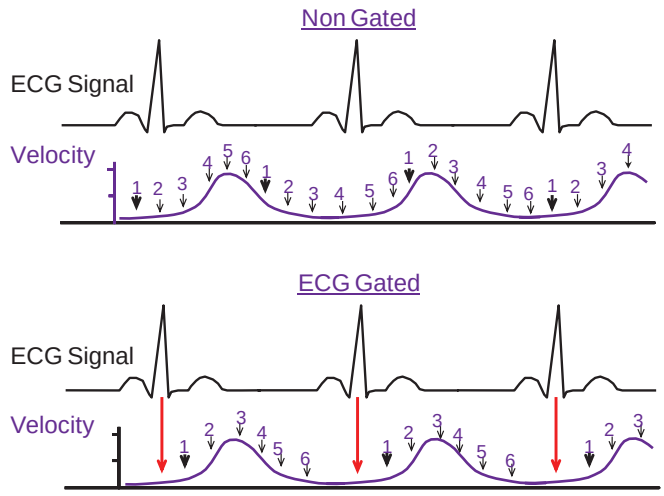

■ **FIGURE 13-30** Motion artifacts occur when data is acquired without consideration of physiologic periodicity. **Top**. The electrocardiogram measures the R-wave at each heartbeat, but data acquisition proceeds in a linear fashion without regard to reproducibility. The result is a set of images degraded with motion artifact, with diagnostic usefulness marginal, at best. **Bottom.** Acquisition of images proceeds with the detection of the R-wave signal and synchronization of the collection of image data in a stepwise fashion over the period between R-waves. A reduced number of images or extended acquisition time is required to collect the data.

magnetic shielding of anatomic structures. Molecular structure and electron orbital characteristics produce fields that shield the main magnetic field and give rise to distinct peaks in the MR spectrum. In the case of proton spectra, peaks correspond to water and fat, and in the case of breast imaging, silicone material is another material to consider. Lower frequencies of about 3.5 parts per million for protons in fat and 5.0 parts per million for protons in silicone occur, compared to the resonance frequency of protons in water (Fig. 13-31). Since resonance frequency increases linearly with field strength, the absolute difference between the fat and water resonance also increases, making high field strength magnets more susceptible to chemical shift artifact.

Data acquisition methods cannot directly discriminate a frequency shift due to the application of a frequency encode gradient or a chemical shift artifact. Water and fat differences therefore cannot be distinguished by the frequency difference induced by the gradient. The protons in fat resonate at a slightly lower frequency than the corresponding protons in water, and cause a shift in the anatomy (misregistration of water and fat moieties) along the frequency encode gradient direction.

A sample calculation in the example below demonstrates frequency variations in fat and water for two different magnetic field and gradient field strengths:

Chemical shift artifact numerical calculation for field strength, with a 3.5-ppm (3.5×10^{-6}) variation in resonance frequency between fat and water results in the following frequency differences:

$$1.5\text{ T: } 63.8 \times 10^{6}\text{Hz} \times 3.5 \times 10^{-6} = 223\text{ Hz}$$

$$3.0\text{ T: } 127.7 \times 10^{6}\text{Hz} \times 3.5 \times 10^{-6} = 447\text{ Hz}$$

Thus, the chemical shift is more severe for higher field strength magnets.

Chemical shift artifact numerical calculation for gradient strength results in the following numerical calculations for a 25-cm (0.25 m) FOV, 256 × 256 matrix:

Low gradient strength: 2.5 mT/m × 0.25 m = 0.000625 T variation, gives frequency range of 0.000625 T × 42.58 MHz/T = 26.6 kHz across FOV and 26.6 kHz/256 pixels = 104 Hz/pixel

High gradient strength: 10 mT/m × 0.25 m = 0.0025 T variation, gives frequency range of 0.0025 T × 42.58 MHz/T = 106.5 kHz across FOV and 106.5 kHz/256 pixels = 416 Hz/pixel.

Thus, a chemical shift occurrence is more severe for lower gradient strengths, since displacement will occur over a large number of pixels. With a higher gradient strength, water and fat are more closely contained within the broader pixel boundary bandwidths. Normal and low bandwidth images are illustrated in Figure 13-32.

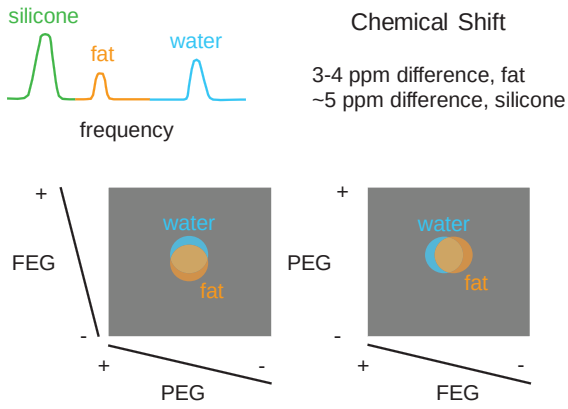

■ **FIGURE 13-31** Chemical shift refers to the slightly different precessional frequencies of protons in different materials or tissues. The shifts (in ppm) are referenced to water for fat and silicone. Fat chemical shift artifacts are represented by a shift of water and fat in the images of anatomical structure, mainly in the frequency encode gradient direction. Swapping the PEG and the FEG will cause a shift of the fat and water components of the tissues in the image.

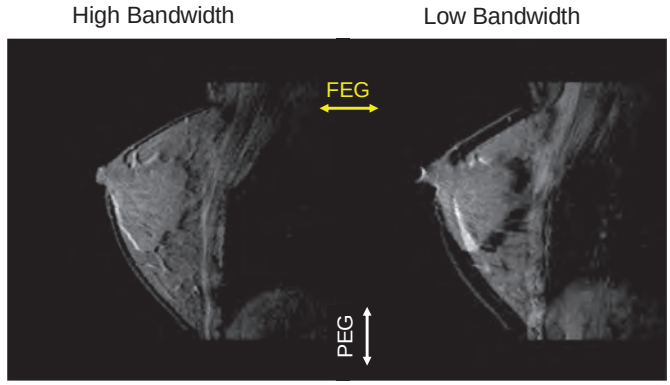

■ **FIGURE 13-32** MR images of the breast, containing glandular and adipose tissue, are acquired under a high bandwidth (32 kHz) and a low bandwidth (4 kHz), illustrating the more severe chemical shift with low readout gradient strength and bandwidth. (Reprinted by permission, Hendrick RE. *Breast MRI: fundamentals and technical aspects*. New York, NY: Springer, 2007.)

RF bandwidth and gradient strength considerations can mitigate chemical shift artifacts. While higher gradient strength can confine the chemical shift of fat within the pixel bandwidth boundaries, a significant SNR penalty occurs with the broad RF bandwidth required to achieve a given slice thickness. A more widely used method is to use lower gradient strengths and narrow bandwidths in combination with off-resonance "chemical presaturation" RF pulses to minimize the fat (or the silicone) signal in the image (Fig. 13-33). Another alternative is to use STIR techniques to eliminate the signals due to fat at the "bounce point." Swapping the phase and frequency gradient directions or changing the polarity of the frequency encode gradient can displace chemical shift artifacts from a specific image region, even though the chemical shift displacement still exists. Identification of fat in a specific anatomic region is easily discerned from the chemical shift artifact displacement caused by changes in FEG/PEG gradient directions.

Chemical Shift Artifacts of the Second Kind

Chemical shift artifacts of the second kind occur with GE images, resulting from the rephasing and dephasing of the echo in the same direction relative to the main magnetic field. Signal appearance is dependent on the selection of TE. This happens because of constructive (in phase) or destructive (out of phase) transverse magnetization events that occur periodically due to the difference in precessional frequencies. At 1.5 T, the chemical shift

■ **FIGURE 13-33** The left image of the lumbar spine is Spin Echo T1 weighted, TR = 450 ms, TE = 14 ms. The right image is T1 weighted with chemical fat saturation pulses, TR = 667 ms, TE = 8 ms. In both images, the FEG is vertically oriented.

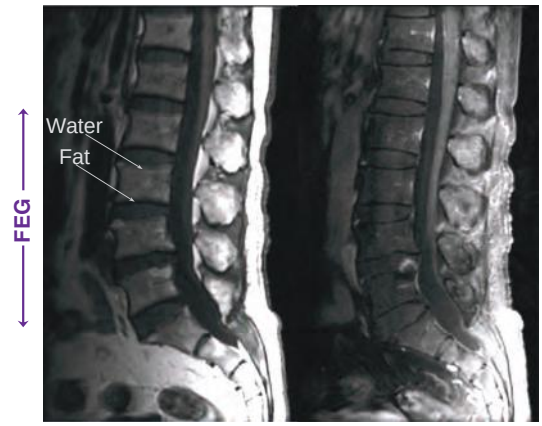

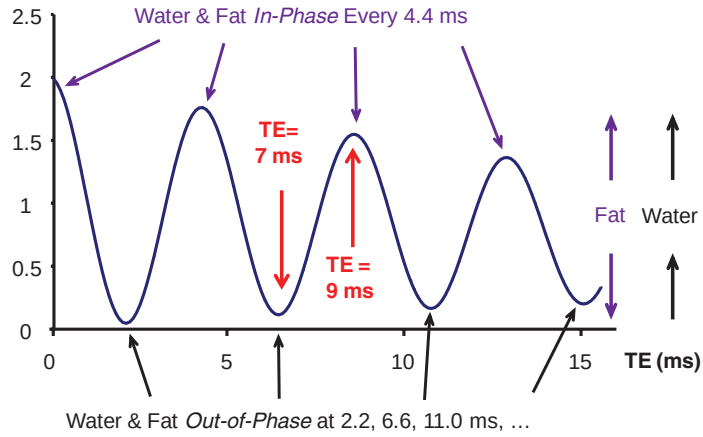

■ **FIGURE 13-34** For GE image sequences, signal intensity of the transverse magnetization vector due to the 220 Hz lower precessional frequency of fat protons, where in-phase magnetization occurs every 4.4 ms (1/220 s^{-1}), and out-of-phase magnetization occurs every 4.4 ms shifted by ½ cycle (2.2 ms). Signal intensity is dependent on the selection of TE, as shown above.

is 220 Hz, and the periodicity of each peak (in phase) between water and fat occurs at 0, 4.5, 9.0, 13.5, …. ms, and each valley (out of phase) at 2.25, 6.75, 11.0, …. ms, as shown in Figure 13-34. Thus, selection of TE at 9 ms will lead to a constructive addition of water and fat, and TE at 7 ms will lead to a destructive addition of water and fat. The in-phase timing will lead to a conventional chemical shift image of the first kind, while the out-of-phase timing will lead to a chemical shift image of the second kind, manifesting a dark rim around heterogeneous water and fat anatomical structures, shown in Figure 13-35.

Ringing Artifacts

Ringing artifact (also known as Gibbs phenomenon) occurs near sharp boundaries and high-contrast transitions in the image, and appears as multiple, regularly spaced parallel bands of alternating bright and dark signal that slowly fades with distance.

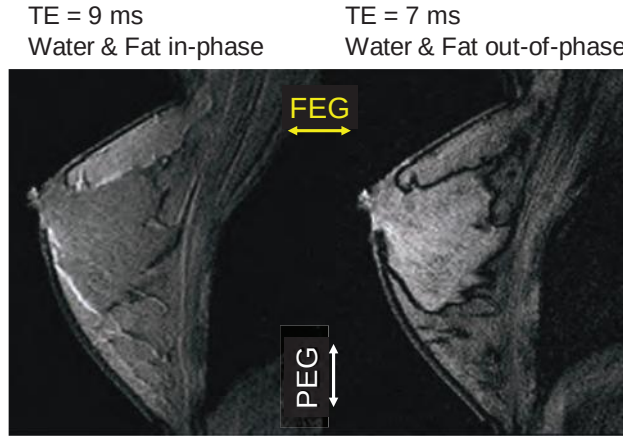

■ **FIGURE 13-35** Breast MRI images show the effect of selecting a specific TE for a GE acquisition. On the left, chemical shift of the "first kind" is shown with TE = 9 ms and water and fat in phase for transverse magnetization, shifted only due to the intrinsic chemical shift differences of fat and water. On the right, chemical shift of the second kind is additionally manifested with TE = 7 ms, due to fat and water being out of phase, creating a lower signal at all fat-water interfaces, and resulting in reduced intensity. (Reprinted by permission, Hendrick RE. *Breast MRI: fundamentals and technical aspects*. New York, NY: Springer, 2007.)

The cause is the insufficient sampling of high frequencies inherent at sharp discontinuities in the signal. Images of objects can be reconstructed from a summation of sinusoidal waveforms of specific amplitudes and frequencies, as shown in Figure 13-36 for a simple rectangular object. In the figure, the summation of frequency harmonics, each with a particular amplitude and phase, approximates the distribution of the object, but initially does very poorly, particularly at the sharp edges. As the number of higher frequency harmonics increase, a better estimate is achieved, although an infinite number of frequencies are theoretically necessary to reconstruct the sharp edge perfectly.

In the MR acquisition, the number of frequency samples is determined by the number of pixels (frequency, k_x, or phase, k_y, increments) across the k-space matrix. For 256 pixels, 128 discrete frequencies are depicted, and for 128 pixels, 64 discrete frequencies are specified (the k-space matrix is symmetric in quadrants and duplicated about its center). A lack of high-frequency signals causes the "ringing" at sharp transitions described as a diminishing hyper- and hypointense signal oscillation from the transition. Ringing artifacts are thus more likely for smaller digital matrix sizes (Fig. 13-37, 256 versus 128 matrix). Ringing artifact commonly occurs at skull/brain interfaces, where there is a large transition in signal amplitude.

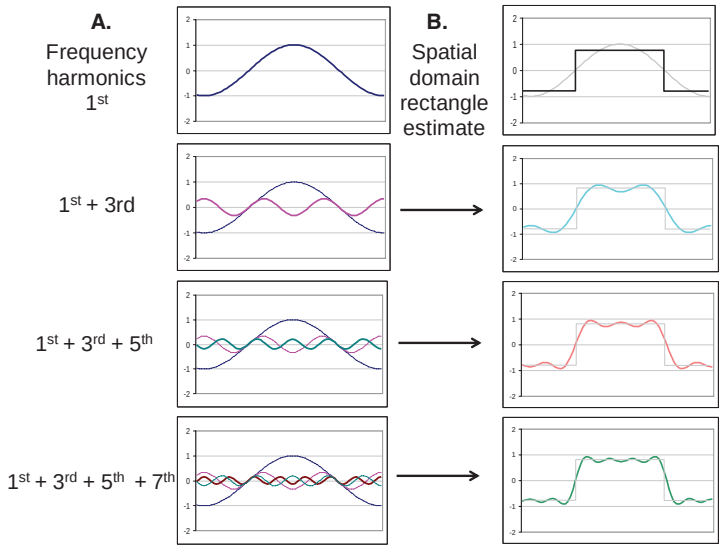

FIGURE 13-36 The synthesis of a spatial object occurs by the summation of frequency harmonics in the MR image. **A. Left column**: frequency harmonics that estimate a rectangle function with progressively higher frequencies and lower amplitudes are shown. **B. Middle column**: As higher frequency harmonics are included, the summed result more faithfully represents the object shape, in this example a rectangle with two vertical edges. The number of frequencies encoded in the MR image is dependent on the matrix size. **C. Right column**: A sharp transition boundary in an MR image is represented with 256 samples better than with128 samples (frequency harmonics in k-space). The amount of ringing caused by insufficient sampling is reduced with a larger number of samples.

C. Sharp transition in MR image:

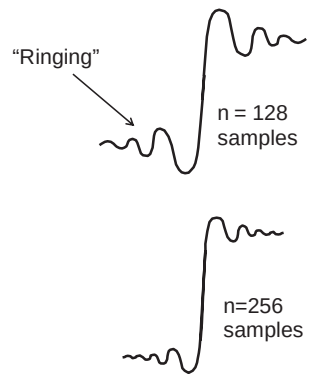

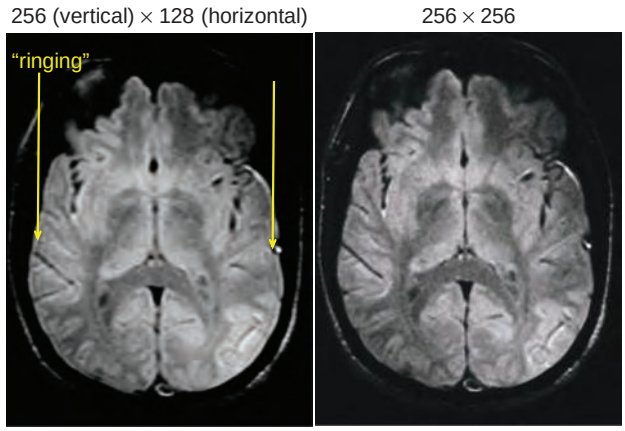

■ **FIGURE 13-37** Example of ringing artifacts caused by a sharp signal transition at the skull in a brain image for a 256 × 128 matrix (left) along the short (horizontal) axis, and the elimination of the artifact in a 256 × 256 matrix (right). The short axis defines the PEG direction.

Wraparound Artifacts

The wraparound artifact is a result of the mismapping of anatomy that lies outside of the FOV but within the slice volume. The anatomy is usually displaced to the opposite side of the image. It is caused by nonlinear gradients or by undersampling of the frequencies contained within the returned signal envelope. For the latter, the sampling rate must be twice the maximal frequency that occurs in the object (the Nyquist sampling limit). Otherwise, the Fourier transform cannot distinguish frequencies that are present in the data above the Nyquist frequency limit, and instead assigns a lower frequency value to them (Fig. 13-38). Frequency signals will "wraparound" to the opposite side of the image, masquerading as low-frequency (aliased) signals.

In the frequency encode direction, a low-pass filter can be applied to the acquired time domain signal to eliminate frequencies beyond the Nyquist frequency. In the phase encode direction, aliasing artifacts can be reduced by increasing the number of phase encode steps (the trade-off is increased image time). Another approach is to move the region of anatomic interest to the center of the imaging volume to avoid the

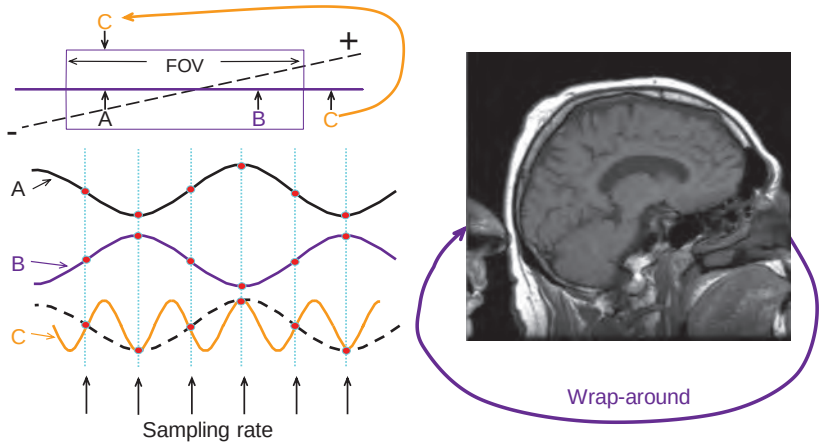

■ **FIGURE 13-38** **Left.** Wraparound artifacts are caused by aliasing. Shown is a fixed sampling rate and net precessional frequencies occurring at position *A* and position *B* within the FOV that have identical frequencies but different phase. If signal from position *C* is at *twice* the frequency of *B* and insufficiently sampled, the same frequency and phase will be assigned to *C* as that assigned to *A*, and therefore will appear at that location. **Right.** A wraparound artifact example displaces anatomy from one side of the image (or outside of the FOV) to the other side.

overlapping anatomy, which usually occurs at the periphery of the FOV. An "antialiasing" saturation pulse just outside of the FOV is yet another method of eliminating high-frequency signals that would otherwise be aliased into the lower frequency spectrum. This example of wrap-around artifact is easy to interpret. In some cases, the artifact is not as well delineated (e.g., the top of the skull wrapping into the brain).

Partial Volume Artifacts

Partial volume artifacts arise from the finite size of the voxel over which the signal is averaged. This results in a loss of detail and spatial resolution. Reduction of partial volume artifacts is accomplished by using a smaller pixel size and/or a smaller slice thickness. With a smaller voxel, the SNR is reduced for a similar imaging time, resulting in a noisier signal with less low-contrast sensitivity. Of course, with a greater NEX (averages), the SNR can be maintained, at the cost of longer imaging time.

13.6 Magnetic Resonance Spectroscopy

Magnetic resonance spectroscopy (MRS) is a method to measure tissue chemistry (an "electronic" biopsy) by recording and evaluating signals from metabolites by identifying metabolic peaks caused by frequency shifts (in parts per million, ppm) relative to a frequency standard. In vivo MRS can be performed with ^{1}H (proton), ^{23}Na (sodium), and ^{31}P (phosphorus) nuclei, but proton spectroscopy provides a much higher SNR and can be included in a conventional MRI protocol with about 10 to 15 min extra exam time. Uses of MRS include serial evaluation of biochemical changes in tumors, analyzing metabolic disorders, infections and diseases, as well as evaluation of therapeutic oncology treatments for tumor recurrence versus radiation damage. Early applications were dedicated to brain disorders, but now breast, liver, and prostate MRS are also performed. Correlation of spectroscopy results and MR images are always advised before making a final diagnosis.

In MRS, signals are derived from the amplitude of proton metabolites in targeted tissues. In these metabolites, chemical shifts occur due to electron cloud shielding of the nuclei, causing slightly different resonance frequencies, which exist in a frequency range between water and fat. The very small signal amplitudes of the metabolites require suppression of the extremely large (~10,000 times higher) amplitudes due to bulk water and fat protons, as shown in Figure 13-39. This is achieved by using specific chemical saturation techniques, such as CHESS (Chemical Shift-Selective) or STIR (see Chapter 12). In many cases, the areas evaluated are away from fat structures, and only bulk water signal suppression is necessary; however, in organs such as the liver and the breast, suppression of both fat and water are required. Once the water and fat signals are suppressed, localization of the targeted area volume is achieved by either a single voxel or multivoxel technique.

Single voxel MRS sampling areas, covering a volume of about 1 cm^3 are delineated by a STEAM (Stimulated echo acquisition mode) or a PRESS (Point Resolved Spectroscopy) sequence. The STEAM method uses a 90-degree excitation pulse and 90-degree refocusing pulse to collect the signal in conjunction with gradients to define each dimension of the voxel. The PRESS sequence uses a 90-degree excitation and 180-degree refocusing pulse in each direction. STEAM achieves shorter echo times and superior voxel boundaries, but with lower SNR. After the voxel data are collected, a Fourier transform is applied to separate the composite signal into individual frequencies, which are plotted as a trace for a normal brain spectrum (Fig. 13-40). The resulting line widths are based on homogeneity of the main magnetic field as

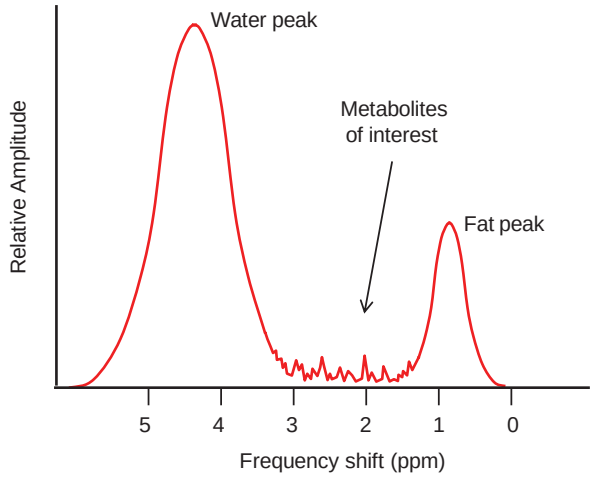

■ **FIGURE 13-39** MRS metabolites of interest in comparison to the water and fat peaks commonly used for imaging. In order to isolate the very small signals, chemical saturation of the water (and fat when present) signal is essential.

well as the magnetic field strength. Higher field strengths (e.g., 3.0 T) will improve resolution of the peaks and corresponding SNR.

Multivoxel MRS uses a CSI (Chemical Shift Imaging) technique to delineate multiple voxels of approximately 1 cm^3 volume in 1, 2, or 3 planes over a rectangular block of several centimeters, achievable with more sophisticated equipment and longer scan times. This is followed by MRSI (Magnetic Resonance Spectroscopic Imaging) where the signal intensity of a single metabolite in each voxel is color encoded for each voxel according to concentration and the generated parameter maps superimposed on the anatomical MR image. In practice, the single voxel technique is used to make the initial diagnosis because the SNR is high and all metabolites are represented in the MRS trace. Then, a multivoxel acquisition to assess the distribution of a specific metabolite is performed.

Proton MRS can be performed with short (20 to 40 ms), intermediate (135 to 145 ms), or long (270 to 290 ms) echo times. For short TE, numerous resonances from metabolites of lesser importance (with shorter T2) can make the spectra more difficult to interpret, and with long echo times, SNR losses are too severe. Therefore, most MRS acquisitions use a TE of approximately 135 ms at 1.5 T. Metabolites of interest for brain spectroscopy are listed in Table 13-2.

Applications of MRS are achieved through the interpretation of the spectra that are obtained from the lesion, from its surroundings, and presumably healthy tissue in

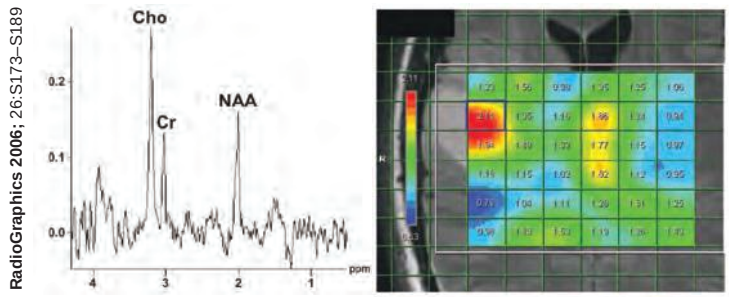

■ **FIGURE 13-40** **Left:** Intermediate echo (TE=135 ms) single voxel spectrum is shown, positioned over an anaplastic oligoastrocytoma brain lesion. Note the elevated Choline peak and lowered Creatine and NAA peaks. **Right:** Multivoxel spectrum is color coded to the Choline / Creatine ratio, illustrating the regional variation of the metabolites corresponding to tumor. From Al-Okaili RN, Krejza J, Wang S, Woo JH, Melhem ER. *Advanced MR Imaging Techniques in the Diagnosis of Intraaxial Brain Tumors in Adults.* Radiographics 2006; 26: S173-S189. By permission.

TABLE 13-2 METABOLITES IN MRS AT 1.5 T

ABBREVIATION	METABOLITE	SHIFT (PPM)	PROPERTIES/SIGNIFICANCE IN THE BRAIN
Cho	Phosphocholine	3.22	Membrane turnover, cell proliferation
Cr	Creatine	3.02 and 3.93	Temporary store for energy-rich phosphates
NAA	*N*-acetyl-L-aspartate	2.01	Presence of intact glioneural structures
Lactate		1.33 (inverted)	Anaerobic glycolysis
Lipids	Free fatty acids	1.2–1.4	Necrosis

the same scan. Main criteria include the presence or absence of pathologic metabolites (lactate or lipids) and the relationships between the concentrations of choline, creatine, and NAA as ratios. Spectra are usually scaled to the highest peak, and y-axis values will usually differ between measurements, so caution must be observed to avoid potential misdiagnoses.

In a tumor, high cell turnover causes an increase in choline concentration along with a corresponding depression of the NAA peak caused by the loss of healthy glioneural structures. In addition, the creatine peak may also be reduced depending on the energy status of the tumor; it is often used to serve as an internal reference for calculating ratios of metabolites. When a lipid peak is observed, this is a sign of hypoxia and the likelihood of a high-grade malignancy. Table 13-3 lists qualitative findings for MRS spectroscopy in evaluating brain tumors for the ratios of NAA/Cr, NAA/Cho, and Cho/Cr. Examples of single voxel and multivoxel spectra are shown in Figure 13-40, illustrating the use of the spectral peaks for diagnostic interpretation of the ratios, and a MRSI color-encoded graphic display of the spatial distribution of findings. There is certainly much more than determining ratios, and differential diagnoses are often clouded by indistinct peaks, poor SNR, and tumor heterogeneity, among other causes. MRS at 3 T field strength enjoys much better SNR, improved spectral resolution, and faster scans. Because of the higher spectral resolution, familiar single target peaks at 1.5 T become a collection of peaks at 3 T.

13.7 Ancillary Components

Ancillary components are necessary for the proper functioning of the MR system. Shim coils are active or passive magnetic field devices that are used to adjust the main magnetic field and to improve the homogeneity in the sensitive central volume of the

TABLE 13-3 RATIOS OF METABOLITE PEAKS IN MRS INDICATING "NORMAL" AND "ABNORMAL" STATUS

METABOLITE RATIO	NORMAL	ABNORMAL
NAA/Cr	2.0	<1.6
NAA/Cho	1.6	<1.2
Cho/Cr	1.2	>1.5

scanner. Gradient coils, as previously discussed, are wire conductors that produce a linear superimposed gradient magnetic field on the main magnetic field. The gradient coils are located inside the cylinder of the magnet, and are responsible for the banging noise one hears during imaging. This noise is caused by the flexing and torque experienced by the gradient coil from the rapidly changing magnetic fields when energized.

Radiofrequency Coils

A wide variety of transmit and receive coils complement a MR scanner. **RF transmitter coils** create an oscillating secondary magnetic field formed by passing an alternating current through a loop of wire. To accomplish excitation and resonance, the created secondary B_1 field must be arranged at right angles to the main magnetic field, B_0. In an air core design with a horizontal field, the RF coil secondary field should be in the transverse or vertical axes, as the B_1 field is created perpendicular to the transmit coils themselves. RF transmitter coils are therefore oriented above, below, or at the sides of the patient, and are usually cylindrical. In most systems, the body coil contained within the bore of the magnet is most frequently used, but also transmitter coils for the head, extremity, and some breast coils are coupled to a receiver coil.

Very often, transmit and receive functions are separated to handle the variety of imaging situations that arise, and to maximize the SNR for an imaging sequence. All **RF receiver coils** must resonate and efficiently store energy at the Larmor frequency. This is determined by the inductance and capacitance properties of the coil. RF transmit and receive coils need to be tuned prior to each acquisition and matched to accommodate the different magnetic inductance of each patient. Receiver coils must be properly placed to adequately detect the MR signal.

Proximity RF coils include volume or bird-cage coils, the design of choice for brain imaging, the single-turn solenoid for imaging the extremities and the breasts, and the saddle coil. These coils are typically operated as both a transmitter and receiver of RF energy (Fig. 13-41). *Volume coils* encompass the total area of the anatomy of interest and yield uniform excitation and SNR over the entire imaging volume. However, because of their relatively large size, images are produced with lower SNR than other types of coils. Enhanced performance is obtained with a process known as quadrature excitation and detection, which enables the energy to be transmitted and the signals to be received by two pairs of coils oriented at right angles, either electronically or physically. This detector manages two simultaneous channels known as the real (records MR information in phase with a reference signal) and the imaginary (records MR information 90 degree out of phase with the reference signal) channels, and increases the SNR up to a factor of $\sqrt{2}$. If imbalances in the offset or gain of these detectors occur, then artifacts will be manifested, such as a "center point" artifact.

Surface coils are used to achieve high SNR and high resolution when imaging anatomy near the surface of the patient, such as the spine. They are typically receive-only designs, and are usually small and shaped for a specific imaging exam and for patient comfort. The received signal sensitivity, however, is limited to the volume located around the coil at a depth into the patient equal to the radius of the coil, which causes a loss of signal with depth. There are now intracavitary coils for endorectal, endovascular, endovaginal, esophageal, and urethral local imaging, and can be used to receive signals from deep within the patient. In general, a body coil is used to transmit the RF energy and the local coil is used to receive the MR signal.

Phased array coils consisting of multiple coils and receivers are made of several overlapping loops, which extend the imaging FOV in one direction (Fig. 13-41). The

■ **FIGURE 13-41** Radiofrequency surface coils improve image quality and SNR for specific examinations. Upper left is a dedicated head and neck coil. Upper right is a dedicated head coil; the lower left and lower right images illustrate the two components of an 8 channel phased array coil for body imaging.

small FOV of each individual coil provides excellent SNR and resolution, and each is combined to produce a composite image with the advantages of the local surface coil, so that all data can be acquired in a single sequence. Phased array coils for the spine, pelvis, breast, cardiac, and temperomandibular joint applications are commonly purchased with an MR system for optimal image quality.

Multi-channel encoding coils with as many as N = 32 elements allow for detection and encoding based upon the detection of a sensitivity map of the signals near the coil. These coils are used in *parallel imaging* to fill N multiple lines of k-space per TR interval, by assigning certain coil responses to specific regions as the data are acquired simultaneously and using software to link them electronically. By filling k-space quicker, the scan time can be reduced by the number of elements in the coil. However, since each line of k-space is encoded by separate coils, the gap between each line for a specific coil is N times greater than if k-space had been filled normally. Since the FOV dimension in the phase encode direction is inversely proportional to the spacing, the size of the FOV is reduced to 1/N its original size, and as a result, aliasing of signals outside of the FOV in the phase encode direction occurs, and each coil response produces a wrapped image. To overcome the aliasing, the system uses the sensitivity profile of each coil to calculate where the signal is coming from relative to the coil based on its amplitude—the signal generated near the coil has a higher amplitude than the signal furthest away. Using this process (called SENSE, ASSET, GRAPPA, iPAT by the various manufacturers), the image is unwrapped and combined with the unwrapped images from the other coils to form one summed image of the slice, with high SNR and resolution (see Figure 13-9). Parallel imaging can be used to either reduce scan time or improve resolution, in conjunction with most pulse sequences. Downsides include image misalignment when combining images due to patient motion, and increase in chemical shift artifacts, due to a range of frequencies mapped across each coil. Nevertheless, multi-coil parallel imaging techniques are now common and increasing in use.

RF coil safety requires regular inspection of the coil condition, including the conductive wires leading to the coils from the connectors. These wires have the capacity to transmit heat, which may burn the insulating material of the wires or burn the patient. It is important to ensure that the coils are not looped and do not touch the patient or the bore of the magnet. Damage to the insulation requires immediate repair, as this could result in extreme heating, fire, and potential harm to the patient.

MR System Subcomponents

The control interfaces, RF source, detector, and amplifier, analog to digital converter (digitizer), pulse programmer, computer system, gradient power supplies, and image display are crucial components of the MR system. They integrate and synchronize the tasks necessary to produce the MR image (Fig. 13-42).

The operator interface and computer systems vary with the manufacturer, but most consist of a computer system, dedicated processor for Fourier transformation, image processor to form the image, disk drives for storage of raw data and pulse sequence parameters, and a power distribution system to distribute and filter the direct and alternating current. The operator's console is located outside of the scan room, and provides the interface to the hardware and software for data acquisition.

13.8 Magnet Siting, Quality Control

Magnet Siting

Superconductive magnets produce extensive magnetic fringe fields, and create potentially hazardous conditions in adjacent areas. In addition, extremely small signal amplitudes generated by the protons in the body during an imaging procedure have a frequency common to commercial FM broadcasts. Thus, two requirements must

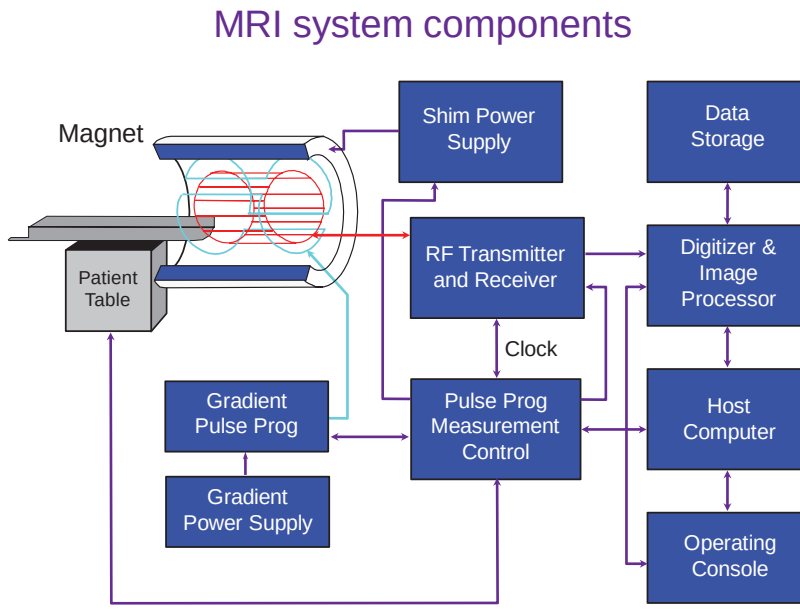

■ **FIGURE 13-42** A block diagram of a typical MRI system shows the components and interfaces between subsystems. Not shown is the **Faraday cage that surrounds the magnet assembly** to eliminate environmental RF noise.

be considered for MR system siting: protect the local environment from the magnet system and protect the magnet system from the local environment.

Fringe fields from a high field strength magnet can extend quite far—roughly equal to αB_0, where α is a constant dependent on the magnet bore size and magnet configuration. Fringe fields can potentially cause a disruption of electronic signals and sensitive electronic devices. An unshielded 1.5-T magnet has a 1-mT fringe field at a distance of approximately 9.3 m, a 0.5-mT field at 11.5 m, and a 0.3-mT field at 14.1 m from the center of the magnet. Magnetic shielding is one way to reduce fringe field interactions in adjacent areas. Passive (e.g., thick metal walls close to the magnet) and active (e.g., electromagnet systems strategically placed in the magnet housing) magnetic shielding systems permit a significant reduction in the extent of the fringe fields for high field strength, air core magnets (Fig. 13-43). Patients with pacemakers or ferromagnetic aneurysm clips must avoid fringe fields above 0.5 mT. Magnetically sensitive equipment such as image intensifiers, gamma cameras, and color TVs are severely impacted by fringe fields of less than 0.3 mT, as electromagnetic focusing in these devices is disrupted.

Administrative control for magnetic fringe fields is 0.5 mT, requiring controlled access to areas that exceed this level. Magnetic fields below 0.5 mT are considered safe for the patient population. Disruption of the fringe fields can reduce the homogeneity of the active imaging volume. Any large metallic object (elevator, automobile, etc.) traveling through the fringe field can produce such an effect.

Environmental RF noise must be reduced to protect the extremely sensitive receiver within the magnet from interfering signals. The typical approach for stray RF signal protection is the construction of a Faraday cage, an internal enclosure consisting of RF attenuating copper sheet and/or copper wire mesh. The room containing the MRI system is typically lined with copper sheet (walls) and mesh (windows). This is a costly construction item but provides effective protection from stray RF noise (Fig. 13-44).

Field Uniformity

In addition to magnetic field strength, field uniformity is an important characteristic, expressed in parts per million (ppm) over a given volume, such as 40 cm^3. This is based upon the precessional frequency of the proton, which is determined from the

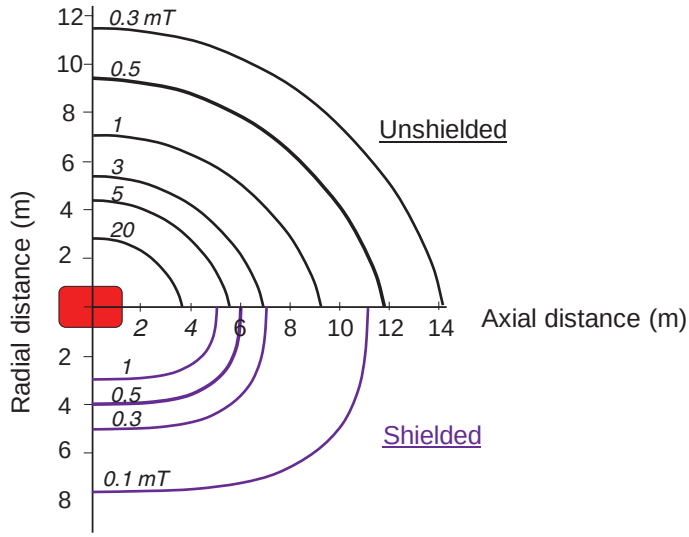

■ **FIGURE 13-43** An unshielded (top half of diagram) and shielded (bottom half of diagram) 1.5 T magnet and the magnetic fringe field strengths plotted with radial distance (vertical axis) and axial distance (horizontal axis).

■ **FIGURE 13-44** The MR scanner room requires protection from extraneous radiofrequency signals. This is achieved with the installation of a "Faraday cage" comprised of copper sheet that lines the inner walls of the room (**left**), copper mesh covering the operator viewing window (not shown), and a copper lined door and doorjamb with an inflatable bladder conductor (note switch above the door handle) to seal the door (**middle and upper right**). A leak in the Faraday cage will result in RF artifacts that will occur at specific frequencies as streaks across the image, perpendicular to the FEG direction. (**Lower right**. FEG is vertical, PEG is horizontal.)

proton gyromagnetic ratio. At 1.5 T, the precessional frequency is 1.5 T × 42.58 MHz/T = 63.8 MHz = 63.8 × 10^6 cycles/s, and a specification of 2 ppm homogeneity (2×10^{-6}) gives a frequency uniformity of about 128 cycles/s (Hz) over the volume. Typical homogeneities range from less than 1 ppm for a small FOV (e.g. 150 mm) to greater than 10 ppm for a large FOV (e.g., 400 mm). Field uniformity is achieved by manipulating the main field peripherally with passive and active "shim" coils, which exist in proximity to the main magnetic field. These coils interact with the fringe fields and adjust the variation of the central magnetic field.

Quality Control

Like any imaging system, the MRI scanner is only as good as the weakest link in the imaging chain. The components of the MR system that must be periodically checked include the magnetic field strength, magnetic field homogeneity, system field shimming, gradient linearity, system RF tuning, receiver coil optimization, environmental noise sources, power supplies, peripheral equipment, and control systems among others. A QC program should be designed to assess the basic day-to-day functionality of the scanner. A set of QC tests is listed in Table 13-4. Qualitative and quantitative measurements of system performance should be obtained on a periodic basis, with a test frequency dependent on the likelihood of detecting a change in the baseline values outside of normal operating limits.

The American College of Radiology has an MRI accreditation program that specifies requirements for system operation, QC, and the training requirements of technologists, radiologists, and physicists involved in scanner operation. The accreditation process evaluates the qualifications of personnel, equipment performance, effectiveness of QC procedures, and quality of clinical images—factors that are consistent with the maintenance of a state-of-the-art facility.

TABLE 13-4 RECOMMENDED QC TESTS FOR MRI SYSTEMS

High-contrast spatial resolution
Slice thickness accuracy
Slice position accuracy
RF center frequency tuning
Geometric accuracy and spatial uniformity
Signal uniformity
Low-contrast resolution (sensitivity)
Image artifact evaluation
Operational controls (e.g., table movement control and alignment lighting checks)
Preventive maintenance logging and documentation
Review of system log book and operations

MRI phantoms are composed of materials that produce MR signals with carefully defined relaxation times. Some materials are aqueous paramagnetic solutions; pure gelatin, agar, silicone, or agarose; and organic doped gels, paramagnetic doped gels, and others. Water is most frequently used, but it is necessary to adjust the T1 and T2 relaxation times of (doped) water, so that images can be acquired using pulse sequence timing for patients (e.g., this is achieved by adding nickel, aqueous oxygen, aqueous manganese, or gadolinium). For example, the ACR MR Accreditation phantom (Fig. 13-45) is a cylindrical phantom of 190 mm inside diameter and 148 mm inside length. It is filled with a 10 millimolar solution of nickel chloride and 75 millimolar sodium chloride. Inside the phantom are several structures that are used in a variety of tests for scanner performance. In this phantom, seven quantitative tests are made by scanning the phantom with specific instructions, and include geometric accuracy, high contrast spatial resolution, slice thickness accuracy, slice position accuracy, image intensity uniformity, percent signal ghosting, and low-contrast object detectability. Details

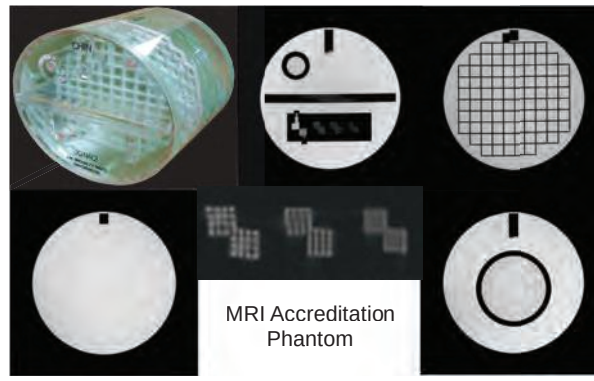

■ **FIGURE 13-45** The ACR accreditation phantom (upper left) and selected images scanned from the phantom are shown above. Upper middle is the spatial resolution module, and just below is a magnification image of the test targets. The upper right shows the geometric distortion module, the lower right is the low contrast sensitivity module, and the lower left is the uniformity module. Not all images are shown; specific details are described in the accreditation documentation available on the ACR website, http://www.acr.org.

on measurement analysis, recommended action criteria, and causes of failure/corrective action are included in the guidance. Some phantoms have standards with known T1, T2, and proton density values to evaluate the quantitative accuracy of the scanner, and to determine the ability to achieve an expected contrast level for a given pulse sequence. Homogeneity phantoms determine the spatial uniformity of transmit and receive RF magnetic fields. Ideal performance is a spatially uniform excitation of the protons and a spatially uniform sensitivity across the imaged object.

13.9 MR Bioeffects and Safety

Although ionizing radiation is not used with MRI and MRS, perception of the general public is that MR is a very safe modality, safety aspects are often an afterthought, particularly in terms of operational activities and training of personnel who work in the area and around the magnet. There are very many important bioeffects and safety issues to be considered for MR. These include the presence of strong magnetic fields, RF energy, time-varying magnetic gradient fields, cryogenic liquids, a confined imaging device (claustrophobia), and noisy operation (gradient coil activation and deactivation, creating acoustic noise). Patients with implants, prostheses, aneurysm clips, pacemakers, heart valves, etc., should be aware of considerable torque on the devices which when placed in the magnetic field, could cause serious adverse effects. Nonmetallic implant materials can also lead to significant heating under rapidly changing gradient fields. Consideration of the distortions and artifacts on the acquired images and possibility of misdiagnosis are also a concern. Ferromagnetic materials inadvertently brought into the imaging room (e.g., an IV pole) are attracted to the magnetic field and can become a deadly projectile to the occupant within the bore of the magnet. Many unfortunate deaths have been attributed to carelessness and lack of a safety culture around an MR scanner. Signage exists in three categories to help identify MR-compatible materials. "MR safe" is a square green sign, and is put on materials and objects that are wholly nonmetallic; "not MR safe" is round red, and is placed on all ferromagnetic and many conducting metals; "MR conditional" signage is triangular yellow, placed on objects that may or may not be safe until further investigation is performed. These signs are shown in Figure 13-46.

In extreme emergencies, the superconducting magnet can be turned off by a manually controlled "quench" procedure. Even under the best circumstances, the quench procedure subjects the magnet to a 260 degrees temperature difference in a short period of time. If performed too quickly, major physical damage to the magnet

■ **FIGURE 13-46** MR labeling includes on the left, MR safe materials that have been found not to interact with the strong MR field or disrupt operation; in the middle, NOT MR safe labels that contraindicate bringing materials with this designation past Zone 2 (see discussion later in this section; on the right, more consideration required before bringing such labeled objects into the scan room).

TABLE 13-5 MRI SAFETY GUIDELINES

ISSUE	PARAMETER	VARIABLES	SPECIFIED VALUE
Static magnetic field	Magnetic field (B_0)	Maximum strength	3.0 T
	Inadvertent exposure	Maximum	0.0005 T
Changing magnetic field (dB/dt)	Axial gradients	$\tau > 120$ μs	<20 T/s
		12 μs $< \tau <$ 120 μs	<2400/τ (μs) T/s
		$\tau <$ 12 μs	<200 T/s
	Transverse gradients		<3× axial gradients
	System		<6 T/s
RF power deposition	Temperature	Core of body	<18°C
		Maximum head	<38°C
		Maximum trunk	<39°C
		Maximum extremities	<40°C
	Specific absorption	Whole body (average)	<4 W/kg
	rate (SAR)	Head (average)	<3 W/kg
		Head or torso per gram	<8 W/kg
		Extremities per gram	<12 W/kg
Acoustic noise levels		Peak pressure	200 pascals
		Average pressure	105 dBA

τ rise time of gradients.
[a]In some clinical applications, higher field strengths (e.g., 4.0 T) are allowed.

can occur. Because of risks to personnel, equipment, and physical facilities, manual quenches should only be initiated after careful considerations and preparation. Uncontrolled quenching is the result of a sudden loss of superconductivity in the main magnet coils, which can result in the explosive conversion of liquid helium to gas, and jeopardize the safety of those in the room and adjacent areas. In the event of insufficient gas outflow, oxygen can be displaced and build up of pressure in the room can prevent the entry door from being easily opened.

MRI is considered "safe" when used within the regulatory guidelines required of the manufacturers by the Food and Drug Administration (Table 13-5). Serious bioeffects are demonstrated with static and varying magnetic fields at strengths significantly higher (10 to 20 times greater) than those used for typical diagnostic imaging.

Static Magnetic Fields

The long-term biologic effects of high magnetic field strengths are not well known. At lower magnetic field strengths, there have not been any reports of deleterious or nonreversable biologic effects, either acute or chronic. With very high field strength magnets (e.g., 4 T or higher), there has been anecdotal mention of dizziness and disorientation of personnel and patients as they move through the field. With systems in excess of 20 T, enzyme kinetic changes have been documented, increased membrane permeability shown, and altered biopotentials have been measured. These effects have not been dem-

onstrated in magnetic fields below 10 T. Effects on ECG traces have shown an increased amplitude of the *T* wave, presumably due to the magneto-hemodynamic effect, caused by conductive fluid such as blood moving across a magnetic field. When this occurs, sometimes the elevated *T* wave will be mistaken for the desired *R* wave, creating an insufficient gating situation. For this reason, it is recommended that ECG leads are not used for patient monitoring, but rather an alternative such as pulse oximetry be used.

Varying Magnetic Field Effects

The time-varying magnetic fields encountered in the MRI system are due to the gradient switching used for localization of the protons. Magnetic fields that vary their strength with time are generally of greater concern than static fields because oscillating magnetic fields can induce electrical current flow in conductors. The maximum allowed changing gradient fields depend on the rise times of the gradients, as listed in Table 13-5. At extremely high levels of magnetic field variation, effects such as visual phosphenes (the sensation of flashes of light being seen) can result because of induced currents in the nerves or tissues. Other consequences such as bone healing and cardiac fibrillation have been suggested in the literature. The most common bioeffect of MR systems is tissue heating caused by RF energy deposition and/or by rapid switching of high strength gradients. RF coils and antennas can present burn hazards when electrical currents and conductive loops are present, and must have proper insulation—both electrical and thermal.

RF Exposure, Acoustic Noise Limits, Specific Absorption Rate

RF exposure causes heating of tissues. There are obvious effects of overheating, and therefore a power deposition limit is imposed by governmental regulations on the manufacturers for various aspects of MRI and MRS operation. Table 13-5 lists some of the categories and the maximum values permitted for clinical use. The rationale for imposing limits on static and varying magnetic fields is based on the ability of the resting body to dissipate heat buildup caused by the deposition and absorption of thermal energy. Other indicators, such as acoustic noise levels and pressure amplitudes, are determined from limits that are shown to have reversible (unaffected) outcomes for clinically approved sequences. Hearing protection should always be available to the patient. For research sequences and procedures that have not been approved by the FDA, patients or volunteers are to have hearing protection in place.

Pregnancy-related Issues and Pediatric Patient Concerns

Pregnant healthcare staff and physicians are permitted to work in and around the MR environment throughout all stages of pregnancy and assist as needed in setting up the patient and the exam. However, they are not to remain in the magnet scanning room (Zone 4). Regarding the scanning of pregnant patients, current data have not yielded any deleterious effects on the developing fetus with common examinations, and no special considerations are warranted, as long as the benefit-risk-ratio of doing the study is that for any other typical patient. Another consideration is the administration of contrast, which should not be routinely provided. A well-documented consideration to administer contrast based on the overwhelming potential benefit to the patient or fetus relative to the risk of exposing them to gadolinium-based agents and potential deleterious effects of free gadolinium ions, as there are studies that have documented that the agents do pass the placental barrier and do enter the fetus.

For pediatric patients, the largest issues are sedation and monitoring. Special attention to sedation protocols, adherence to standards of care regarding sedation guidelines, and monitoring patients during the scan with MR-safe temperature monitoring and isolation transport units are crucial to maintaining patient safety.

MR Personnel and MR Safety Zones

The American College of Radiology has published a white paper describing the recommendations for MR safety in general, and MR safety "zones" and MR personnel definitions in particular in their 2007 publication (ACR white paper reference). MR safety policies, procedures, and safe practices are suggested in the guidance. In an effort to maintain a buffer zone around the "always on" magnet, MR safety zones are categorized from Zone 1 to Zone 4. Zone 1 is the area freely accessible to the general public, in essence everywhere outside of the MR magnet area and building. Zone 2 represents the interface between Zone 1 and Zone 3—typically the reception area, where patients are registered and MR screening questions take place. Zone 3 is a restricted area comprised of the MR control room and computer room that only specific personnel can access, namely, those specifically trained as MR personnel (described below) and appropriately screened patients and other individuals (nurses,

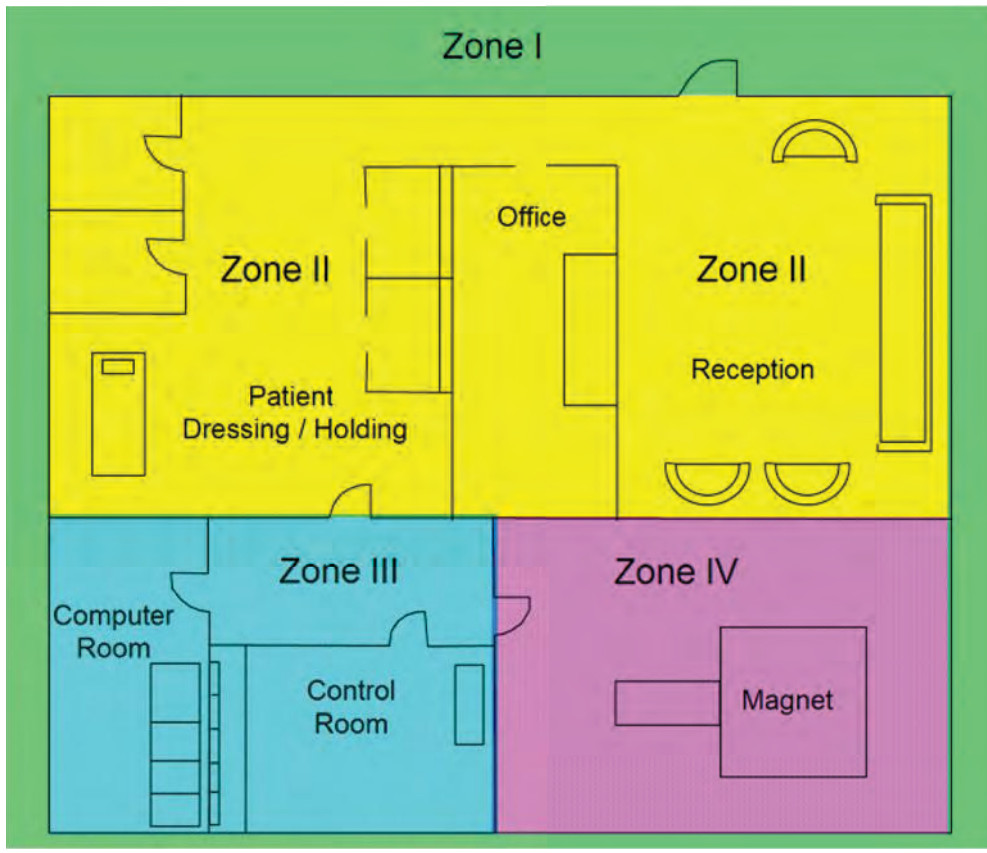

■ **FIGURE 13-47** Zoning concept for describing areas in an MR system environment include Zone 1, unrestricted access; Zone 2, interface between unrestricted and restricted areas; Zone 3, restricted area only allowed for MR personnel and screened individuals; Zone 4, the area of the scanner and high magnetic field strength. (Adapted from Kanal E., et.al. Guidance Document for Safe MR Practices: 2007.)

support staff). Zone 4 represents the MR magnet room, and is always located within the confines of Zone 3. Demarcation of these zones should be clearly marked and identified. Figure 13-47 illustrates the zoning concept.

Furthermore, there are personnel definitions describing criteria that must be achieved before access can be granted to Zone 3 and Zone 4 areas. *Non-MR personnel* are patients, visitors, for staff who do not have the appropriate education or training that meet the criteria for Level 1 or Level 2 MR personnel. *Level 1 MR personnel* have passed minimal safety and education training on MR safety issues and have a basic understanding of the effects of MR magnets, dangers of projectiles, effects of strong magnetic fields, etc. These individuals can work in Zone 3 and Zone 4 areas without supervision or oversight; examples are MR office staff, patient aides, and custodial staff. *Level 2 MR personnel* are more extensively trained in the broader aspects of MR safety issues, for example, understanding the potential for thermal loading, burns, neuromuscular excitation, and induced currents from gradients. These individuals are the gatekeepers of access into Zone 4, and take the action and the leadership role in the event of a patient code, ensuring that only properly screened support staff are allowed access. Those responding to a code must be made aware of and comply with MR safety protocols. Examples of personnel designated as Level 2 include MR technologists, MR medical physicists, radiologists, and department nursing staff.

Designated personnel are required to continuously maintain their safety credentials, by acquiring continuous education credits throughout the year on MR safety aspects, and taking an annual test and achieving a minimum passing score.

13.10 Summary

Meeting the needs of the MR exam and using the equipment safely and effectively requires the understanding of the basic physics underpinnings described in Chapter 12, and the details of advanced acquisition methods, image characteristics, artifacts/pitfalls, and MR safety/bioeffects covered in this chapter. The reader is encouraged to keep up with the rapid developments of MRI and MRS by referring to recent literature and websites dedicated to MRI education and technological advances.

REFERENCES AND SUGGESTED READINGS

American College of Radiology MRI Accreditation Program, Phantom Test Guidance and other documentation for the MRI accreditation program, available at http://www.acr.org/accreditation/mri/mri_qc_forms.aspx, accessed May 30, 2011.

Hendrick RE. *Breast MRI: fundamentals and technical aspects*. New York, NY: Springer, 2007.

Kanal E, Barkovich AJ, Bell C, et.al. ACR guidance document for safe MR practices: 2007. *AJR Am J Roentgenol.* 2007;188:1–27.

NessAiver M. *All you really need to know about MRI physics.* Baltimore, MD: Simply Physics, 1997.

Al-Okaili RN, Krejza J, Wang S, Woo JH, Melhem ER. *Advanced MR Imaging Techniques in the Diagnosis of Intraaxial Brain Tumors in Adults.* Radiographics 2006; 26: S173-S189.

Westbrook C, Kaut-Roth C, Talbot J. *MRI in practice*. 3rd ed. Malden, MA: Blackwell Publishing, 2005.